Hampton Roads Crossing Study Supplemental Environmental Impact Statement: Evaluation of Potential Impact on Surface Water Elevation, Flow, Salinity, and Bottom Shear Stress
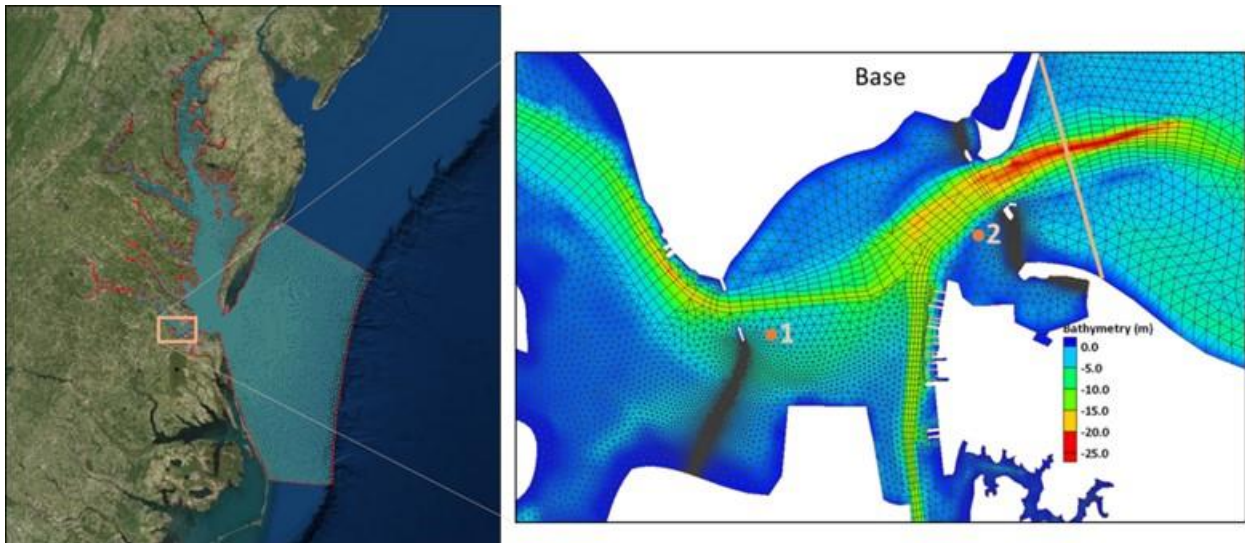
A Report to:

Virginia Department of Transportation
Environmental Division
1401 East Broad Street,
Richmond, Virginia 23219

by

Joseph Zhang, Harry Wang, Zhou Liu, Mac Sisson, and Jian Shen

Virginia Institute of Marine Science
Department of Physical Sciences
Gloucester Point, Virginia 23062

Special Report No. 453

In Applied Marine Science and Ocean Engineering

January 17, 2017

Table of Contents

LIST OF TABLES

LIST OF FIGURES

Executive Summary

The purpose of this study is to evaluate the potential impacts of the proposed alternatives for the highway crossing in Hampton Roads on physical characteristics of surface water elevation, flow, salinity, and bottom shear stress. The analysis is part of the Virginia Department of Transportation (VDOT), the Federal Highway Administration, and other stakeholders' Supplemental Environmental Impact Statement (SEIS) for Hampton Roads Crossing Study (HRCS). This study was built upon previous effort in the same area (Boon et al. 1999) whereby VIMS' (Virginia Institute of Marine Science) EFDC model (Environmental Fluid Dynamics Code) was used to study the impact of the bridge-tunnel infrastructure on the physical characteristics. Due to limitations of the technology at the time, bridge pilings were not resolved directly; instead, they are parameterized by the porosity. In the present study, the state-of-the-art, unstructured-grid modeling system SCHISM (Semi-implicit, Cross-scale, Hydroscience System Model) was used, which allows the model domain to cover the entire Chesapeake Bay and, at the same time, enables the local higher-resolution grid to resolve the bridge pilings in explicitly simulating the impacts of bridge piling under 4 scenarios: Alternative A (I64 at HRBT), Alternative B (I64 at HRBT, I-564 connector, VA I-64 connector and VA I64), Alternative C (I-664, I-564, VA I64 connector and I664 connector) and Alternative D (corridors included in all the other alternatives).

The SCHISM model was first calibrated with the observation data including water level, ADCP (Acoustic Doppler Current Profile) at 4 locations, and 20 salinity and temperature data measurements across the lower Chesapeake Bay, James River, and Elizabeth River for the existing condition of the year 2011. The model results compared very well with the comprehensive observation data, collected by NOAA (National Ocean Atmospheric Administration), EPA Chesapeake Bay Program, and USGS (US Geological Survey) and further validated over the years of 2010 - 2013. This confirms the skills of the SCHISM model being a validated base case (no-build condition) which can be used for scenario runs. The analyses of the impacts were conducted by comparing the difference between the base case versus the scenario runs for different alternatives using local analysis and global analysis. The former focuses on the localized effect of changes at any single point location whereas the latter takes into consideration the percentage of the total area associated with class intervals of the changes deviated from the base case. Here, the term '*global*' is used to refer to the entire region from the mouth of the James River upstream to the James River Bridge within which the transportation infrastructures are proposed. By combining the global and local analyses, a balanced view of assessment from both large scale as well as local scale is achieved in a objective manner.

The local analysis of scenario runs for the surface water elevation consists of evaluating changes of tidal amplitudes and phases. The change of amplitudes are all below 1mm at the backdrop of near 1 meter tidal range (on the order of one tenth of 1%). The phase changes are less than 0.3 degrees out of 360 degrees of freedom (on the order of one tenth of 1%). The average flux of tidal flow change from all scenarios is on the order of a few m^3/s (out of several hundred to several thousand m^3/s) or less than 1% change for all alternatives. Small changes were observed in time history of surface and bottom currents around the proposed bridge piling. An examination of the spatial (plan-view) distribution of the instantaneous current fields revealed that most of the changes were caused by local deviations in the direction and phase, rather than the magnitude of the current. The vorticity analysis were further conducted to quantify these changes and confirm that the changes are all localized in nature. A significant large eddy feature occupies the Hampton Roads Flats was intact except that it shows only a very minor change in phase in response to all the alternatives. Salinity changes were observed in the

vicinity of bridges on pilings, especially those for Alternative D. This was primarily a response to piling-induced turbulence, increased vertical mixing, and the elimination of surface-to-bottom salinity gradients immediately around pilings. No changes were observed in the longitudinal salinity distribution along the channel axis of the James River in response to any of the alternatives except a notable increase of the bottom salinity in two semi-enclosed coastal basins: Mill Creek and Willoughby Bay. The sediment erosion and deposition potential is quantified using the bottom shear stress. The change in the latter is mostly confined near the proposed pilings. The bottom shear stress generally decreases both upstream and downstream of the pilings but increases between the pilings. The decreases (~ -0.1 Pa) occur mostly near the tunnel islands of I64 due to reduced flow there. The addition of I564 in Alternative B only causes a smaller decrease there (~ -0.02Pa), because the flow near the entrance of Elizabeth River is not as strong as that in James River. More blocking of flow by the I664 expansion in Alternative C leads to similar decreases in the bottom stress (~ -0.1Pa) near the tunnel islands, but the increases (~0.1 Pa) on the north and west sides of southern tunnel are also observed. The changes in Alternative D are approximately equal to the sum of changes in Alternatives B & C. These changes are mostly correlated to those in the averaged flow: the flow velocity tends to slow down both upstream and downstream due to the blocking effects of the pilings and tunnel islands, but tends to increase between pilings due to more constriction there.

To make assessment of the overall impact of the alternatives on the lower James River, a global analysis with the areas of variation taken into consideration is necessary. The technique involves generating an area-weighted frequency histogram and cumulative frequency function (with hourly intervals) for a year-long comparison of parameters predicted by the base case versus the 4 scenarios. By dividing the aforementioned differences into class intervals and plotting the frequency distribution, it was found that all variables have a central tendency toward zero deviation. The 95th percentile values were then selected to represent the conservative estimate of the differences of the 4 alternatives deviated from the base case. The variables selected are 95th percentile deviation of the surface current, bottom current, surface salinity, bottom salinity, and the bottom shear stress: also included are the reference values obtained from 90th and 95th of the base case, as shown in the table below. When the 95th percentile values of the alternatives A, B, C, D are divided by the reference values, the *percentage impact relative to the base case* are obtained.

Impacts analysis based on quantified deviation from base case due to HRCS SEIS Alternatives using global analysis					
Difference (from Base Case):	**Alternative A**	**Alternative B**	**Alternative C**	**Alternative D**	**Reference values** from Base case
Surface Current	0.10 cm/s	0.11 cm/s	0.15 cm/s	**0.15 cm/s**	**24 - 28 cm/s**
Bottom Current	0.05 cm/s	0.05 cm/s	0.10 cm/s	**0.11 cm/s**	**10 - 12 cm/s**
Surface Salinity	0.17 ppt	0.21 ppt	0.32 ppt	**0.33 ppt**	**22 - 24 ppt**
Bottom Salinity	0.14 ppt	0.18 ppt	0.26 ppt	**0.28 ppt**	**24 - 26 ppt**
Bottom Shear Stress	0.002 pa	0.002 pa	0.003 pa	**0.0045 pa**	**0.23 - 0.25 Pascal**

These percentage impacts are all less than 1-2%, which are considered small from an environmental risk point-of-view. To characterize the residence time change, the differences in the water age (the transit time of the water from the upstream of the James River moving downstream) between the base case and the 4 alternatives were also compared and were found to be generally small – less than 0.1 day near the proposed bridge structures except that near the mouth of the Elizabeth River where the change was about 1 day. In conclusion, the new study, conducted under VDOT planning level which does not assume full design/construction details, confirms the results from the previous investigation results that the changes

due to the projects are mainly local in nature and the overall impacts on the lower James as a whole are relatively small compared to the "no-build" base case.

1. Background

The Virginia Department of Transportation (VDOT), in cooperation with the Federal Highway Administration (FHWA) as the lead federal agency, is preparing a Supplemental Environmental Impact Statement (SEIS) for the Hampton Roads Crossing Study (HRCS) located in the cities of Chesapeake, Hampton, Newport News, Norfolk, Portsmouth, and Suffolk, Virginia. The SEIS re-evaluates the findings of the 2001 HRCS Final Environmental Impact Statement (FEIS) and Record of Decision (ROD). Pursuant to the National Environmental Policy Act (NEPA) of 1969, as amended, FHWA is preparing a SEIS because of the time that has lapsed since the 2001 FEIS and new information indicating significant environmental impacts not previously considered. The SEIS, prepared in accordance with the implementing regulations of NEPA (23 CFR §771.130), is intended to aid in ensuring sound decision making moving forward by providing a comparative understanding of the potential effects of the various options. Information in this report, prepared by VIMS and described below, will support discussions presented in the SEIS.

Based on a previous study (Boon et al. 1999), the tidal heights and currents were not substantially altered except immediately adjacent to the new structures. The residual eddy near the Elizabeth River entrance diminished in 2 alternatives (Alternatives 2 and 9 there). Due to the enhanced mixing near those structures, salinity stratification is reduced in the near field, which affects the residual circulation pattern. Similarly, sedimentation was also slightly reduced near the structures. Overall, only small impacts on physical variables were observed in the near field. Since the bridge pilings were not resolved in that study, further research is required to corroborate these findings. As there are many such pilings along the bridges (e.g., some alternatives call for one piling every 20-25 m), these structures *collectively* may exert some impact on the overall physical characteristics of the river. Similarly, since scouring is a highly localized process, the collection of those structures may also influence the sediment transport pattern nearby. How far upstream/downstream this influence propagates will be the subject of study in this project using a high-resolution grid (with the smallest grid cell size comparable to the smallest bridge piling) unstructured-grid model developed at VIMS.

Five alternatives are under consideration for the Draft SEIS and are assessed in this technical report. The proposed limits of the four build alternatives are shown on **Figure 1**. This technical report, prepared in support of the Draft SEIS, will assess existing conditions and environmental impacts along the Study Area Corridors for each alternative. Each alternative is comprised of various roadway alignments, used to describe the alternatives and proposed improvements.

The No-Build Alternative ('Base')

This alternative includes continued routine maintenance and repairs of existing transportation infrastructure within the Study Area Corridors, but there would be no major improvements.

Alternative A

Alternative A begins at the I-64/I-664 interchange in Hampton and creates a consistent six-lane facility by widening I-64 to the I-564 interchange in Norfolk. A parallel bridge-tunnel would be constructed west of the existing I-64 HRBT. Based on input received during previous studies, VDOT and FHWA have agreed that improvements proposed in the HRCS SEIS to the I-64 corridor would be largely confined to existing right-of-way. To meet this commitment, Alternative A considers a six-lane facility whose configurations are summarized in Table 1. The total number of new pilings added is ~280. The numbers

of new pilings for this and other alternatives below are determined by the GIS shapefile provided by VDOT, within which it giving exact locations of piers in each of the alternatives.

Table 1: Alternative A Lane Configurations

Roadway Alignments	Existing Lanes	Proposed Lanes
I-64 (Hampton)	6	6
I-64 (HRBT and Norfolk)	4	6

Alternative B

Alternative B would include all of the improvements included under Alternative A. The Study Area Corridor also includes the existing I-564 corridor that extends from its intersection with I-64 west towards the Elizabeth River. I-564 would be extended to connect to a new bridge-tunnel across the Elizabeth River (I-564 Connector). A new roadway (164 Connector) would extend south from the I-564 connector, along the east side of Craney Island, and connect to existing VA 164. VA 164 would be widened from this intersection west to I-664. Alternative B lane configurations are summarized in Table 2. The number of new pilings added is ~450.

Table 2: Alternative B Lane Configurations

Roadway Alignments	Existing Lanes	Proposed Lanes
I-64 (Hampton)	6	6
I-64 (HRBT and Norfolk)	4	6
I-564	6	6
I-564 Connector	None	4
VA 164 Connector	None	4
VA 164	4	6

Note: The I-564 Intermodal Connector (IC) project is separate from HRCS that lies between the I-564 Connector and I-564. It would be constructed regardless of whether the HRCS improvements are made and therefore is included under the No-Build Alternative and is not listed with other proposed improvements.

Alternative C

Alternative C includes the same improvements along I-564, the I-564 Connector, and the VA 164 Connector that were considered in Alternative B. This alternative would not include consideration of improvements to I-64 or to VA 164 beyond the connector. Instead, this alternative includes the conversion of two existing lanes on I-564 in Norfolk to transit only. This transit conversion would extend along the I-564 Connector to its intersection with the 164 Connector. At that point, a new bridge structure (I-664 Connector) would continue west and tie into I-664. This alternative also would include widening

along I-664 beginning at I-664/I-64 in Hampton and continuing south to the I-264 interchange in Chesapeake. Alternative C lane configurations are summarized in

Table 3. The total number of new pilings added is ~920.

Table 3: Alternative C Lane Configurations

Roadway Alignments	Existing Lanes	Proposed Lanes
I-664 (from I-64 to the proposed I-664 Connector)	4-6	8 + 2 Transit Only
I-664 (from the proposed I-664 Connector to VA 164)	4	8
I-664 (from VA 164 to I-264)	4	6
I-564	6	4 + 2 Transit Only
I-564 Connector	none	4 + 2 Transit Only
VA 164 Connector	none	4
I-664 Connector	none	4 + 2 Transit Only

Note: The I-564 IC project is separate from HRCS that lies between the I-564 Connector and I-564. It would be constructed regardless of whether the HRCS improvements are made and therefore is included under the No-Build Alternative and is not listed with other proposed improvements.

Alternative D

Alternative D is a combination of the sections that comprise Alternatives B and C. Alternative D lane configurations are summarized in Table 4. The number of new pilings added is ~1200.

Table 4: Alternative D Lane Configurations

Roadway Alignments	Existing Lanes	Proposed Lanes
I-64 (Hampton)	6	6
I-64 (HRBT and Norfolk)	4	6
I-664 (from I-64 to VA 164)	4-6	8
I-664 (from VA 164 to I-264)	4	6
I-664 Connector	None	4
I-564	6	6
I-564 Connector	none	4
VA 164 Connector	none	4
VA 164	4	6

Note: The I-564 IC project is separate from HRCS that lies between the I-564 Connector and I-564. It would be constructed regardless of whether the HRCS improvements are made and therefore is included under the No-Build Alternative and is not listed with other proposed improvements.
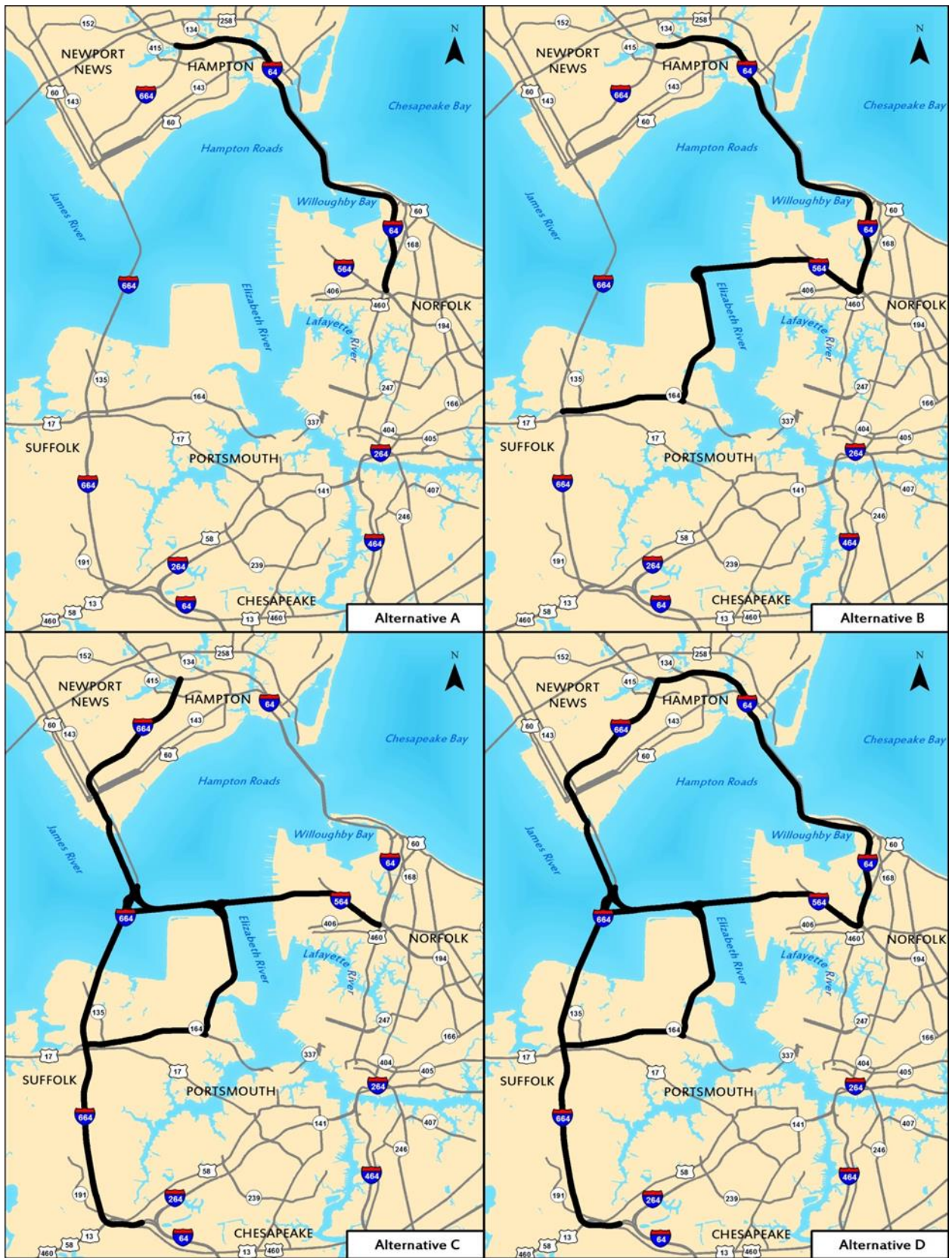
Figure 1: The proposed James River transportation infrastructure Alternatives A, B, C, and D.

2. Approach and observation

In this study we utilize a 3D unstructured-grid model, SCHISM (Semi-implicit Cross-scale Hydroscience Integrated System Model; schism.wiki), which is a derivative product of SELFE v3.1dc (Zhang and Baptista 2008a). It is an open-source, community-supported modeling system, based on unstructured grids in the horizontal and a very flexible coordinate system in the vertical (Zhang et al. 2015, 2016), designed for the seamless simulation of 3D baroclinic circulation across creek-to-ocean scales. It employs a semi-implicit finite-element/finite-volume method together with an Eulerian-Lagrangian method (ELM) to solve the Navier-Stokes equations (in either hydrostatic or non-hydrostatic form). As a result, numerical stability is greatly enhanced and the errors from the "mode splitting" method are avoided; in fact, the only stability constraints are related to the explicit treatment of the horizontal viscosity and baroclinic pressure gradient, which are much milder than the stringent CFL condition. The implicit scheme used in SCHISM often allows the use of 'hyper resolution' (on the order of a few meters) with little penalty on the time step, thus greatly reducing the need to eliminate key physics to fit the computer. The default numerical scheme is 2nd-order accurate in space and time, but optional higher-order schemes have been developed as well (e.g., the dual Kriging ELM proposed by LeRoux et al. 1997). The model also incorporates wetting and drying in a natural way, and has been rigorously benchmarked for inundation problems (Zhang and Baptista 2008b; Zhang et al. 2011) and certified by National Tsunami Hazard Mitigation Program (NTHMP) as a tsunami inundation model (NTHMP 2012). SCHISM-enabled forecasts have been officially adopted by NOAA (http://tidesandcurrents.noaa.gov/ofs/creofs/creofs.html) and Central Weather Bureau (Taiwan) (http://cwb.gov.tw/V7e/forecast/nwp/marine_forecast.htm); California Department of Water Resource (DWR) also disseminates a Bay-Delta simulation package based on SCHISM (http://baydeltaoffice.water.ca.gov/modeling/deltamodeling/models/bay_delta_schism/).

SCHISM solves the hydrostatic form of the Navier-Stokes equations with the Boussinesq approximation. The turbulence closure in SCHISM adopts the generic length scale (GLS) model of Umlauf and Burchard (2003). Air-water heat exchange is accounted for in the model using the bulk aerodynamic model of Zeng et al. (1998), based on Monin-Obukhov's similarity theory. Auxiliary models are also developed to simulate the effects of wind waves and sediment transport, etc. More information about the model and its application cases around the world can be found at www.schism.wiki.

Observational assets

In this study we utilize available observational data from NOAA (http://tidesandcurrents.noaa.gov/tide_predictions.html) and EPA's Chesapeake Bay Program (http://www.chesapeakebay.net/groups/group/21890) in the project area, i.e., Lower Chesapeake Bay (LCB). Figure 2 and Tables 5(a) – 5(b) show the names and locations of these stations, where basic hydrodynamic variables (elevation, velocity, salinity, and temperature) are measured. Year 2011 was chosen as the simulation period because of maximum availability of the data in this year whereas years 2010 and 2012 were used for verification.

Table 5 (a): NOAA tidal gauges in the Lower Chesapeake Bay.

Station_name	Kiptopeke	CBBT	Sewells Point	Money Point

Station ID	8632200	8638863	8638610	8639348

Table 5 (b): Salinity and temperature stations maintained by Chesapeake Bay Program (EPA).

Region	Station							
Lower Bay	CB6.4	CB7.3E	CB7.3	CB7.4N	CB7.4	CB8.1		
James River	RET5.2	LE5.1	LE5.2	LE5.3	LE5.4	LE5.5-W	LE5.6	CB8.1E
Elizabeth River	ELI2	ELD01	EBB01	ELE01	EBE1	LFA01		
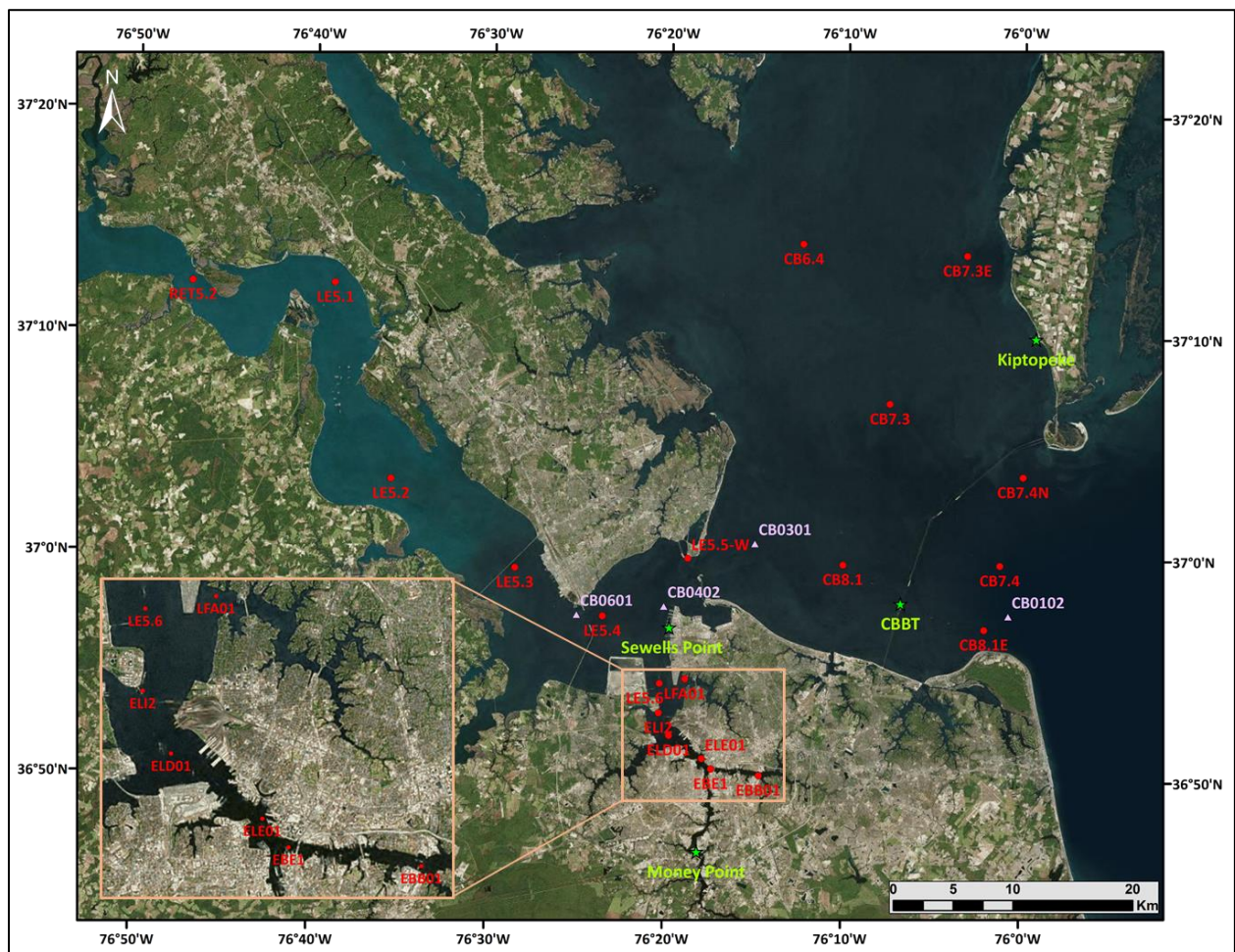
Figure 2: Observation stations used in this paper. Red circles are salinity and temperature stations maintained by Chesapeake Bay Program; green stars are NOAA tidal gauges; purple triangles (CB0102, CB0301, CB0402, CB0601) are NOAA current stations. See Tables 1-2 for more details.

3. Model setup, calibration, and verification

3.1 Model set-up

We first calibrate the model under the existing condition ('Base'), using available observations near LCB. As the results below indicate, the impact of the project site is limited to the LCB and is very minor in the mid and upper Bay. Therefore in generating the grid we deliberately applied higher resolution in the LCB while only maintaining a coarser resolution of up to 400m elsewhere in the Bay. Figs. 3-4 show the domain extent and five grids ('Base', Alternatives A-D). Altogether there are 52,484 nodes, 71,559 triangular elements, and 13,391 quad elements (mostly used to represent the shipping channels) in the Base grid (Fig. 3), 101,117 nodes, 143,821 triangular elements, and 24,503 quad elements in the D grid, including 1850 new bridge pilings (Fig. 4).

Even though a fine resolution of 1-2 m is used near the bridge pilings, we use a large time step of 120s (courtesy of the implicit scheme). The tracer transport is solved using an implicit, 2-limiter method known as TVD^2 which has been shown to be both accurate (due to an anti-diffusion limiter in time) and efficient (Zhang et al. 2016). For turbulence closure, we use a modified Mellor-Yamada scheme (k-kl) from the GLS framework. Watershed loadings in both point and nonpoint source forms predicted from EPA's Bay Program are used in the James River in order to accurately simulate the salinity there. River discharges of the 7 major tributaries (Susquehanna, Patuxent, Potomac, Rappahannock, York, James, and Choptank) of the Chesapeake Bay are taken from the USGS measurement. On the water surface, the atmospheric forcing (including heat fluxes) is from NARR (http://www.emc.ncep.noaa.gov/mmb/rreanl/). The model is first spun up for 0.5 years (from July 1, 2010 to December 31, 2010) and then continues for another 1 year (January-December, 2011); the results shown below are based on year 2011.
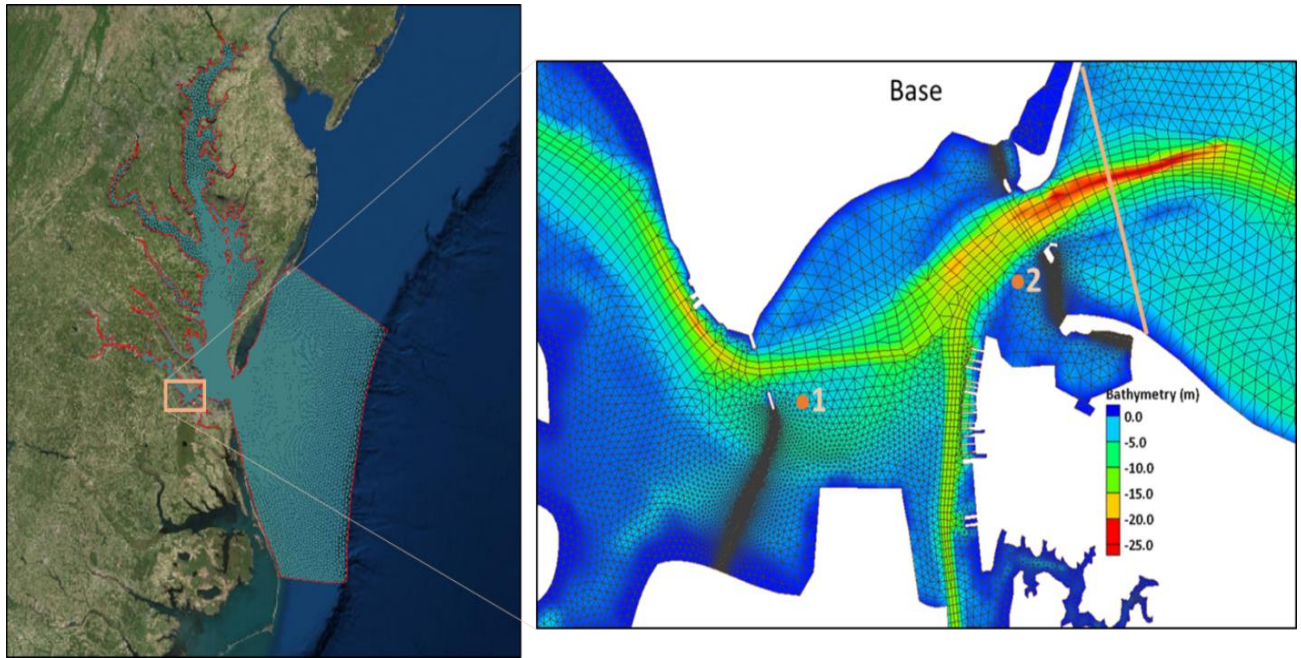
Figure 3: Domain extent and the computational grid for 'Base', with zoom-in near the project area.
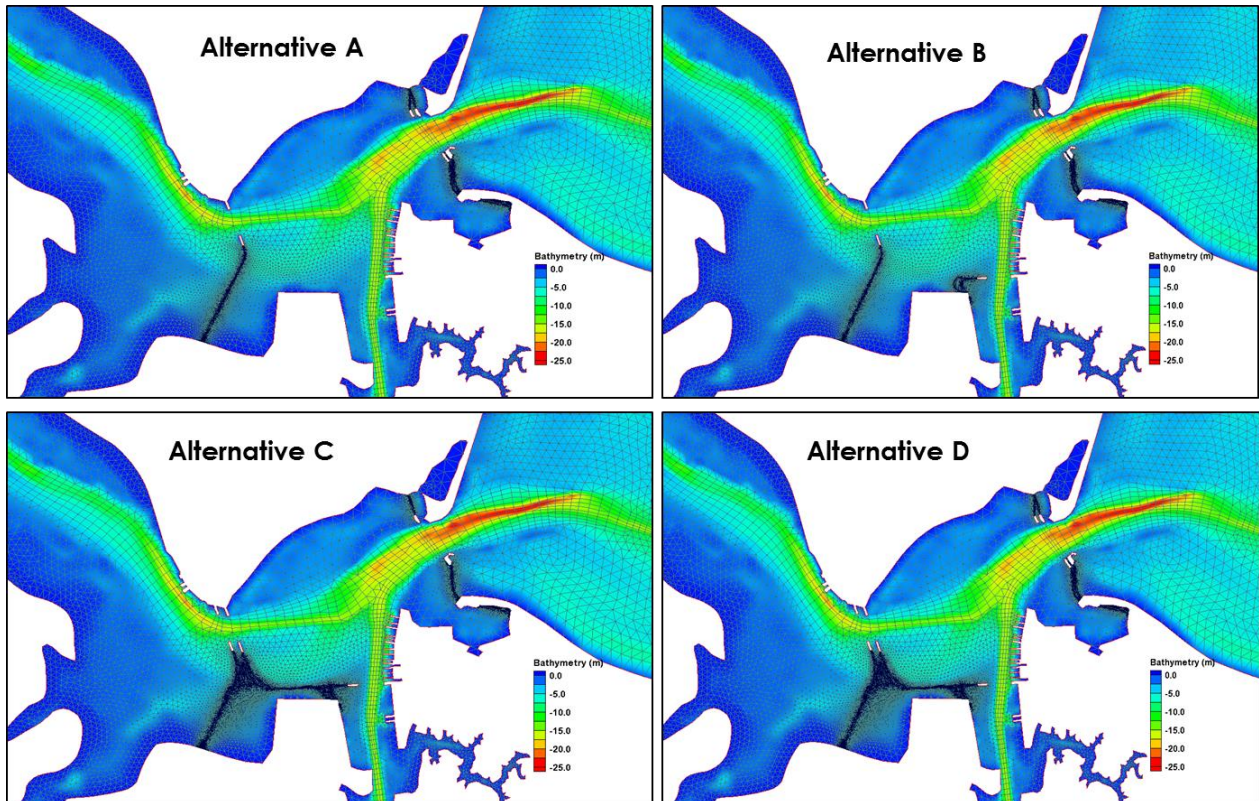
Figure 4: Differences of the grids for Alternatives A-D near the project area.

3.2 Numerical diffusion

The large contrast in grid resolution begs the question of whether the inherent numerical diffusion in the current model may contaminate the transport results. This is not an issue if the numerical diffusion is smaller than the physical diffusion in the system. The physical diffusivity is estimated to be on the order of 10m²/s or larger in estuaries (Fischer 1979; Monismith et al. 2002). SCHISM's inherent numerical diffusivity due to the 2nd-order transport solver is proportional to element area. Therefore, we first assess the numerical diffusion using a simple test.

The test deals a pure 1D problem with a Gauss hill being advected with a uniform 1m/s flow in a long flume. Without any diffusion, the analytical solution is a translation of the hill downstream without deformation. Numerical diffusion would deform the hill causing the amplitude to decrease and standard deviation to increase (i.e. broader peak). The effective numerical diffusion associated with a given grid resolution can then be estimated by comparing the numerical results (at the end of 1 day) against the analytical solution of a pure diffusion equation:

$$\frac{\partial c}{\partial t} = D \frac{\partial^2 c}{\partial x^2}$$

where c is the concentration and D is a diffusivity. Note that this estimate shows little sensitivity to the length of simulation used, suggesting that the effective diffusivity is relatively constant over time.

The results shown in Fig. 5 indicate that the numerical diffusion in the model is always smaller than the physical diffusion; it's only ~0.6 m²/s at the coarsest resolution of 400 m used in the estuary grid. Therefore, the results below are not influenced by the numerical diffusion of the model.
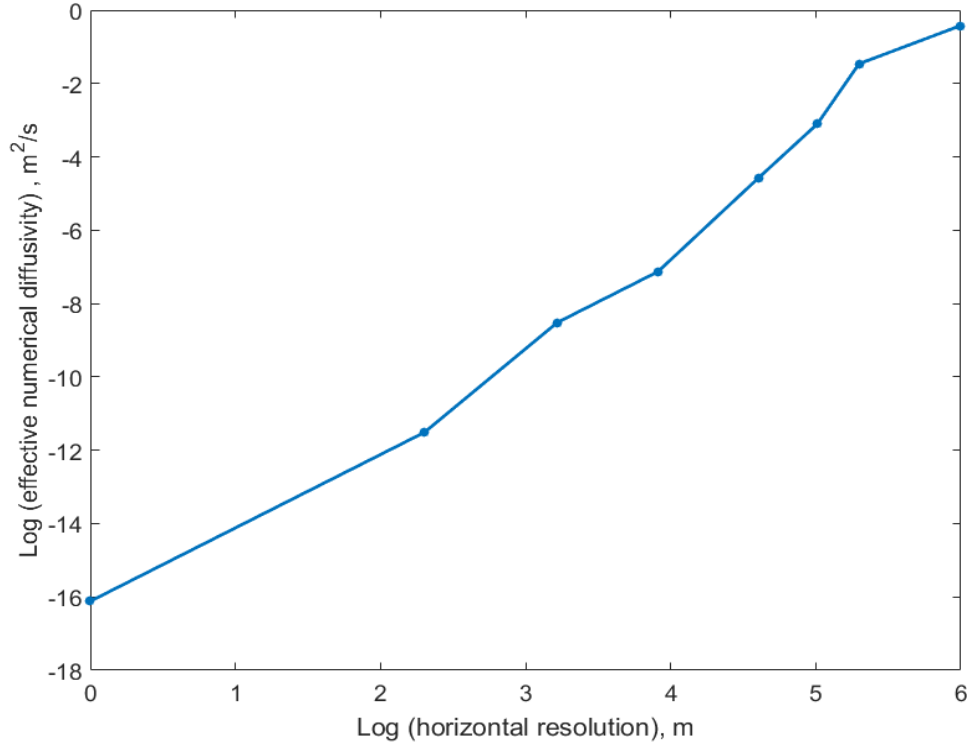
Figure 5: Effective horizontal diffusivity estimated by the Gauss hill test.

10

3.3 Model calibration and verification

A. surface elevation

Chesapeake Bay is a micro-tidal estuary with a tidal range of ~1m in most parts. This can be seen from **Figure 6** which shows the model-data comparison at 4 tide gauges in LCB. Of the 4 gauges, Sewells Point is located nearest to the project site. From Sewells Point into Elizabeth River the tidal amplitude is slightly amplified (see Money Point) due to the funnel-shape geometry (Figure 3). The model is able to accurately capture the variability of the tidal elevation in LCB, with an RMSE of no more than 9 cm.

Similarly, the modeled sub-tidal signals are in good agreement with observations (See Figure 7). In particular, the storm surge associated with Hurricane Irene (near day 234) is well-captured by the model. The comparison of major tidal constituents in this region is shown in Table 6. Over 85% of the tidal energy is contained in the M_2 constituent, which is modeled within 1-2 cm and 1 degree at all gauges; the model tends to slightly under-estimate the amplitude. Larger errors are found in K_1 but the tidal energy associated with this constituent is small.
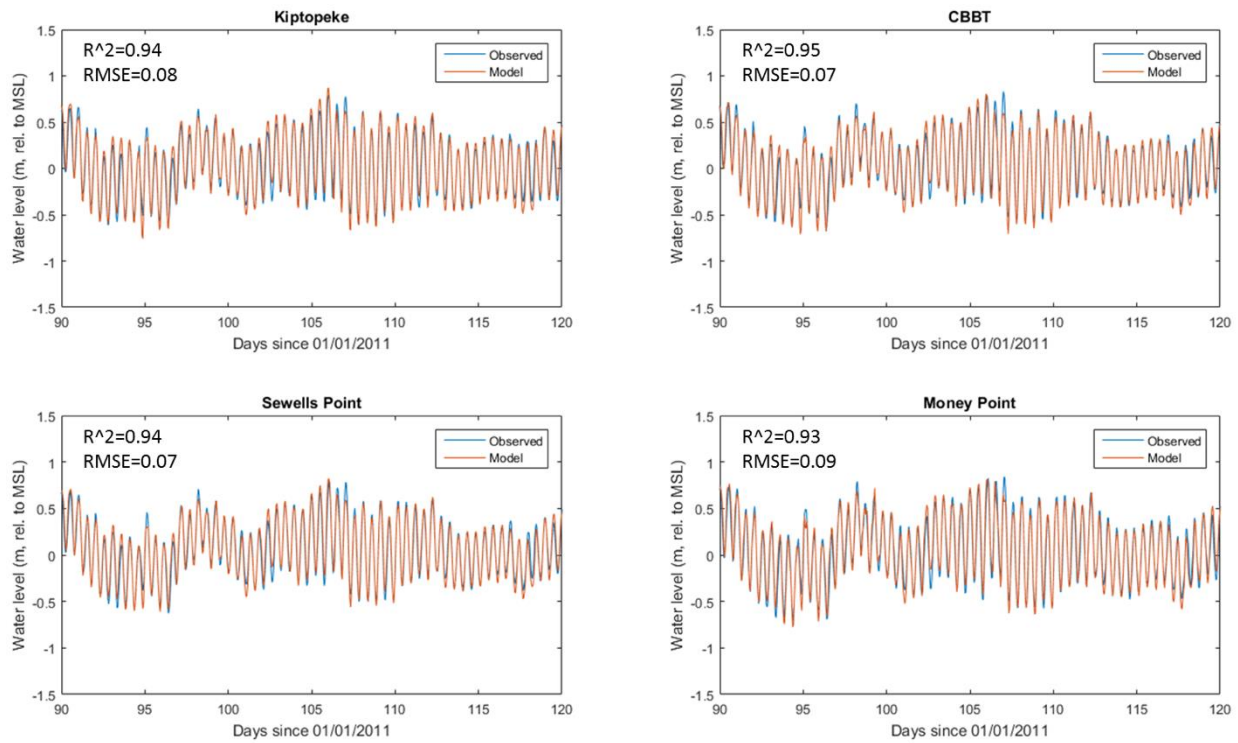
Figure 6: Comparison of total elevation at four stations in the lower Bay and James & Elizabeth River in a 30-day period in 2011.
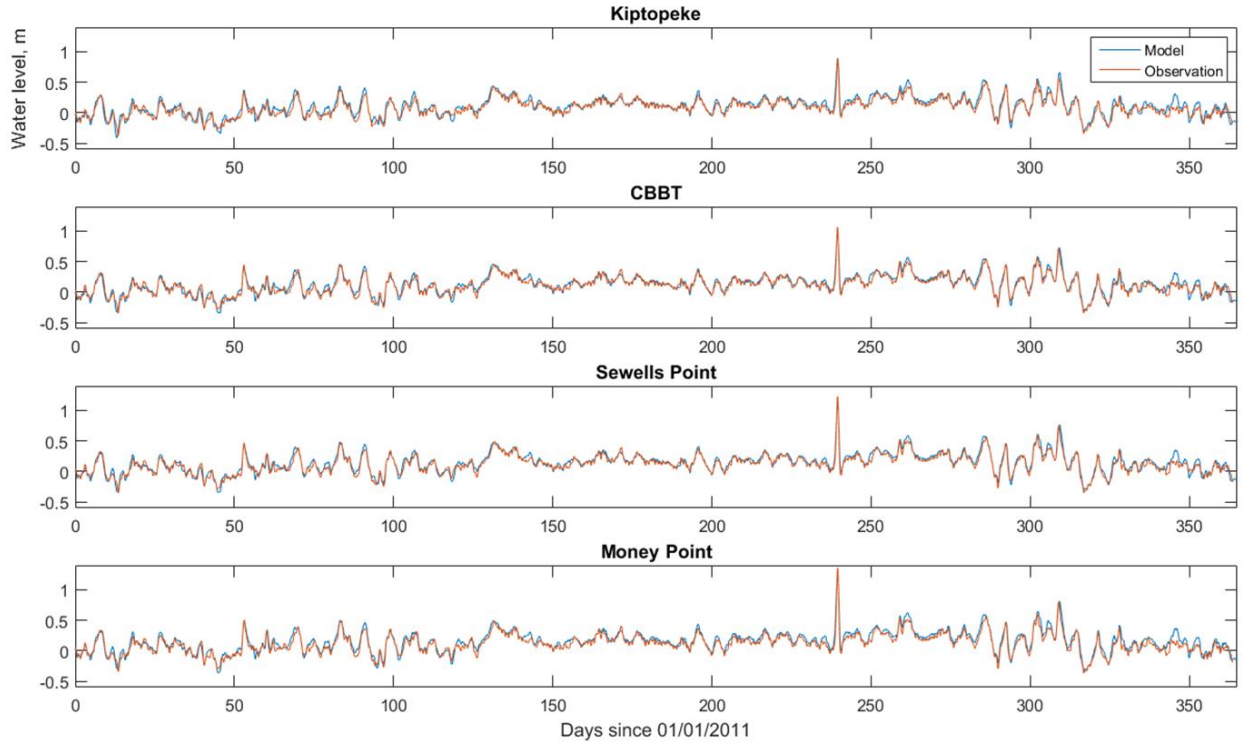
Figure 7: Comparison of sub-tidal signals at the tide gauges.

Table 6: Tidal harmonic constituents at four tide gauges in the Lower Chesapeake Bay.

Station	Amplitudes (m) of tidal harmonic constituents. Note: Error = Model − Data											
	M2		N2		S2		K2		O1		K1	
	Data	Error	Data	Error	Data	Error	Data	Error	Data	Error	Data	Error
Kiptopeke	0.3893	0.0031	0.0894	-0.0012	0.0677	-0.0001	0.0171	0.0003	0.0474	-0.0019	0.0569	-0.0082
CBBT	0.3794	-0.0014	0.0902	-0.0036	0.0683	-0.0024	0.0171	0.0004	0.0449	-0.0030	0.0547	-0.0104
Sewells Point	0.3582	-0.0111	0.0836	-0.0055	0.0635	-0.0039	0.0156	0.0000	0.0395	-0.0025	0.0503	-0.0095
Money Point	0.4127	-0.0174	0.0952	-0.0075	0.0712	-0.0038	0.0178	0.0002	0.0415	-0.0040	0.0526	-0.0101

Station	Phase (degree) of tidal harmonic constituents. Note: Error = Model − Data											
	M2		N2		S2		K2		O1		K1	
	Data	Error	Data	Error	Data	Error	Data	Error	Data	Error	Data	Error
Kiptopeke	97.45	0.72	6.43	0.59	87.38	0.04	225.03	2.02	287.55	8.92	188.98	32.29
CBBT	85.51	-0.63	354.97	-0.67	77.22	-2.20	212.30	1.63	280.75	4.83	179.03	29.88
Sewells Point	111.81	0.13	21.60	-1.27	107.31	-2.92	239.41	2.20	294.35	2.72	194.13	27.12
Money Point	118.38	-0.28	28.78	-2.34	113.10	-1.59	246.09	1.44	296.49	1.25	195.41	27.18

B. Salinity and temperature

12

The salinity variation inside LCB follows distinctive strain-induced periodic stratification (SIPS; Simpson et al. 1990; Burchard and Hetland 2010), modulated by the spring-neap cycle, freshwater discharge, and wind. The spring freshet in March-May pushes salinity lower throughout the Bay and tends to induce the largest stratification. During the dry season of summer and early fall, the river flow reaches its lowest level and this in turn pushes the salinity up the estuary and rivers and suppresses the stratification. Superposed on this seasonal variability are major wind events (e.g. Hurricane Irene in August, 2011) and the accompanying heavy precipitation. The precipitation tends to 'freshen up' the Bay while the effects of the wind depend on specificity of the storm (Cho et al. 2012). In the case of Irene, the predominant wind direction after the landfall was southerly, and as a result the surface salinity increased (and the bottom salinity decreased due to increased turbulence).

The modeled salinity captured the above-mentioned processes and generally has a good skill (see Figure 8), with an averaged RMSE of 2.4 PSU (2.4 PSU in lower Bay, 2.5 PSU in James River, 1.9 PSU in Elizabeth River). The model skill generally deteriorates toward upstream rivers where larger uncertainties exist from watershed loadings and in some cases, bathymetry.

The temperature in LCB has a seasonal signature (See Figure 9). The thermal stratification is usually small and the water column well-mixed in spring and winter due to larger turbulence mixing and weaker surface heating. Significant stratification occurs during summer-fall, primarily due to solar heating. Overturning occurs during fall as the surface water becomes progressively cooler and eventually colder than the bottom water, which has a marine origin. The comparison shown in Figure 9 confirms that the model has a good skill in predicting the water temperature.

Figure 8 (a): Comparison of salinity in (a) lower Bay (b) James River; (c) Elizabeth River.

(b)

Figure 8 (b): Comparison of salinity in (a) lower Bay (b) James River; (c) Elizabeth River.
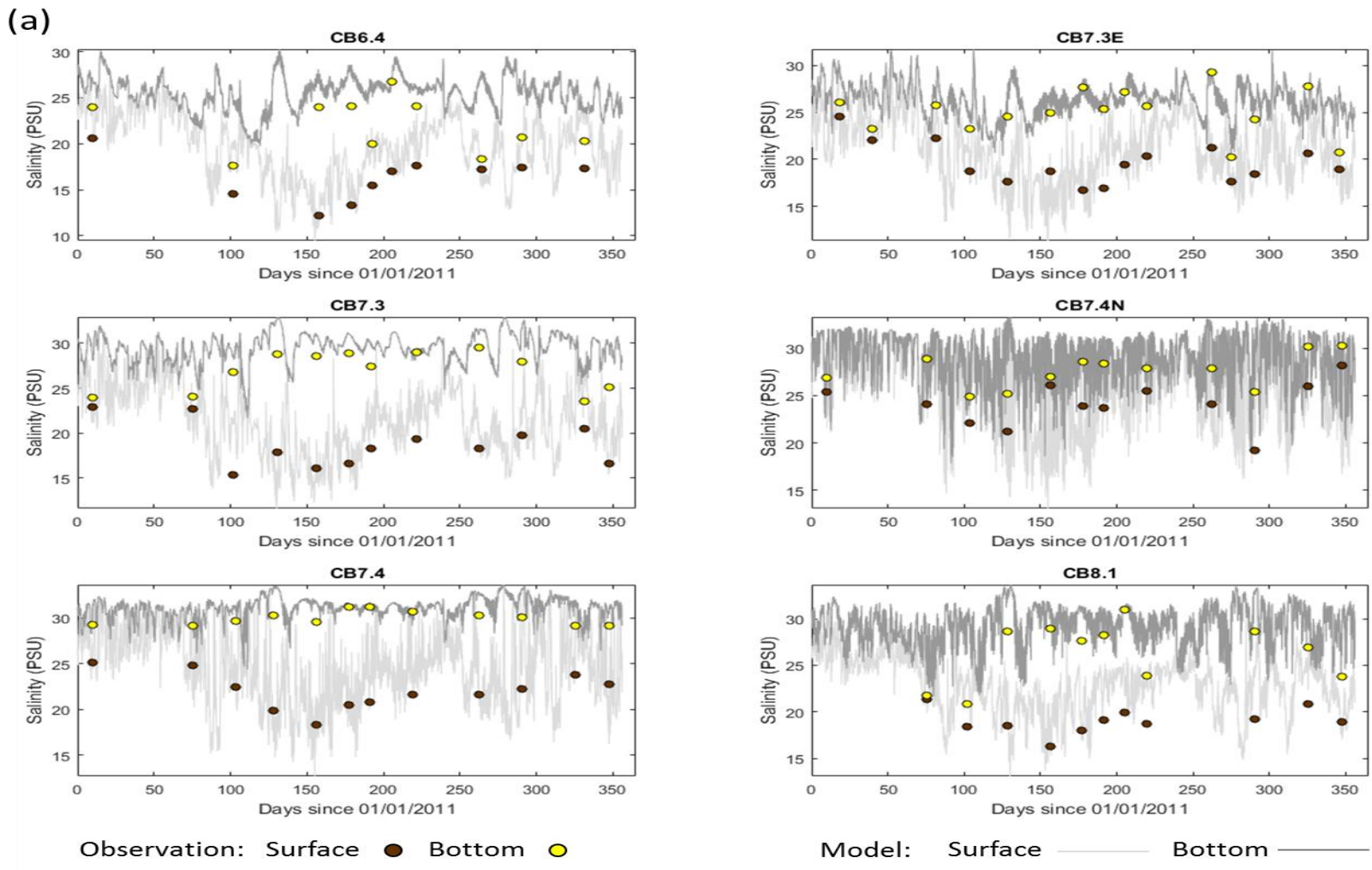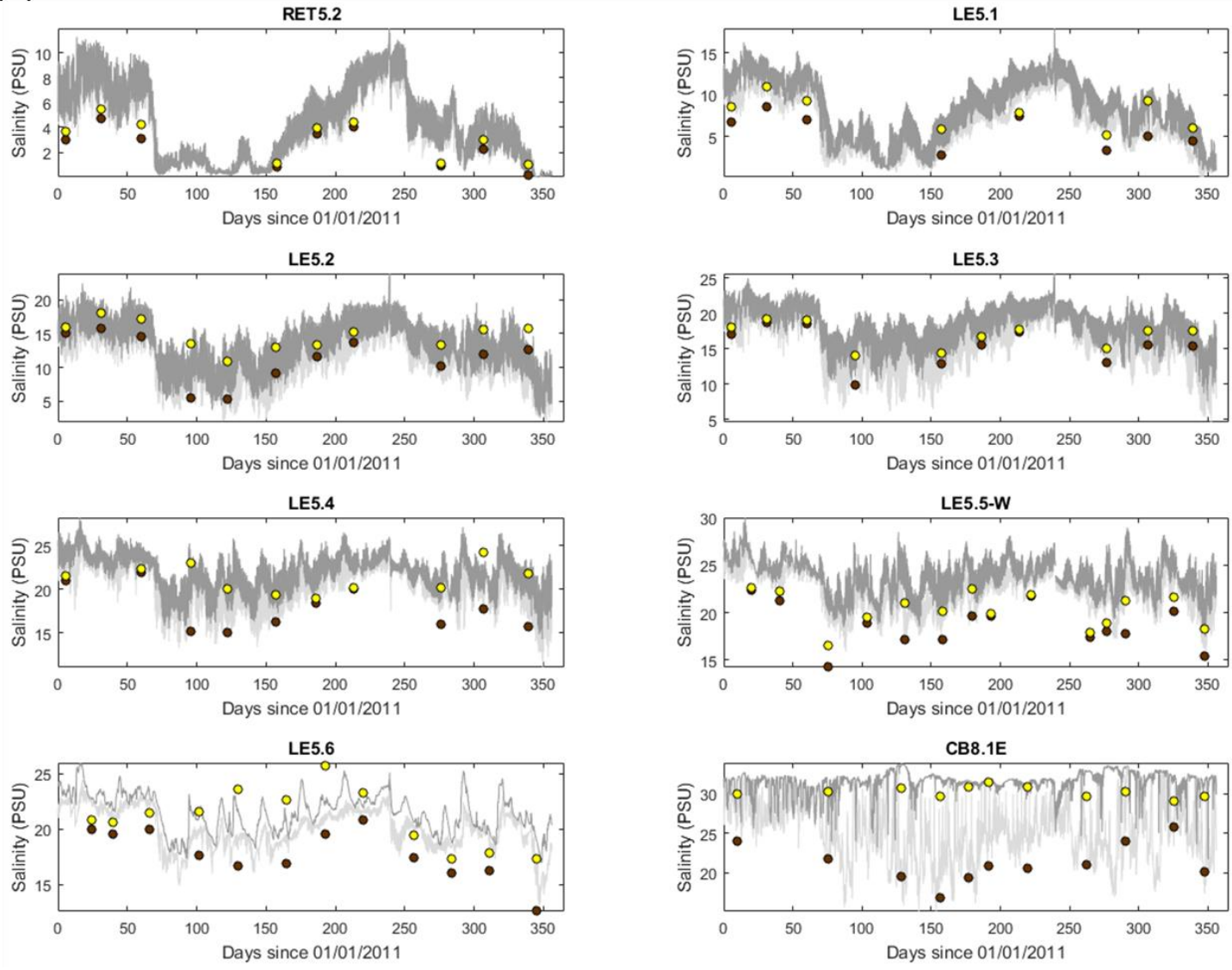
Figure 8 (c): Comparison of salinity in (a) lower Bay (b) James River; (c) Elizabeth River.

(a)
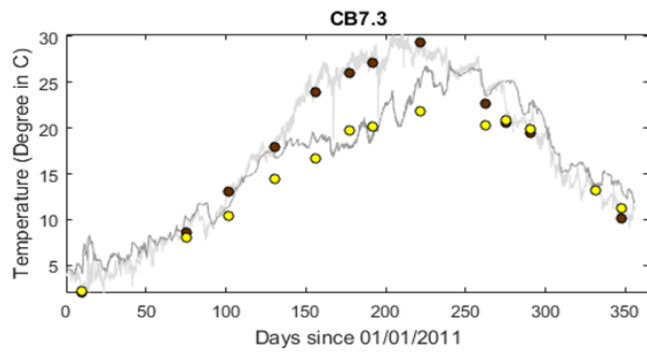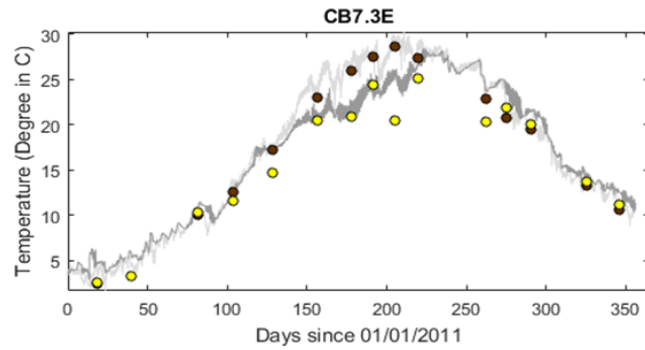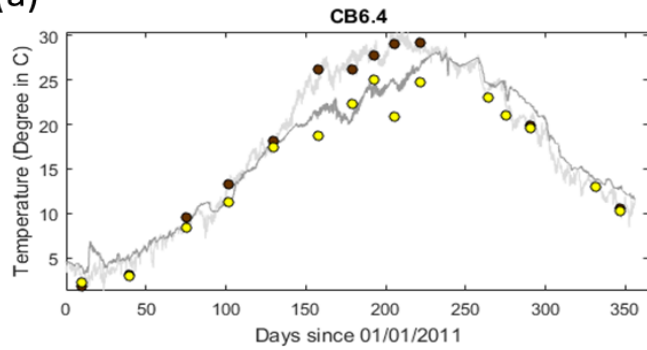
Figure 9 (a): Comparison of temperature in (a) lower Bay (b) James River; (c) Elizabeth River.

(b)

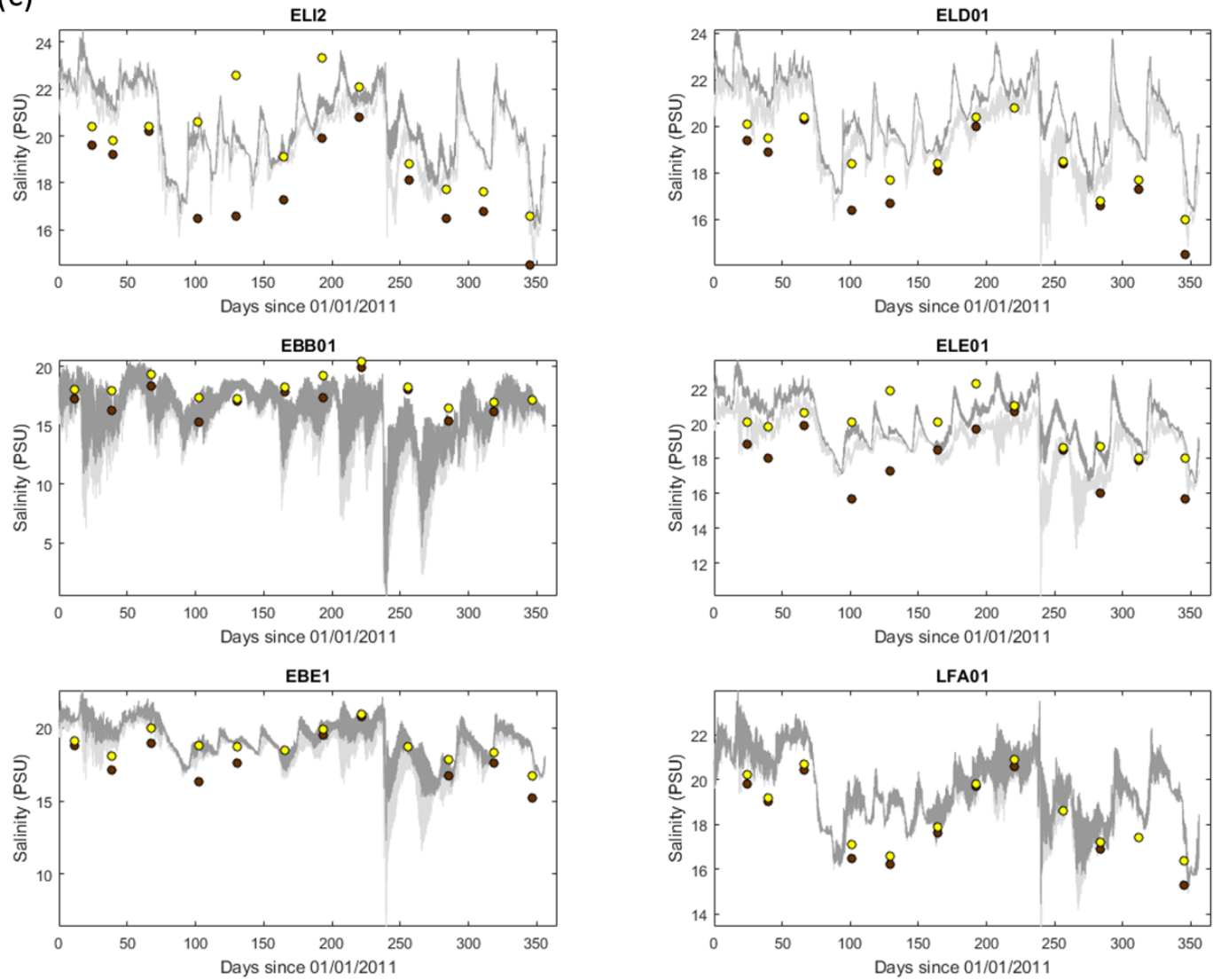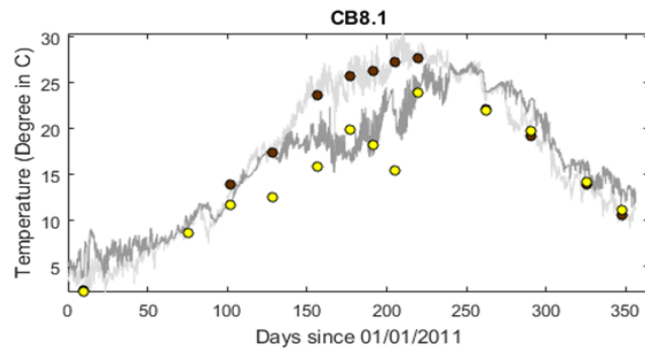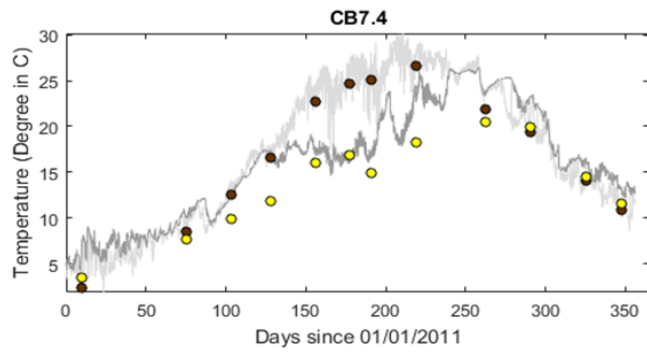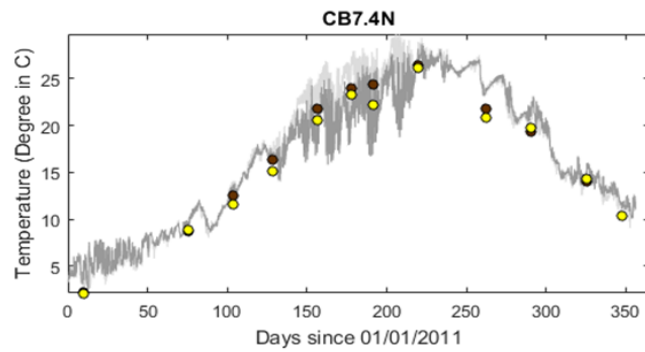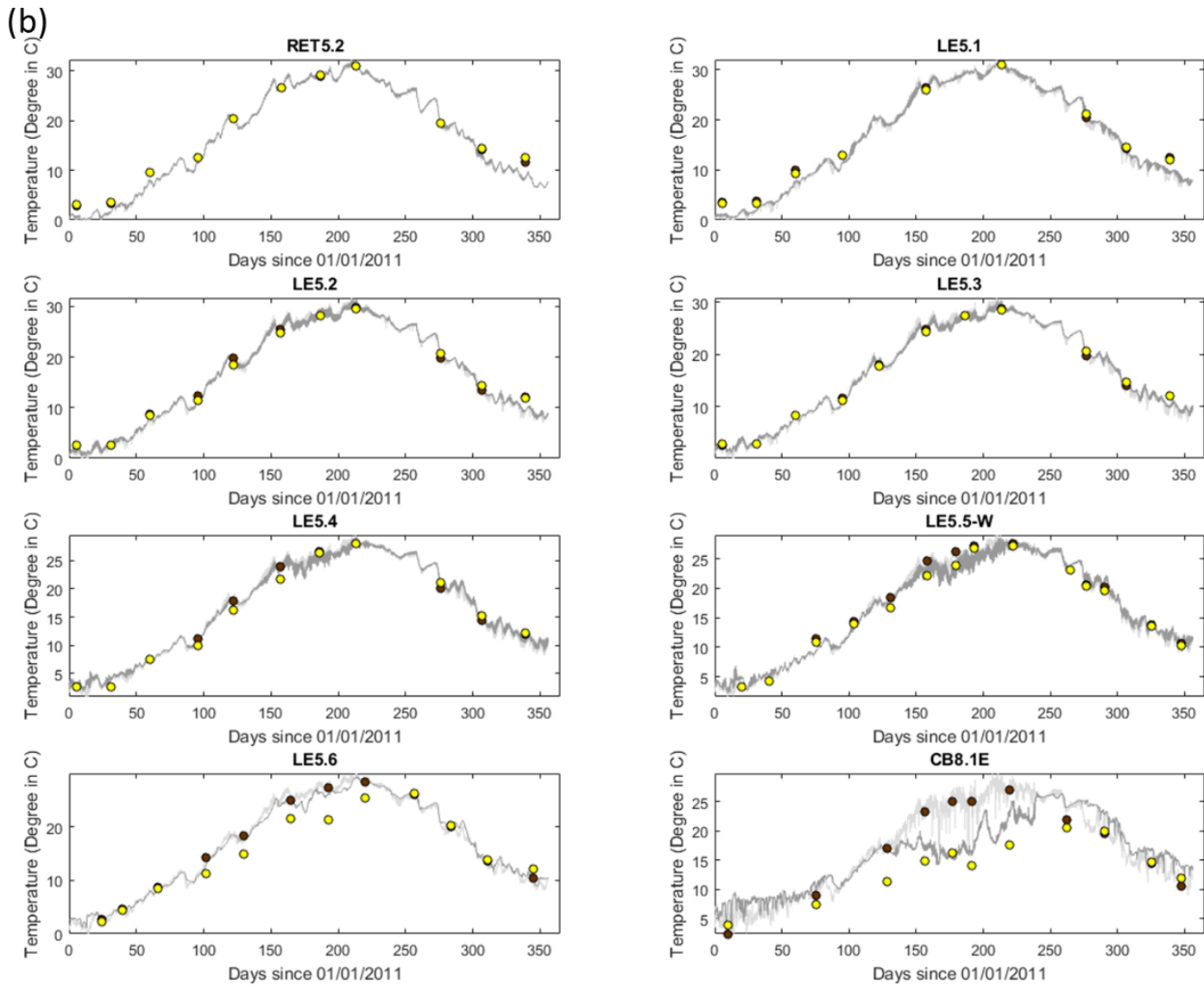Figure 9 (b): Comparison of temperature in (a) lower Bay (b) James River; (c) Elizabeth River.
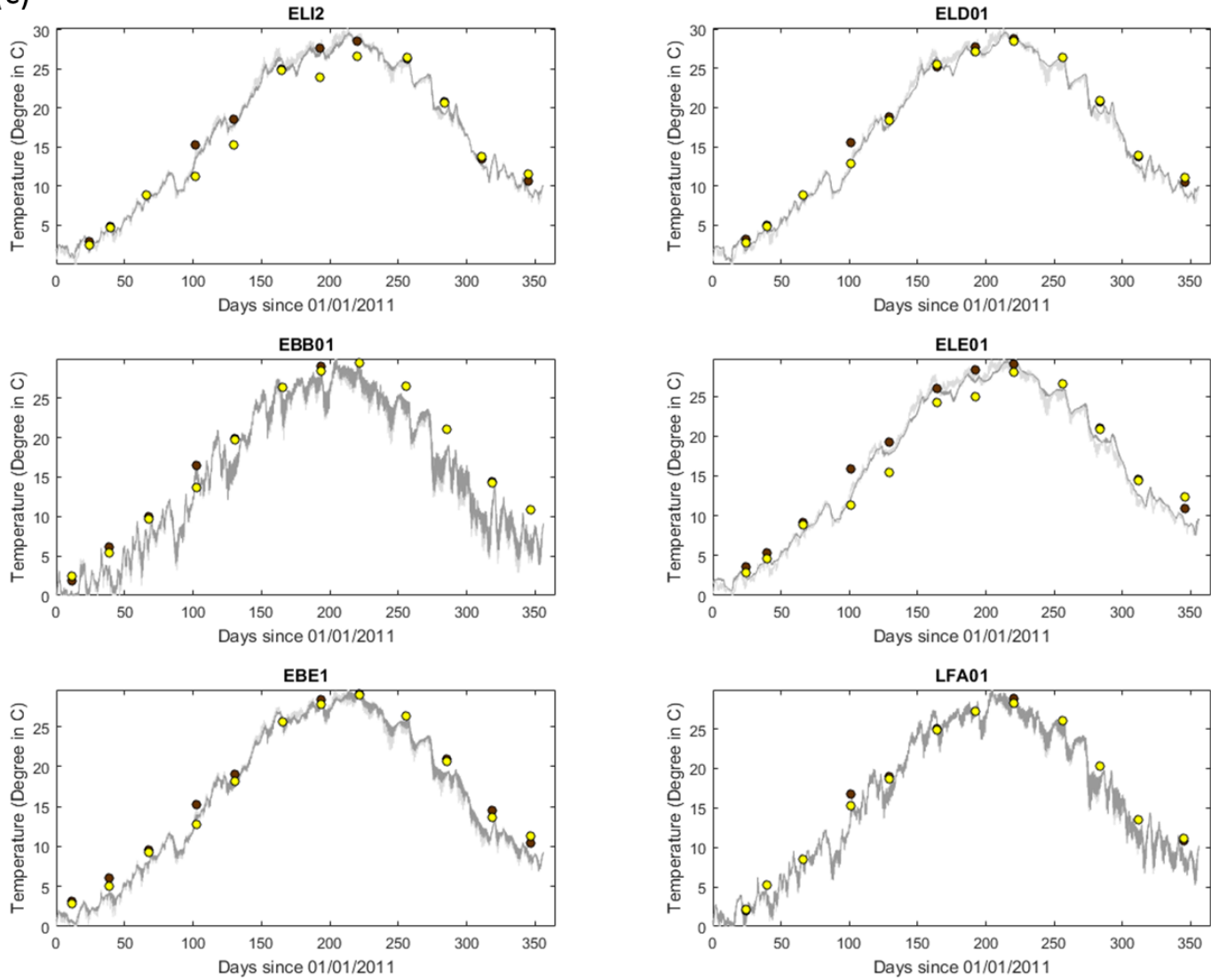
(c)

Figure 9 (c): Comparison of temperature in (a) lower Bay (b) James River; (c) Elizabeth River.

C. Velocity profile

The good model skill for the predicted water density (which is a function of salinity and temperature) suggests that the model is able to accurately represent baroclinic processes such as gravitational circulation. This is confirmed by the comparison of along-channel velocity at 4 ADCP stations (see Figures 10 -13). In general, the model captures the two-layer velocity structure quite well; the averaged R^2 value for the 4 stations is 0.80. Occasional large errors in the near-surface velocity may be related to uncertainties in the wind forcing.

D. Additional model verification for 2011-2013

In the previous section, the model was calibrated principally during the observation-rich year of 2011, in which the model parameters such as bottom friction and turbulence mixing coefficients, were determined. Once the parameters were determined, they were fixed and additional model runs were conducted over different years: years 2010, 2012, and 2013 for verification. Although the observation data in 2010, 2012, and 2013 are not as complete and thorough as those of 2011, they nevertheless serve as an additional check to ensure the parameters are functioning reasonably universally when multi-year simulations were conducted under different conditions. The results for the verification are presented on pages B-1 through page B18 in Appendix B. Among 18 figures presented, Figures B-1 to B-4 show the additional water level analysis for 2010 and 2012; Figures B-5 to Figure B-10 show additional velocity comparisons for July, 2011 and July, 2012; Figures B-11 to B-15 show the comparisons of salinity and temperature over 2010 and 2012 on individual years; Figures B16-B17 show the comparisons of salinity and temperature continuously from January 2011 through December 2013. Lastly, the statistical comparison is presented in Figure B-18. The exercise essentially re-affirms the well-executed skill of performance for SCHISM setup in the Chesapeake Bay.

4. Results from scenario runs

4.1 Local analysis

The addition of new bridge pilings could potential alter the flow pattern near the project area. We start by looking at the impact on some 'integrated' quantities: tidal elevation (which is closely related to tidal prism) and total outflow. For this purpose we look at the tidal harmonic constituents at 2 stations inside the project area (cf. Figure 3), as shown in Table 7 and 8. It is obvious that the changes are marginal on tides and mean-sea levels (cf. Z_0, the roughness height), generally less than ~1mm for all alternatives: the changes are smallest with Alternative A, but the differences between alternatives are indeed small.

Comparisons of flow at the mouth of James River between alternatives are shown in Figure **14**; the differences between Base and the 4 alternatives are again small. To further examine the impact, both tidal and residual components of the flow are analyzed and shown in Tables 9-10. The addition of the new pilings mostly decreases both the amplitude and the mean of the flow by a small amount; e.g., the decrease in the residual flow is on the order of a few m^3/s, or less than 1% in all alternatives (see Table 10). Alternative B affects the flow slightly more than Alternative C, but the difference is subtle. The largest decrease in the residual flow is found in Alternative D. Therefore, the impact on bulk quantities is small, as the ratio between the total area of the new pilings and the total surface area is no more than 1% in all alternatives, despite the presence of a large number of pilings.

Figure 10: Comparison of the along-channel velocity at cb0102. (a) Time series comparison between observations (blue) and model predictions (red) at multiple depths; (b) scatter plots.

Figure 11: Comparison of the along-channel velocity at cb0301. Time series comparison between observations (blue) and model predictions (red) at multiple depths; (b) scatter plots.
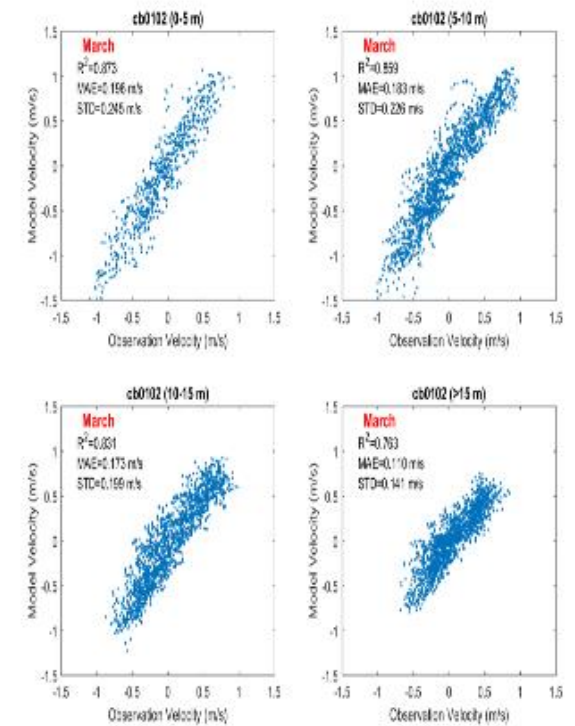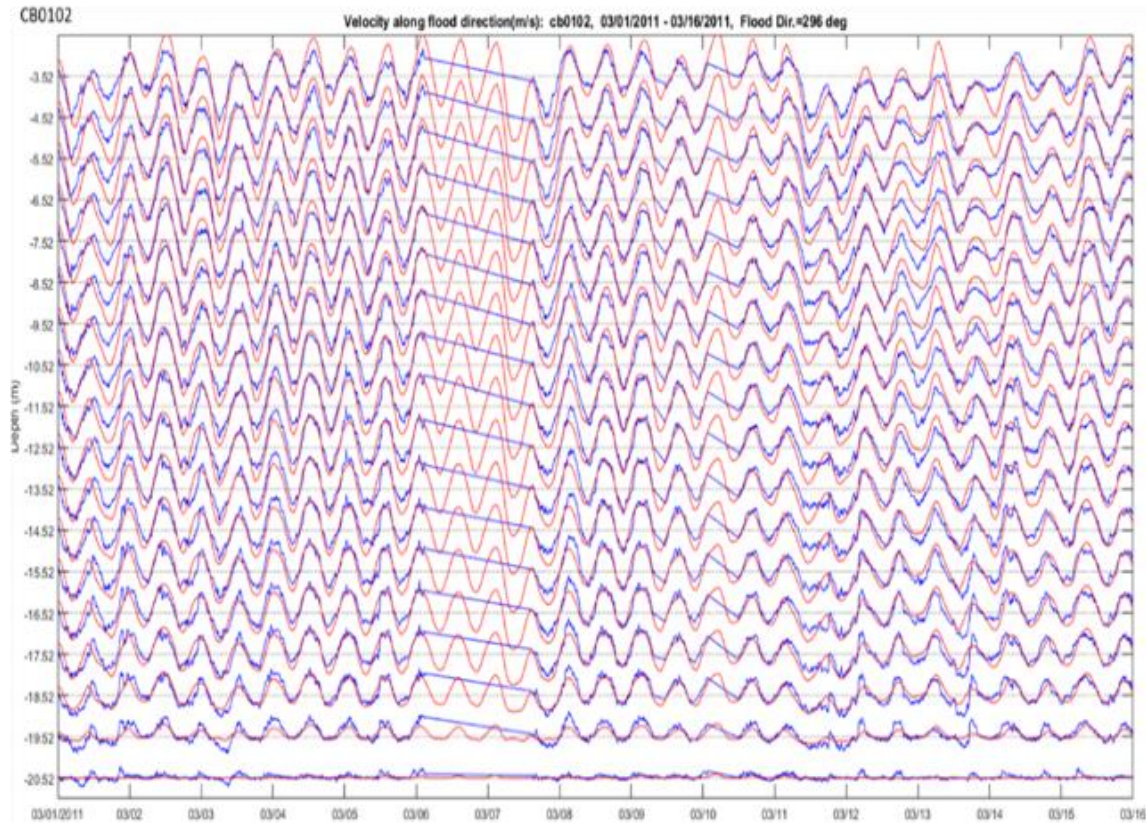
Figure 12: Comparison of the along-channel velocity at cb0402. Time series comparison between observations (blue) and model predictions (red) at multiple depths; (b) scatter plots.
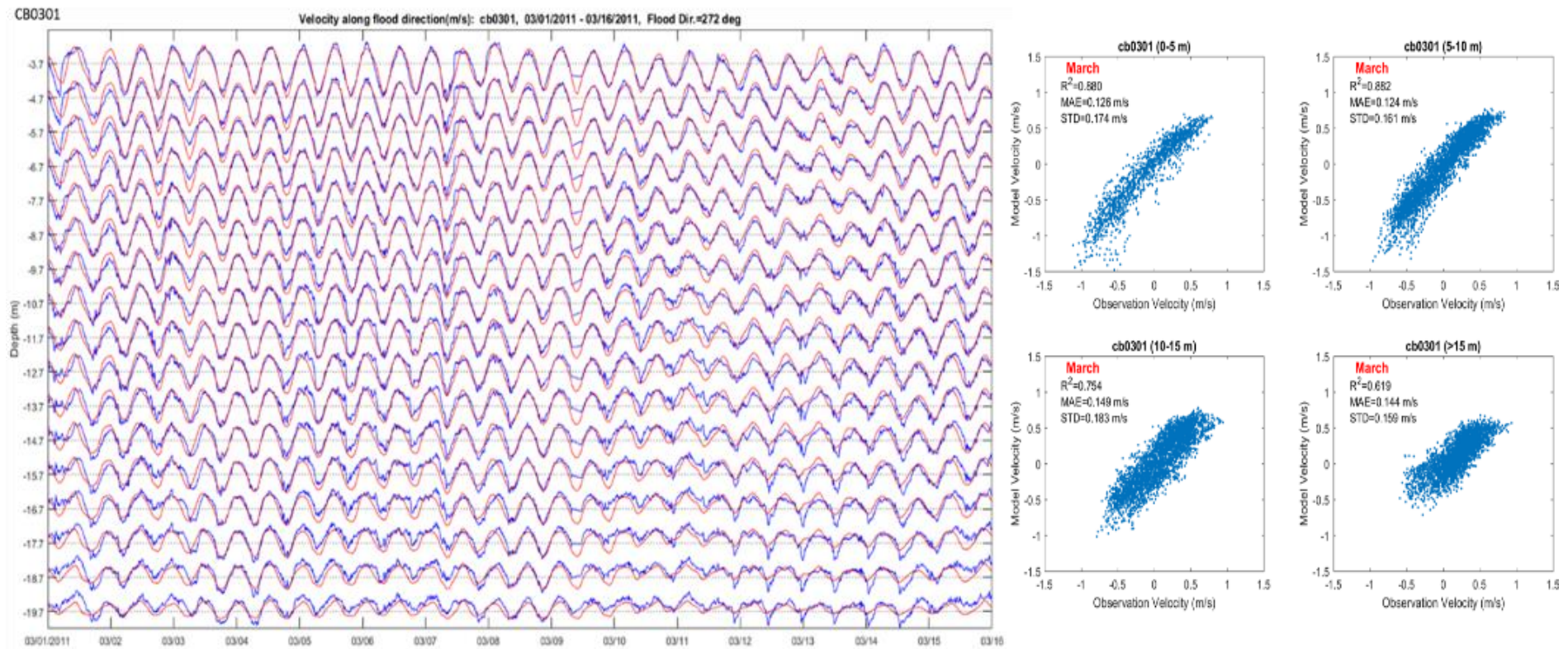
Figure 13: Comparison of the along-channel velocity at cb0601. Time series comparison between observations (blue) and model predictions (red) at multiple depths; (b) scatter plots.
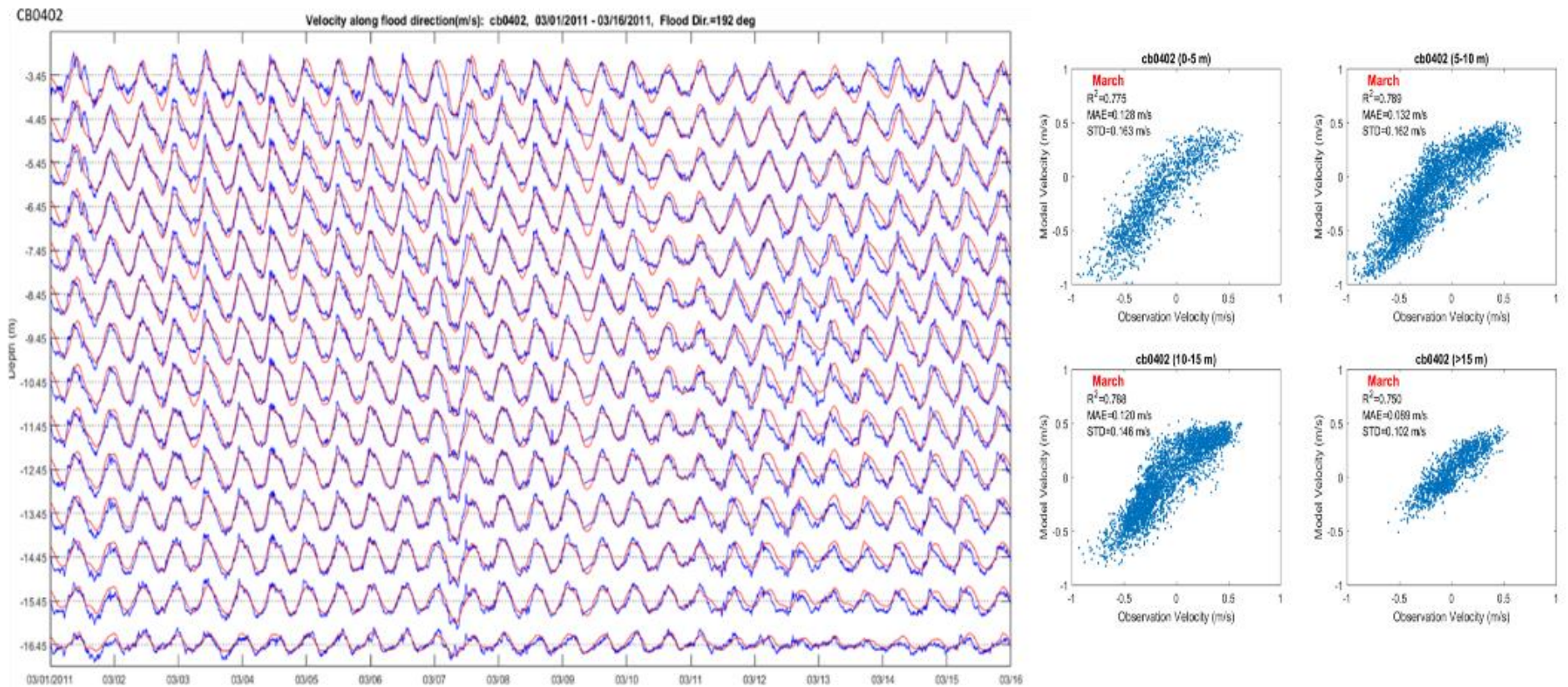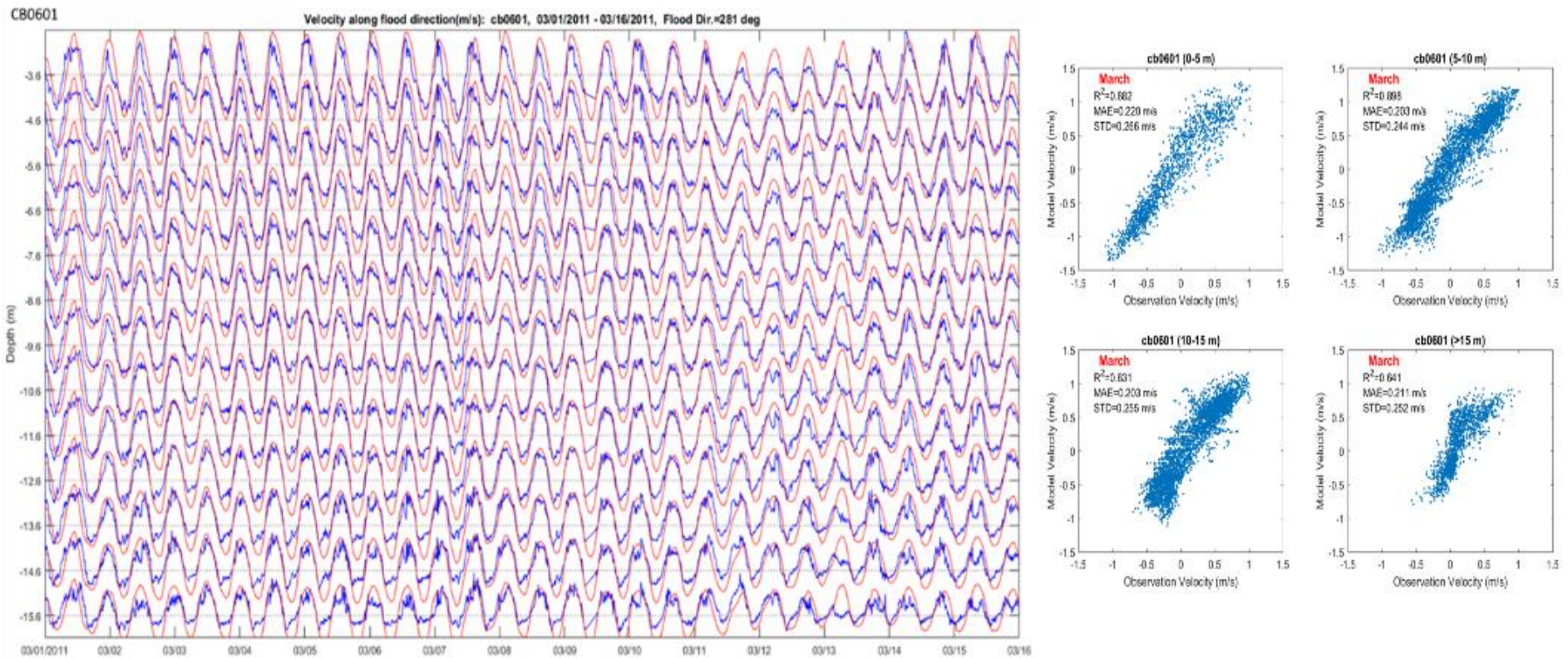
24

Table 7: Comparison of tidal elevation constituents at Station 1 (cf. Figure 3) between alternatives. Note that the phases of the Z_0 constituent are not meaningful.

Location 1	Tidal harmonic constituents								
Amplitude (m)	M_2	N_2	S_2	K_2	O_1	K_1	Q_1	P_1	Z_0
Base	0.3685	0.0820	0.0626	0.0166	0.0370	0.0418	0.0065	0.0100	0.0391
A	0.3687	0.0822	0.0627	0.0166	0.0371	0.0419	0.0065	0.0101	0.0388
B	0.3667	0.0816	0.0623	0.0165	0.0369	0.0416	0.0065	0.0100	0.0391
C	0.3668	0.0816	0.0622	0.0165	0.0371	0.0418	0.0065	0.0100	0.0394
D	0.3652	0.0812	0.0619	0.0165	0.0369	0.0415	0.0065	0.0099	0.0394
Phase(degrees)	M_2	N_2	S_2	K_2	O_1	K_1	Q_1	P_1	
Base	114.84	23.06	106.30	244.15	296.84	220.17	220.43	238.72	
A	115.03	23.31	106.57	244.47	297.05	220.37	220.73	238.99	
B	114.89	23.11	106.33	244.19	296.92	220.27	220.38	238.85	
C	114.81	23.07	106.32	244.21	297.06	220.38	220.82	238.96	
D	114.85	23.11	106.37	244.25	297.13	220.46	220.79	239.00	

Table 8: Comparison of tidal elevation constituents at Station 2 (cf. Figure 3) between alternatives.

| Location 2	Tidal harmonic constituents								
Amplitude (m)	M_2	N_2	S_2	K_2	O_1	K_1	Q_1	P_1	Z_0
Base	0.3474	0.0789	0.0606	0.0158	0.0354	0.0394	0.0063	0.0099	0.0373
A	0.3484	0.0793	0.0608	0.0158	0.0356	0.0397	0.0063	0.0100	0.0371
B	0.3468	0.0788	0.0604	0.0157	0.0355	0.0393	0.0063	0.0099	0.0374
C	0.3478	0.0790	0.0606	0.0158	0.0355	0.0394	0.0063	0.0099	0.0374
D	0.3470	0.0787	0.0604	0.0157	0.0355	0.0393	0.0063	0.0099	0.0376
Phase (degrees)	M_2	N_2	S_2	K_2	O_1	K_1	Q_1	P_1	
Base	106.58	15.43	98.16	235.29	294.58	218.15	217.00	235.97	
A	106.72	15.60	98.35	235.57	294.72	218.30	217.17	236.19	
B	106.58	15.39	98.09	235.26	294.59	218.18	216.80	235.98	
C	106.60	15.44	98.12	235.29	294.63	218.18	217.08	236.00	
D	106.59	15.40	98.08	235.30	294.62	218.20	216.89	235.99	

Table 9: Comparison of harmonics of flow at the mouth of James River between alternatives.

Cross-sectional flux								
Amplitude (m³/s)	M_2	N_2	S_2	K_2	O_1	K_1	Q_1	P_1
Base	28950.9	6063.8	4584.1	1263.3	1884.8	2855.8	277.3	621.4
A	28952.7	6069.3	4585.6	1264.2	1886.2	2861.8	279.1	614.8
B	28835.3	6040.5	4567.7	1258.8	1881.8	2853.1	276.9	612.5
C	28938.4	6060.5	4587.6	1263.9	1885.6	2856.3	278.4	612.1
D	28841.1	6040.2	4572.4	1260.1	1878.5	2848.3	277.3	610.8
Phase (degrees)	M_2	N_2	S_2	K_2	O_1	K_1	Q_1	P_1
Base	76.53	1.64	26.24	165.71	58.94	308.03	0.01	329.45
A	76.70	1.85	26.51	165.96	59.10	308.20	0.03	329.72
B	76.68	1.77	26.33	165.84	59.02	308.13	0.12	329.55
C	76.57	1.63	26.23	165.73	59.01	308.07	0.11	329.59
D	76.62	1.69	26.28	165.81	59.08	308.13	0.27	329.61

Table 10: Comparison of seasonal residual flow at the mouth of James River between alternatives.

Amplitudes of seasonal residual cross-sectional flux (m³/s)				
Alternatives	**Jan-Mar**	**Apr-Jun**	**July-Sept**	**Oct-Dec**
Base	190.71	172.86	70.16	236.21
A	189.45	172.04	69.91	234.66
B	188.80	171.99	69.57	236.28
C	190.44	172.12	69.61	235.98
D	188.57	171.75	69.28	235.62

The yearly averaged bottom and surface salinities for 'Base' suggest a typical estuarine circulation pattern (see Figure 15). The bottom salinity shows a much sharper gradient between the channel and the shoal than the surface salinity, as the channel serves as the main conduit for ocean water to intrude into the river. The surface salinity over the channel is slightly lower than that over the shoal, enhancing the 2-layer gravitational circulation in the channel. The average bottom-surface salinity difference is 2-5 PSU over the channel (see Figure 15). Figures 16-19 show the differences in the averaged salinity between the 4 alternatives and the Base. All alternatives are found to increase the surface and bottom salinity, albeit at a different rate. In particular, the increases in Alternative A are the smallest (<0.5 PSU) and mostly

(a) Total Cross-Sectional Flux

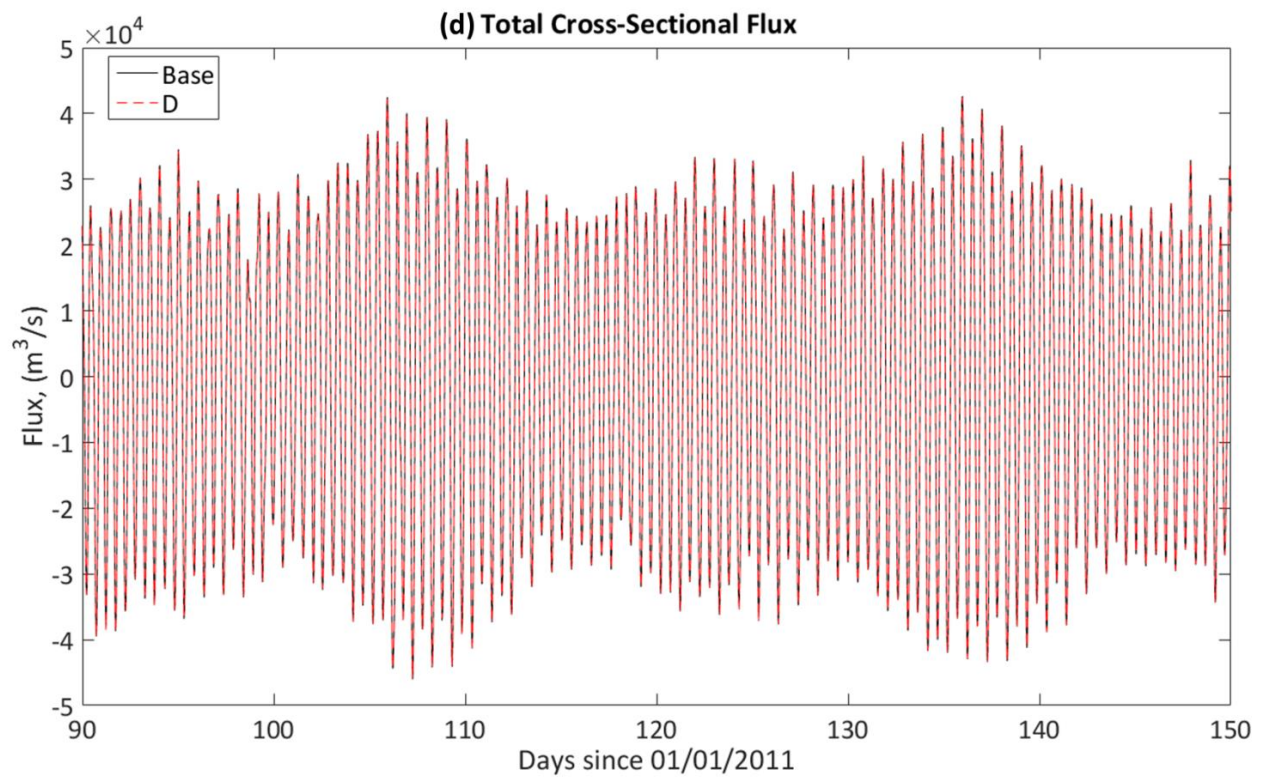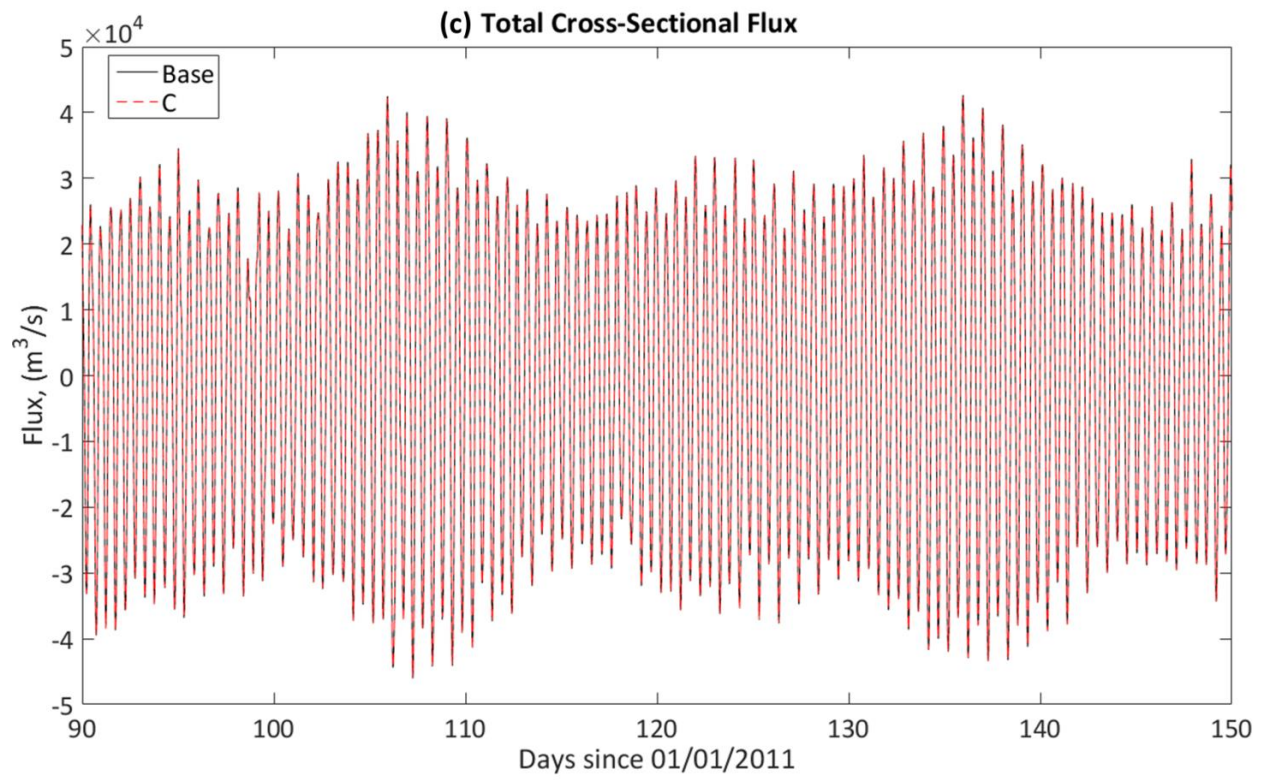**(b) Total Cross-Sectional Flux**
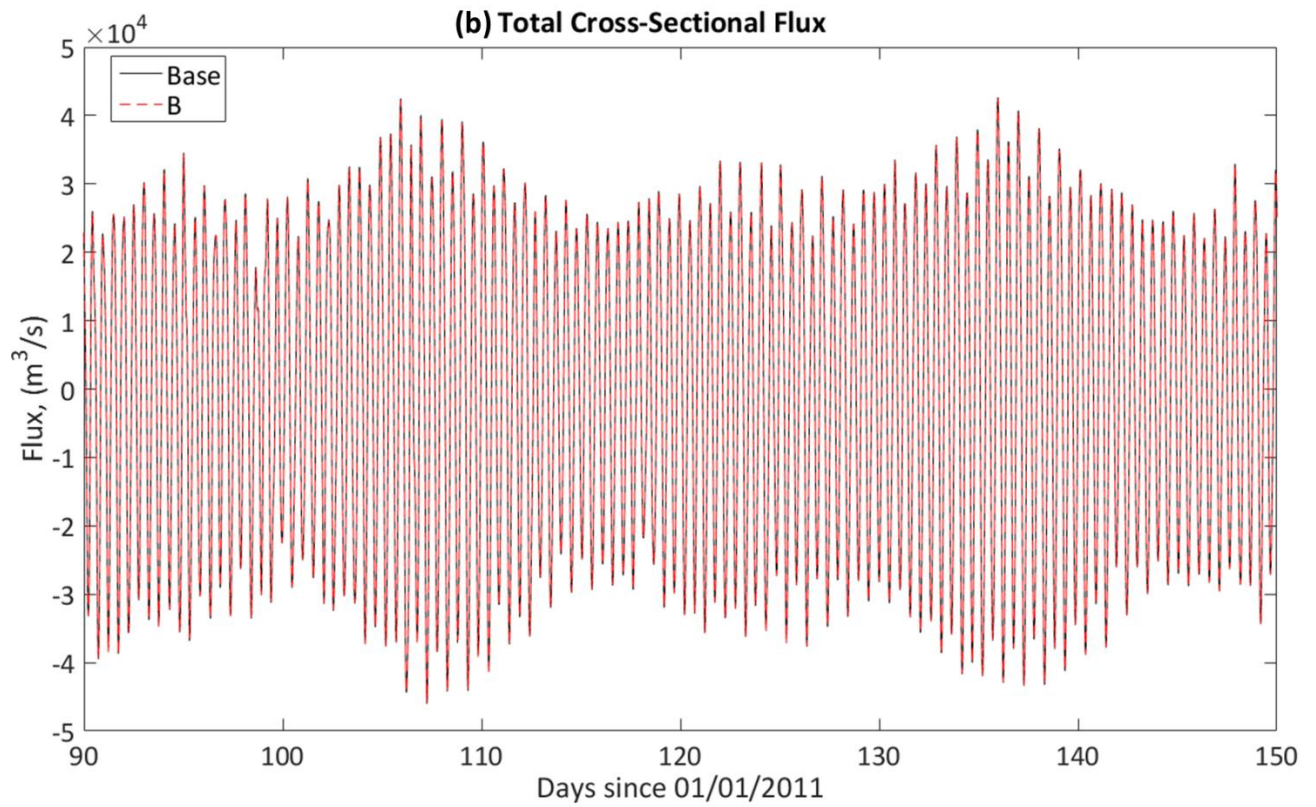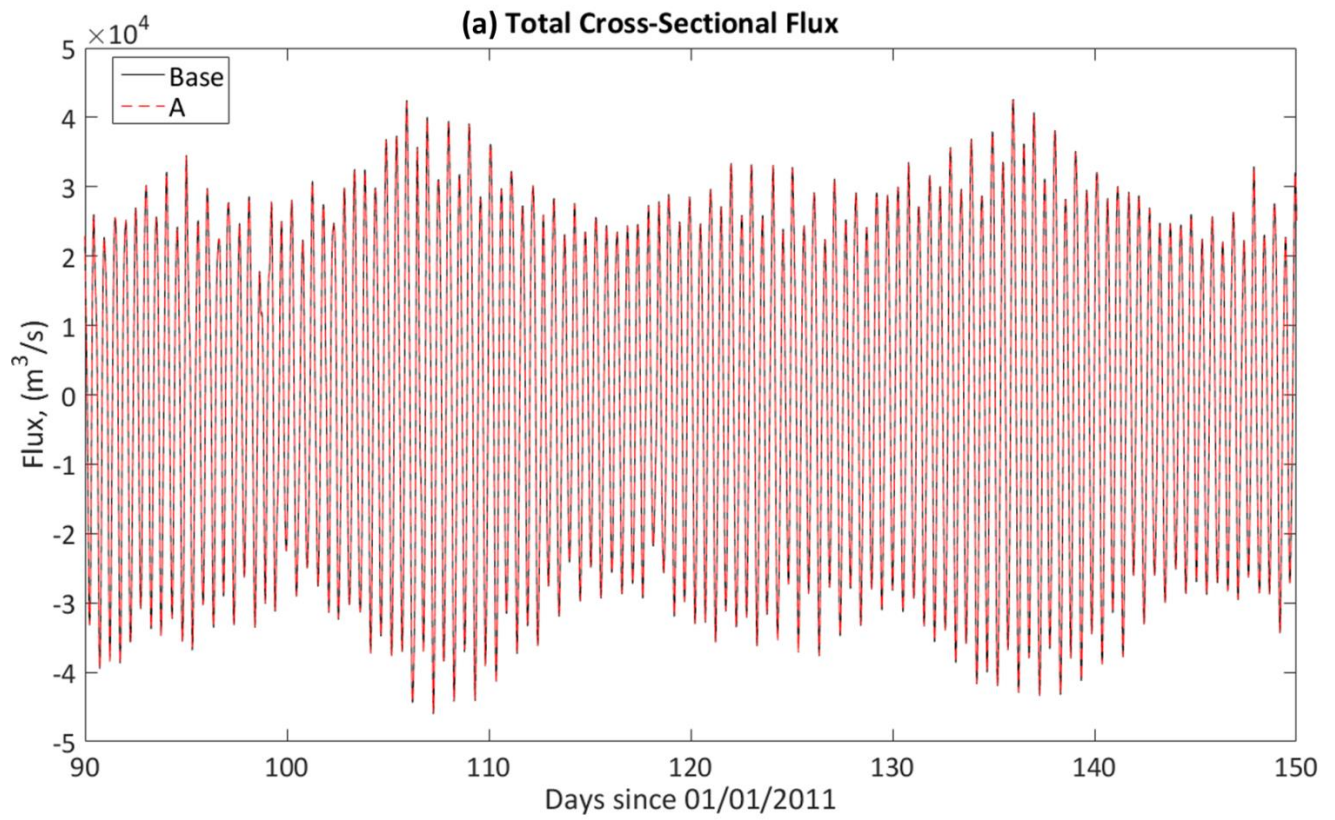
Figure 14: Comparison of time series of flow at the mouth of James River between Base and 4 alternatives. The positive values indicate flow into the river.

confined near the added lanes of I64. More flow blocking in front of the semi-enclosed Willoughby Bay to the south and Mill Creek to the north leads to increased salinity there, and also the increased flow propagates more into the main Bay at the surface than at the bottom, due to larger flow velocity at the surface (See Figure 16). The addition of the I-564 Connector and the VA 164 Connector near the entrance of Elizabeth River in Alternative B has larger effects on the salinity, with up to 1 PSU increase there and into Elizabeth River (**Figure 17**). On the other hand, a similar addition of the I-564 Connector and the VA 164 Connector, and expansion in I664 (including from I-64 to the proposed I-664 Connector, from the proposed I-664 Connector to VA 164, and from VA 164 to I-264) in Alternative C result in even larger increases (up to 1.5 PSU) north and west of Craney Island (**Figure 18** vs. **Figure 17**), suggesting stronger blocking of flow in that area by the new pilings. The increases in Alternative D are similar to those resulting from the sum of Alternatives B&C, particular at the surface; the increases of the bottom salinity in the semi-enclosed Willoughby Bay and Mill Creek are slightly larger than those in Alternative B (**Figure 19** vs. **Figure 17**), suggesting that the added flow blocking due to the new I664 and I564 pilings has helped increase the retention of the intruded salt water. In all alternatives, the increase in the surface salinity is larger than that in the bottom salinity. This results in less vertical stratification, which is consistent with the fact that the added new bridge pilings enhance local turbulence mixing. In general, the largest increase in salinity is related to Alternative D. The salinity change is less than 0.1 PSU ~4km outside the James River entrance, suggesting minimal impact on the main Bay.

The spatial pattern of the residual flows in the lower James River for base and alternatives were shown in Figure 20 (a) – (e). By inter-comparisons of (a) – (e) of the Figure 20, the large cyclonic, eddy structure occupied the entire Hampton Road tidal flat from I-664 to I-64 remains largely unchanged, with only subtle changes in its mean position. Local changes near the new pilings, however, still can be seen (e.g., northeast of Craney Island in **Figure 20**b vs. **Figure 20**c). The addition of connectors to I664 in Alternatives C&D only slightly perturbed the mean flow near the connectors as compared to Alternative B (Figure 20). On the other hand, close examination of the surface vorticity field reveals increase in vorticity in the project area. The expansion of I64 in Alternative A increases the vorticity not only near I64 but also ~6km upstream, in the Elizabeth River and in the Willoughby Bay (**Figure 21**a vs. **Figure 21**b); the latter is due to horizontal transport of turbulence. The additional pilings in the I564 and I664 Connectors in Alternative B generally increase the vorticity in the project area (**Figure 21**b vs. **Figure 21**c). On the other hand, the expansion of I664 and I564 in Alternative C creates new vorticity both upstream and downstream (**Figure 21**a vs. **Figure 21**d). The change in the vorticity pattern in Alternative D can be roughly thought of as the sum of Alternatives B&C (**Figure 21**e). The increase serves as an effective horizontal mixing mechanism that explains the increase in bottom salinity in some areas (e.g. northern shallow shoal in **Figure 19**b).

One other potential impact of the tunnel island and the bridge piling is on the residence time of the flow in the projected area. To quantify the influence of pilings on the residence time, we calculate the water age in the James River using the method developed by Shen and Haas (2004). Initially the tracer age concentration is 0 everywhere and non-zero concentration is injected at the upstream boundary of James River. The age calculation reaches a quasi-steady state after about 120 days, and Figure 22 shows the age distribution near the project area. Since the water age is 0 at the river boundary, the age shown in Figure 22 can also be construed as the residence time, which is 90-100 days in this area, with slightly larger values for the semi-enclosed areas.
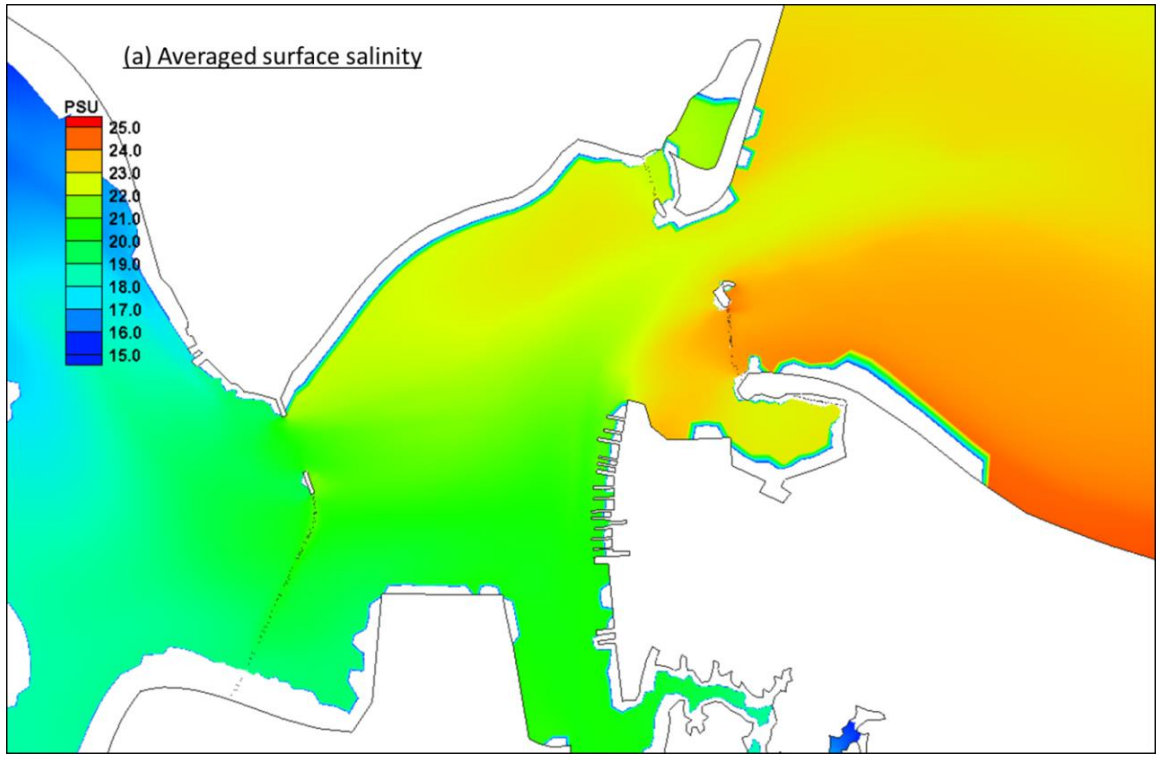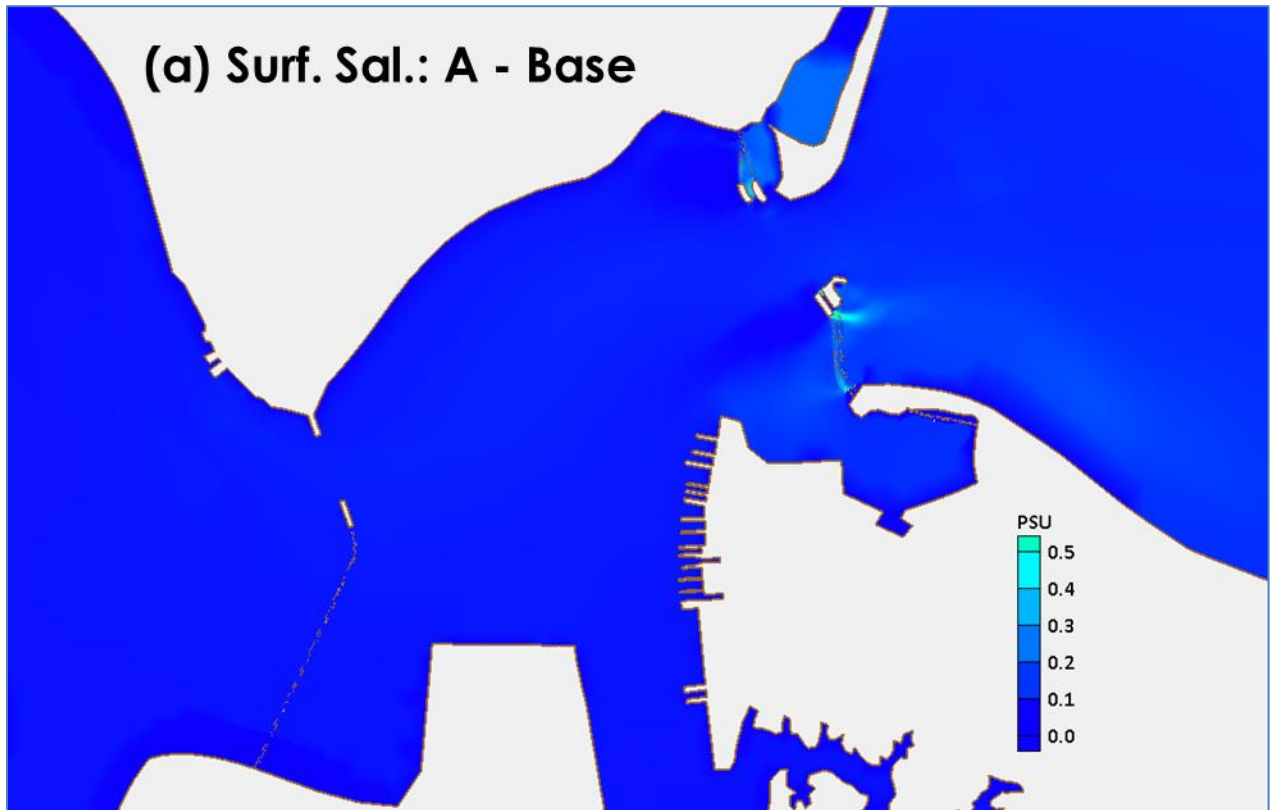
(a)
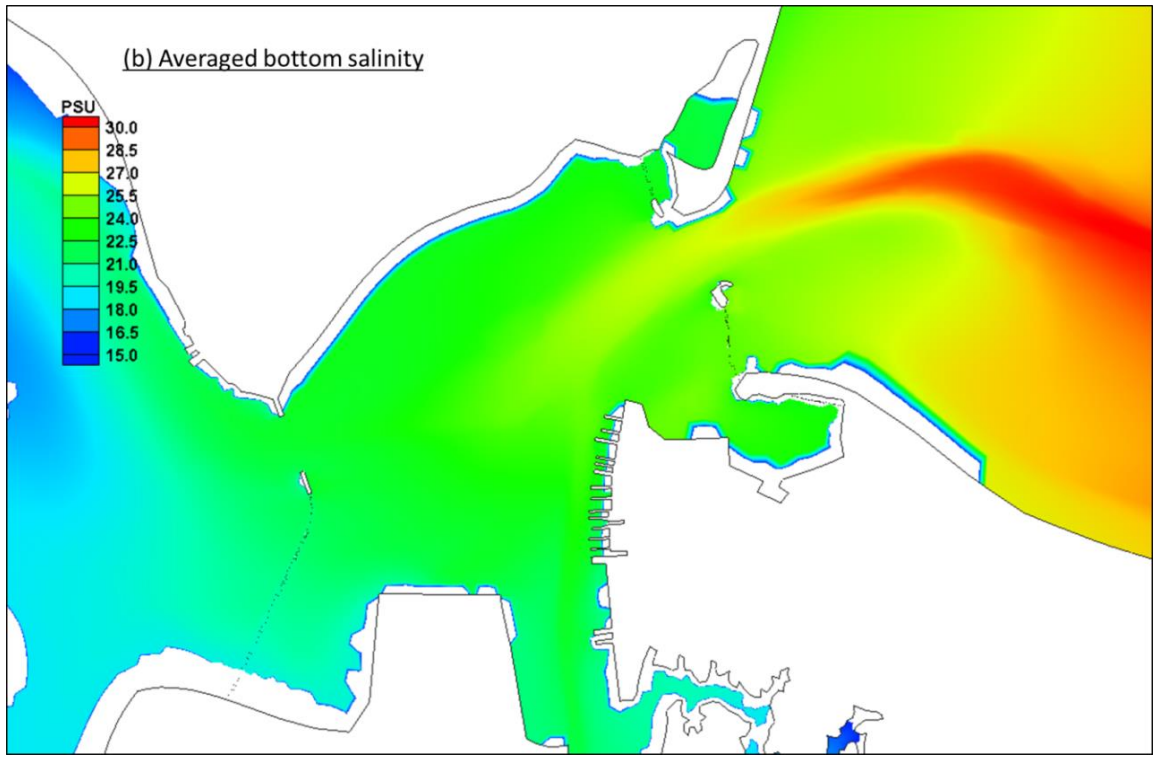
(b)

Figure 15: Averaged (a) surface and (b) bottom salinity near the project site for year 2011 from Base. Note that the color schemes are different.
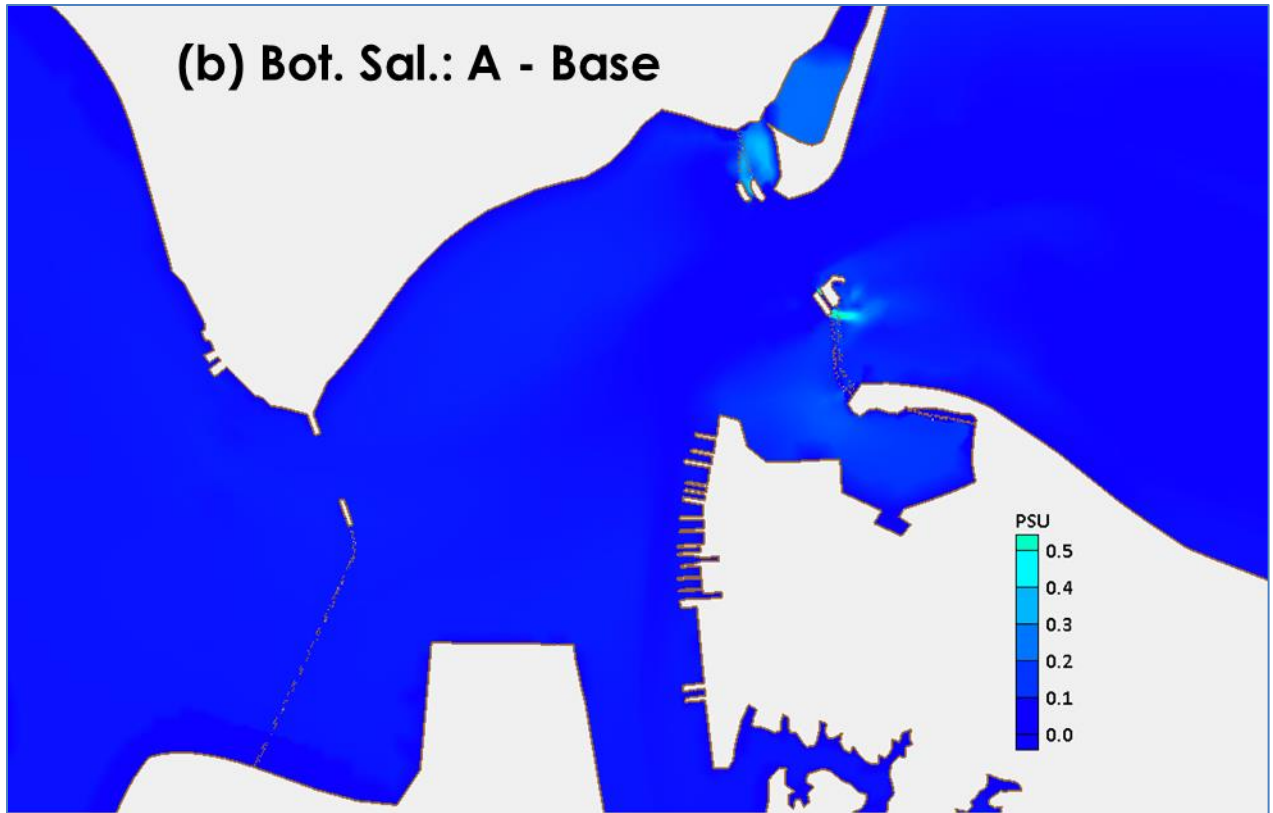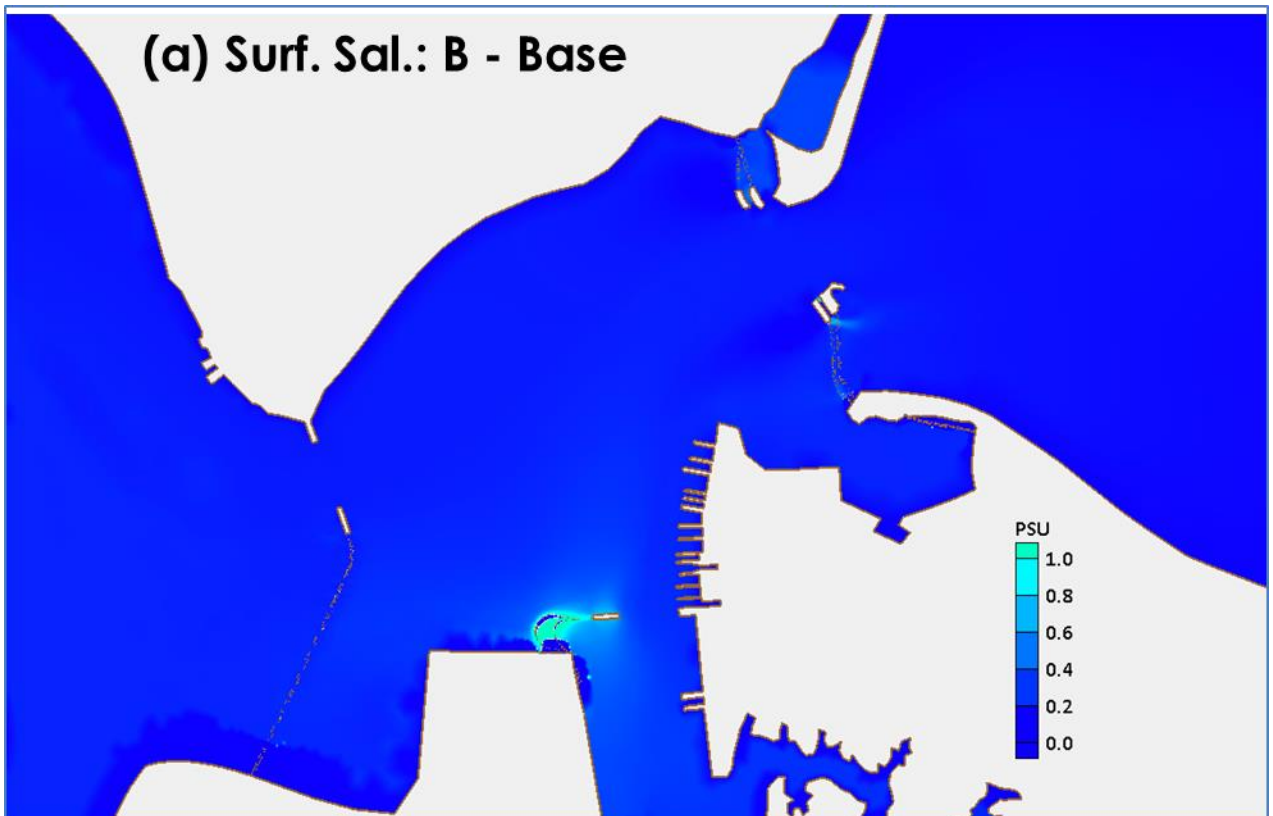
Figure 16: Averaged salinity difference between Alternative A and Base, at (a) surface and (b) bottom.
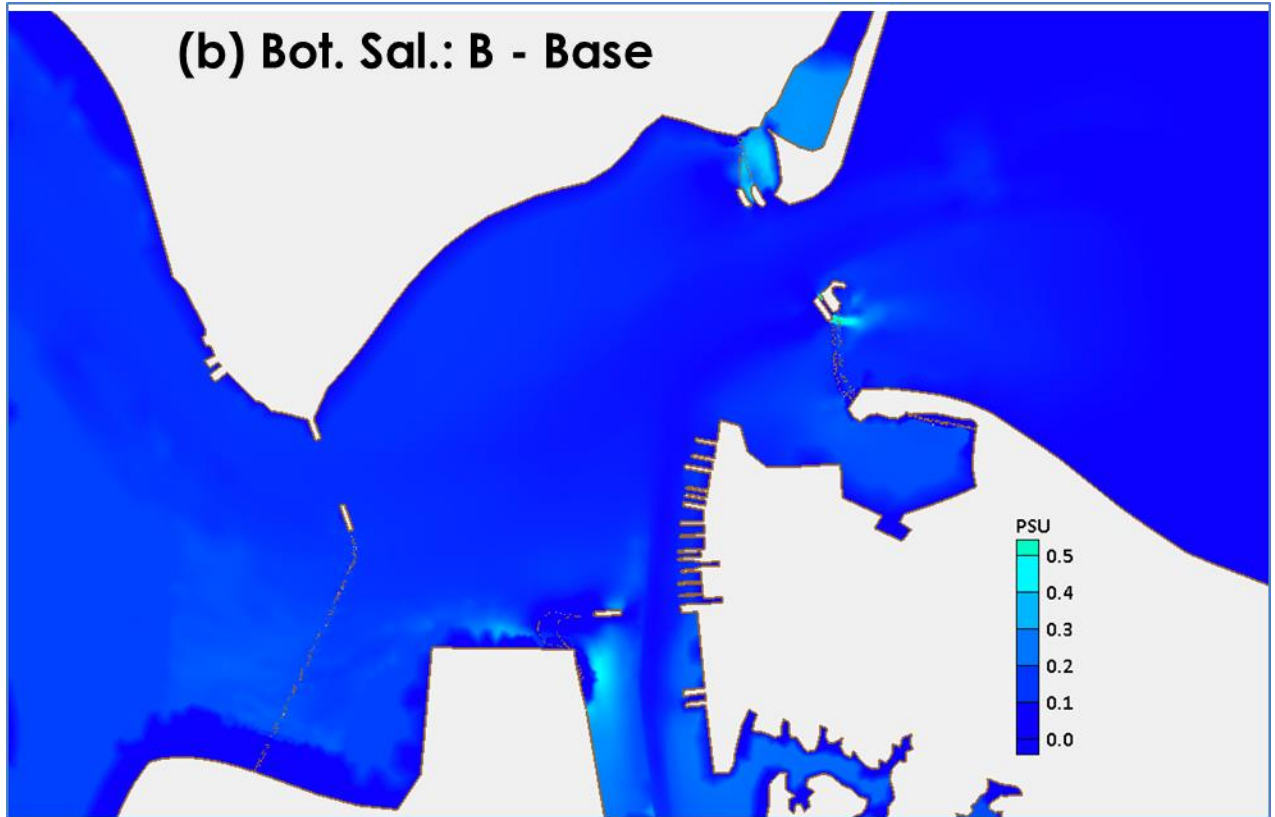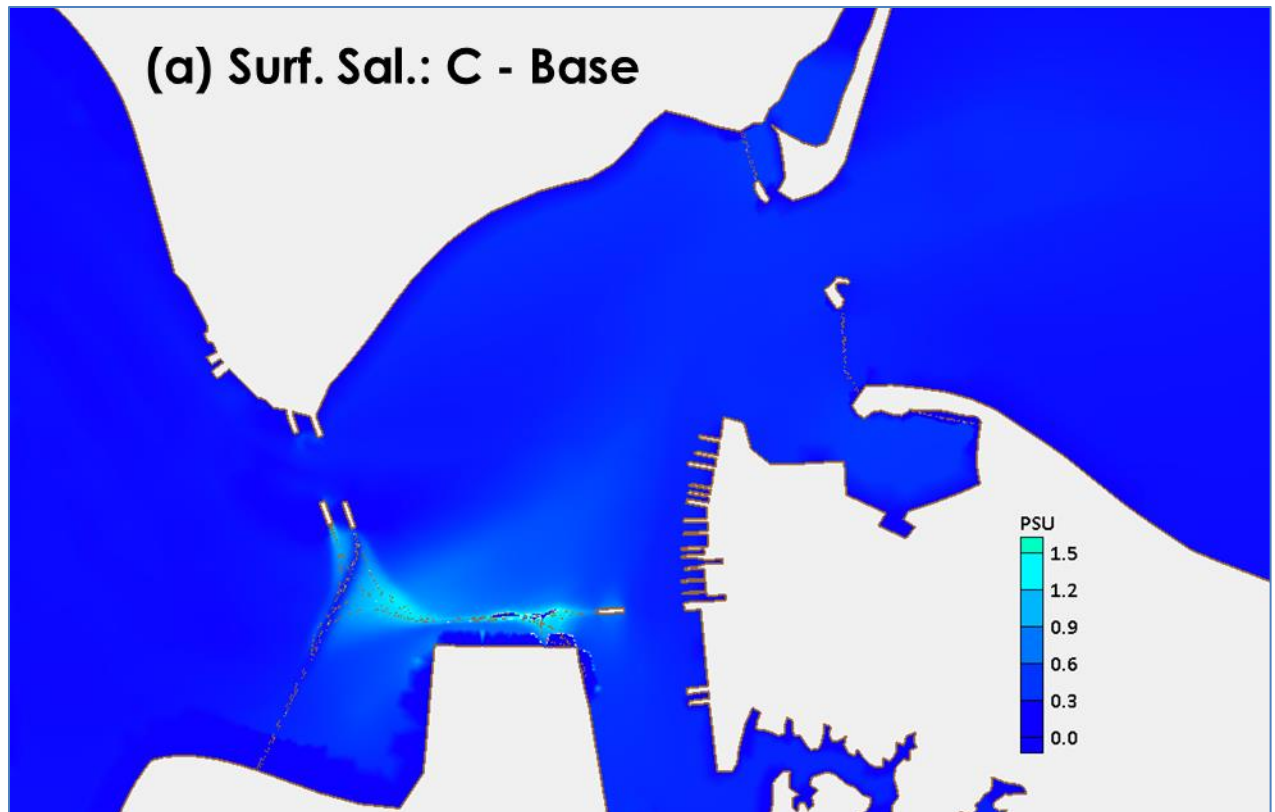
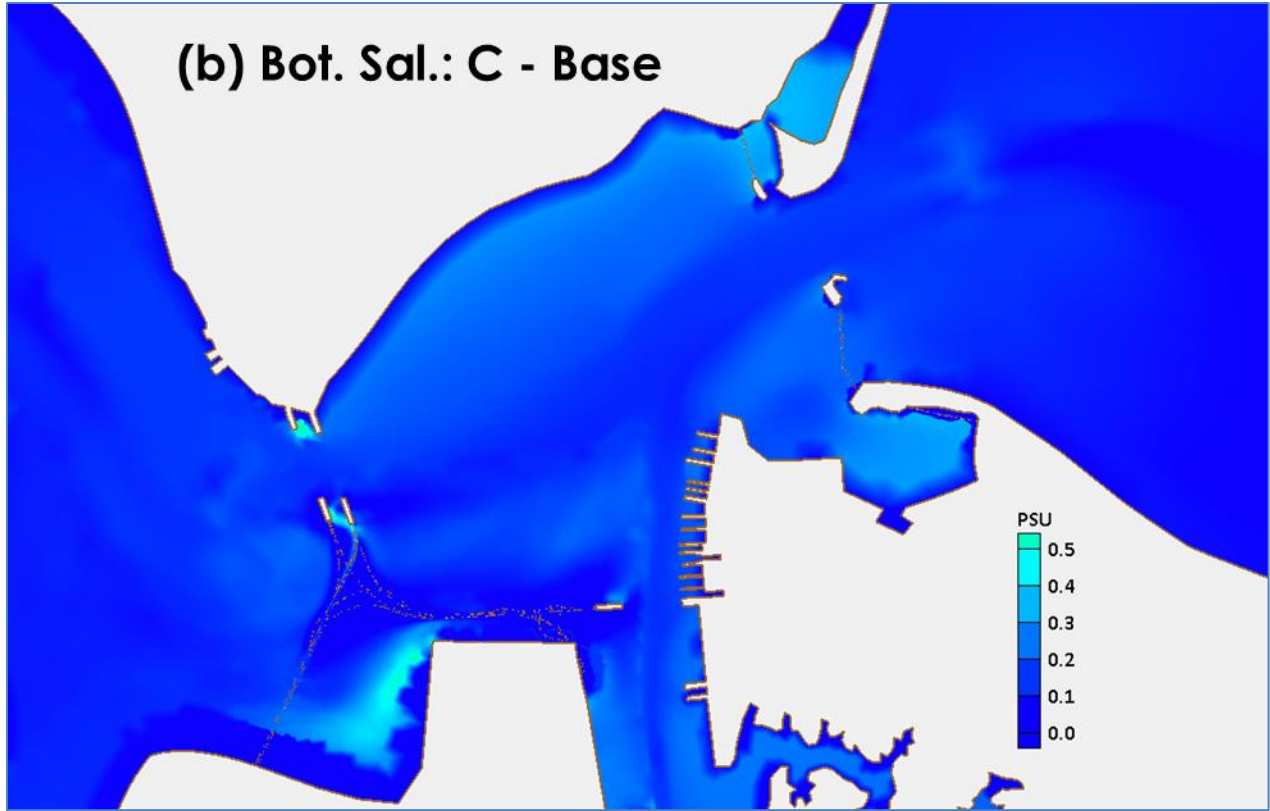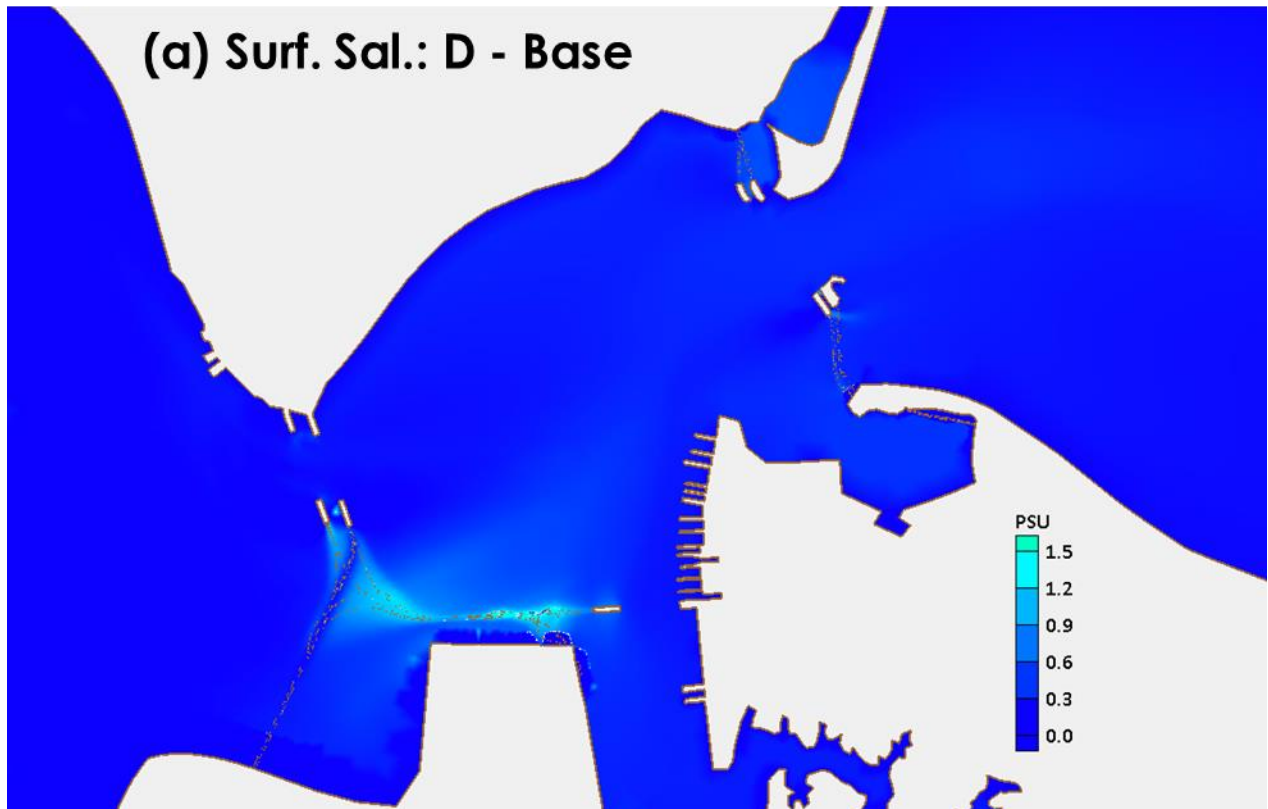Figure 17: Averaged salinity difference between Alternative B and Base, at (a) surface and (b) bottom.

Figure 18: Averaged salinity difference between Alternative C and Base, at (a) surface and (b) bottom.
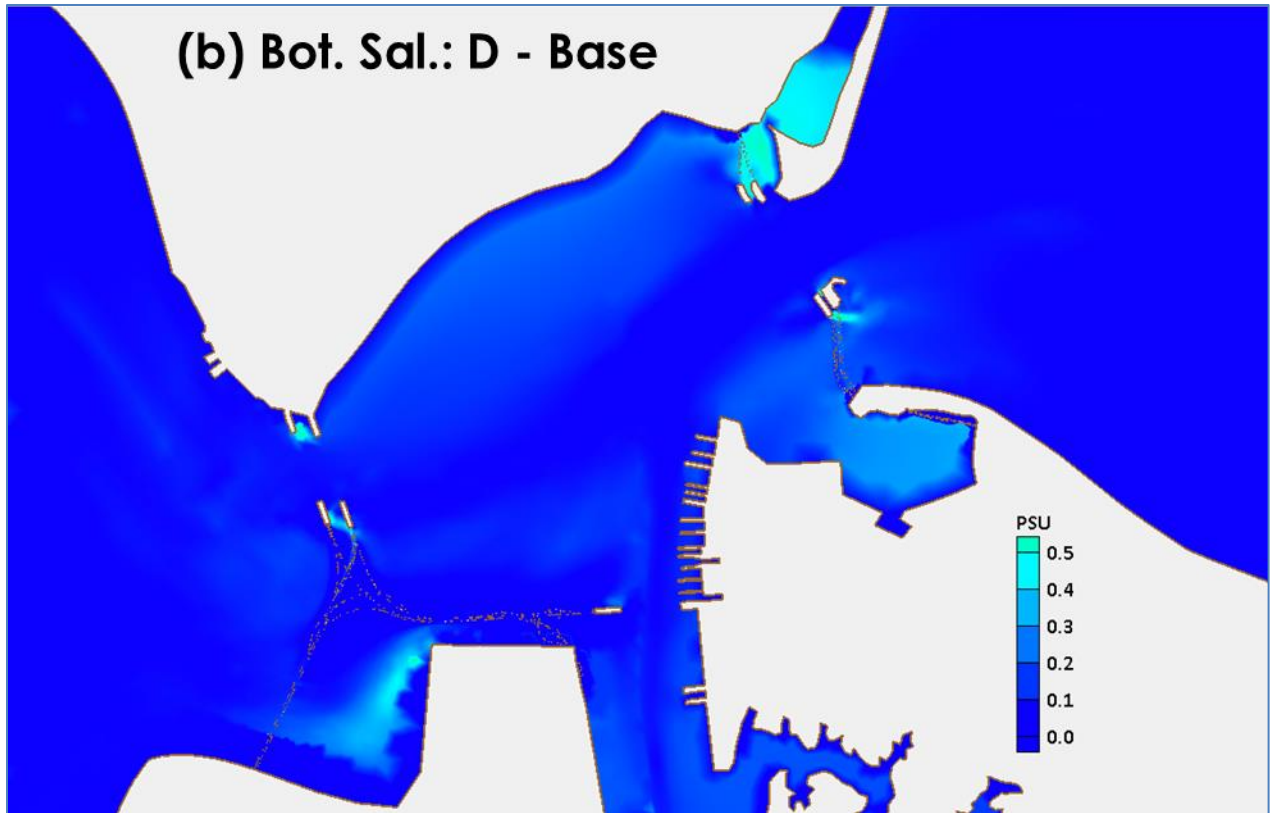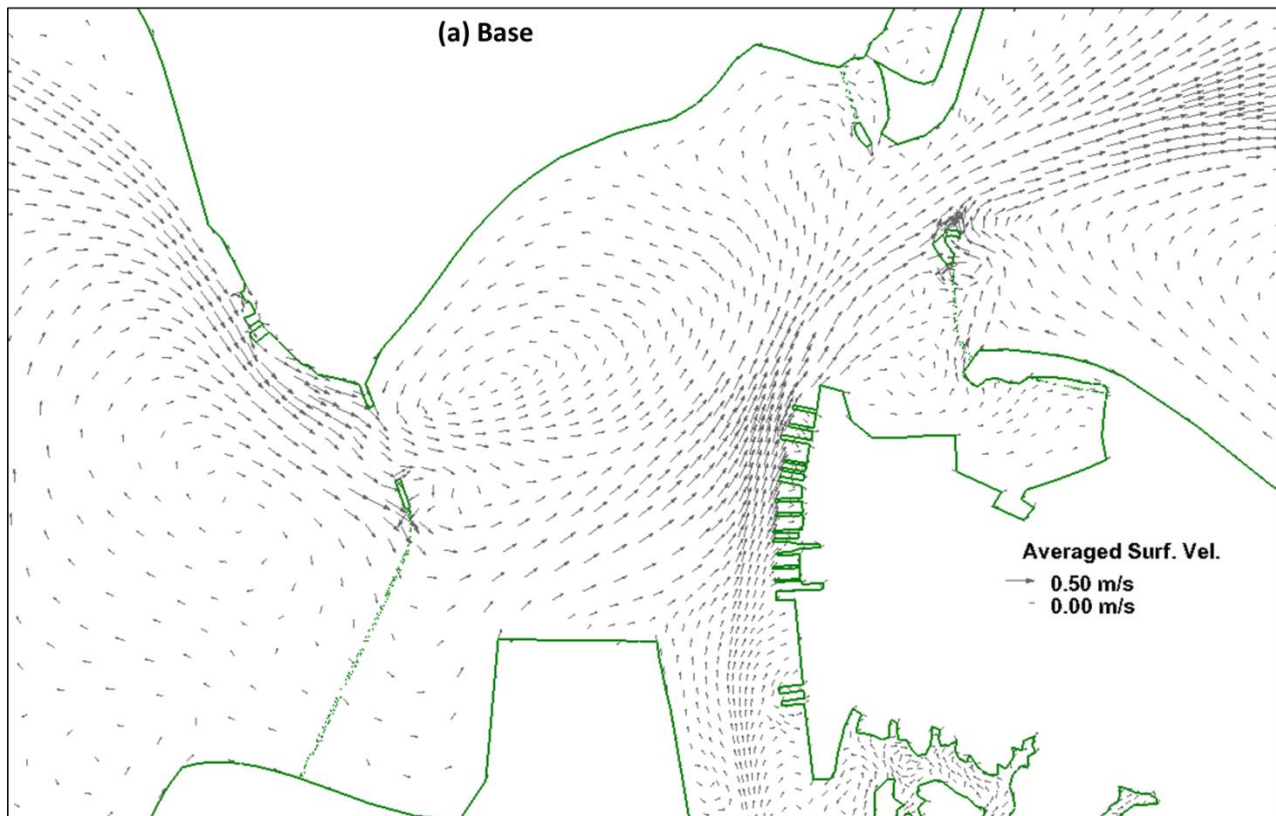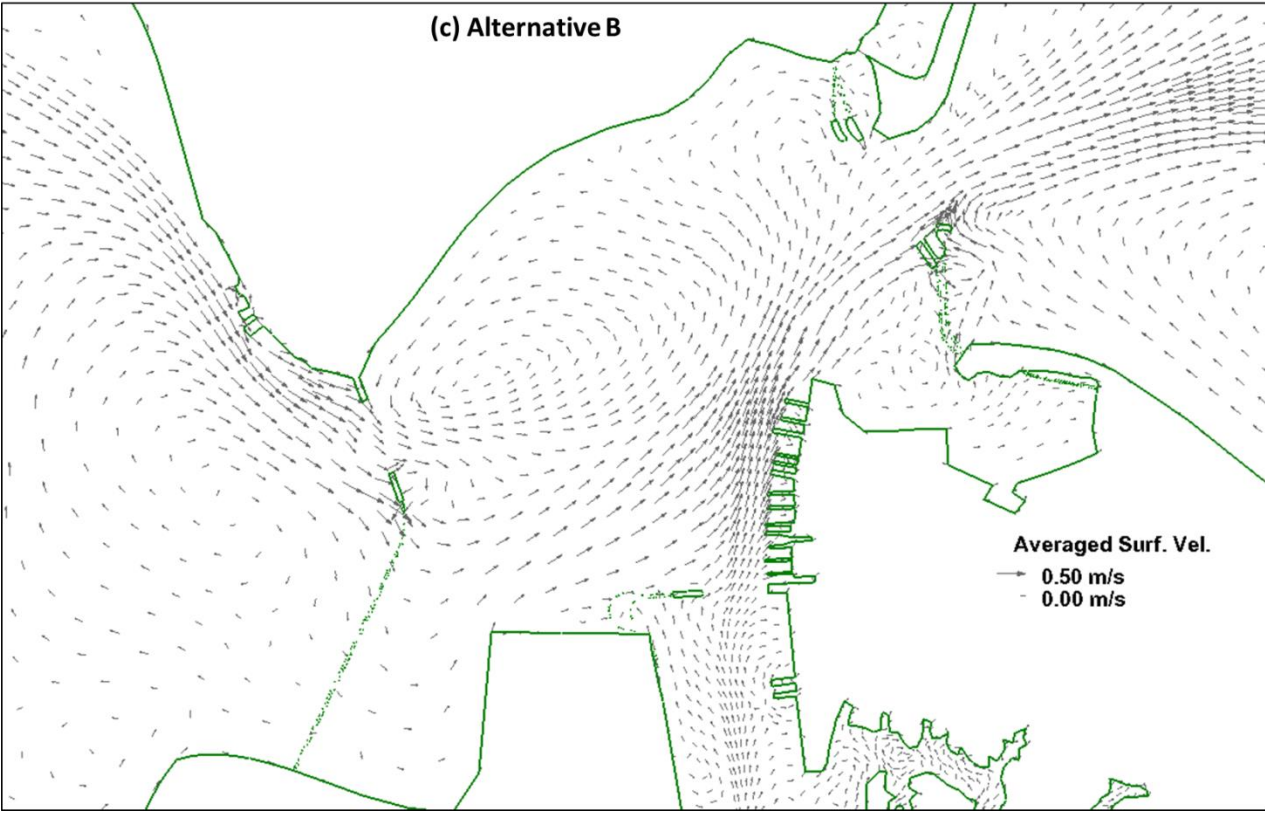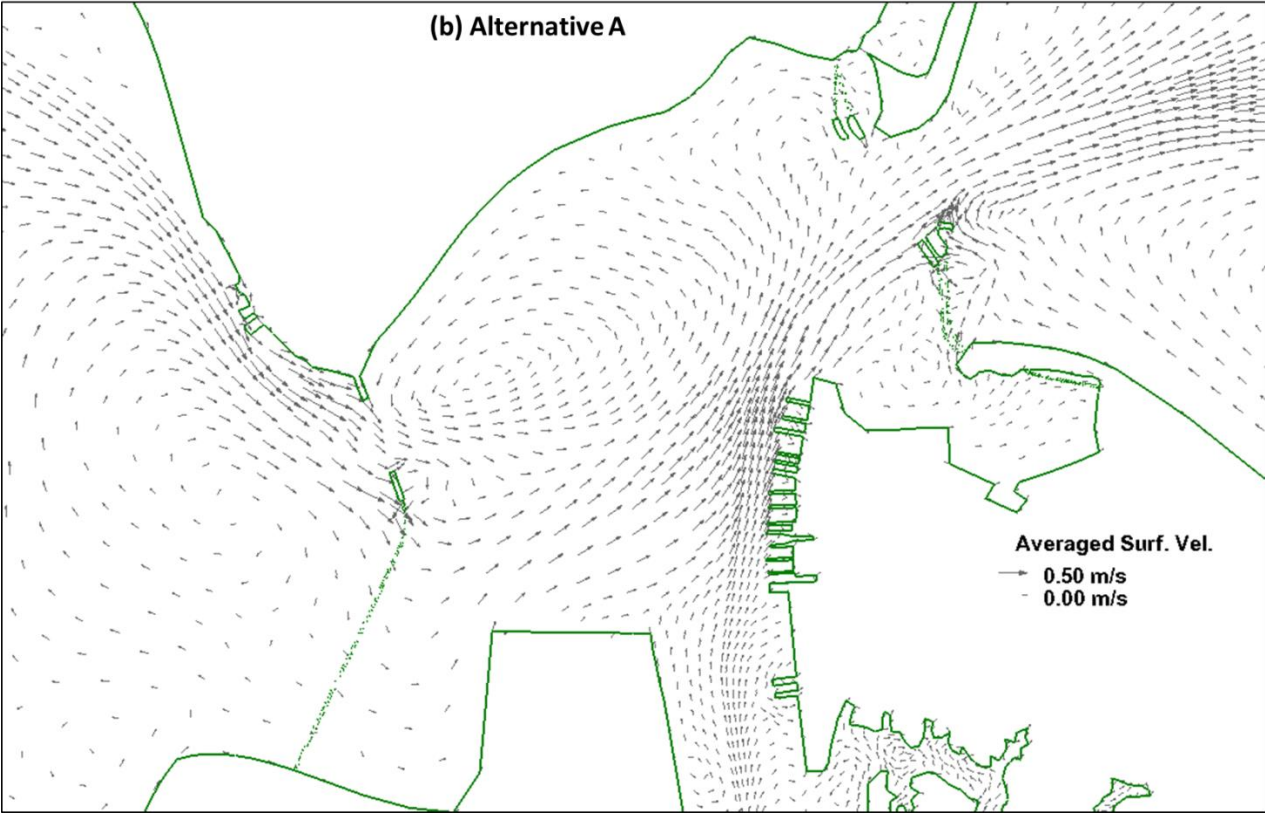
Figure 19: Averaged salinity difference between Alternative D and Base, at (a) surface and (b) bottom.

(b) Alternative A

Averaged Surf. Vel.

→ 0.50 m/s
- 0.00 m/s

(c) Alternative B

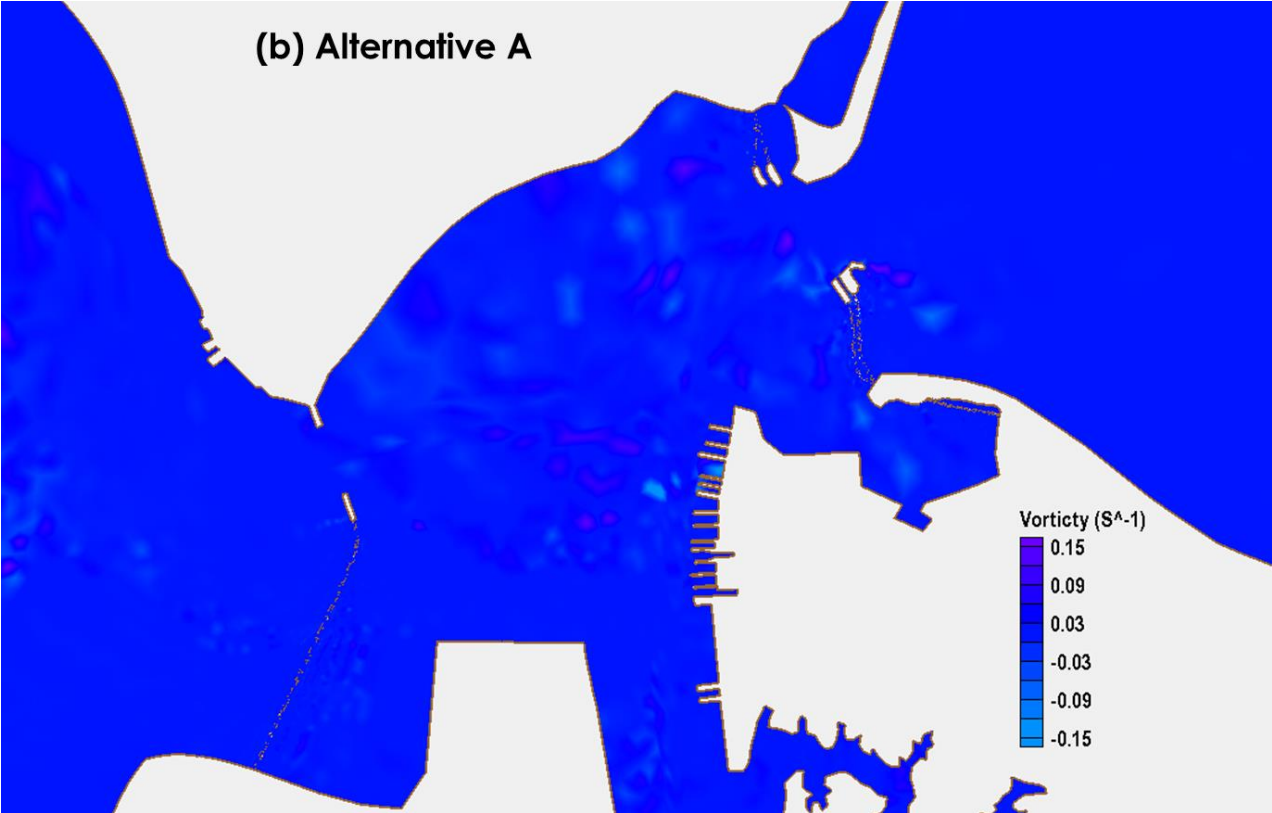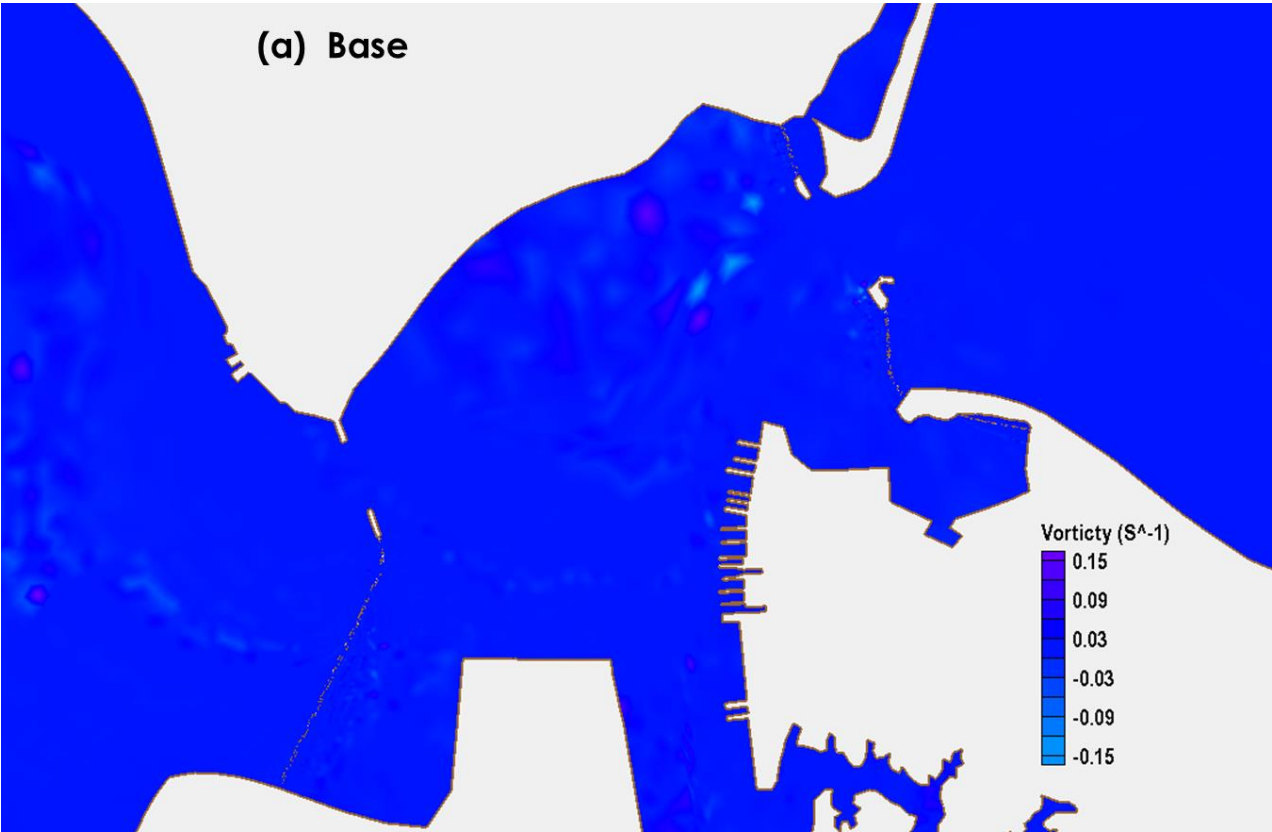Averaged Surf. Vel.
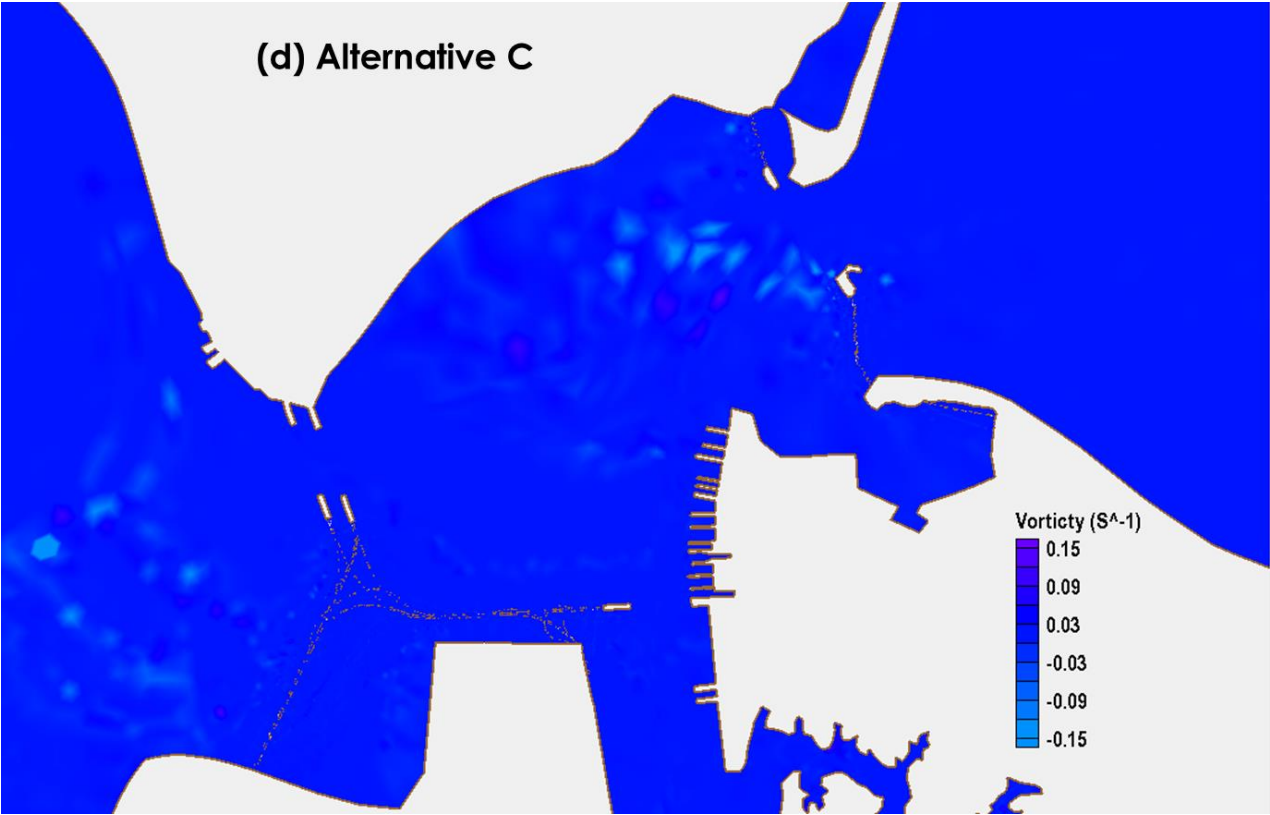
→ 0.50 m/s
- 0.00 m/s

36
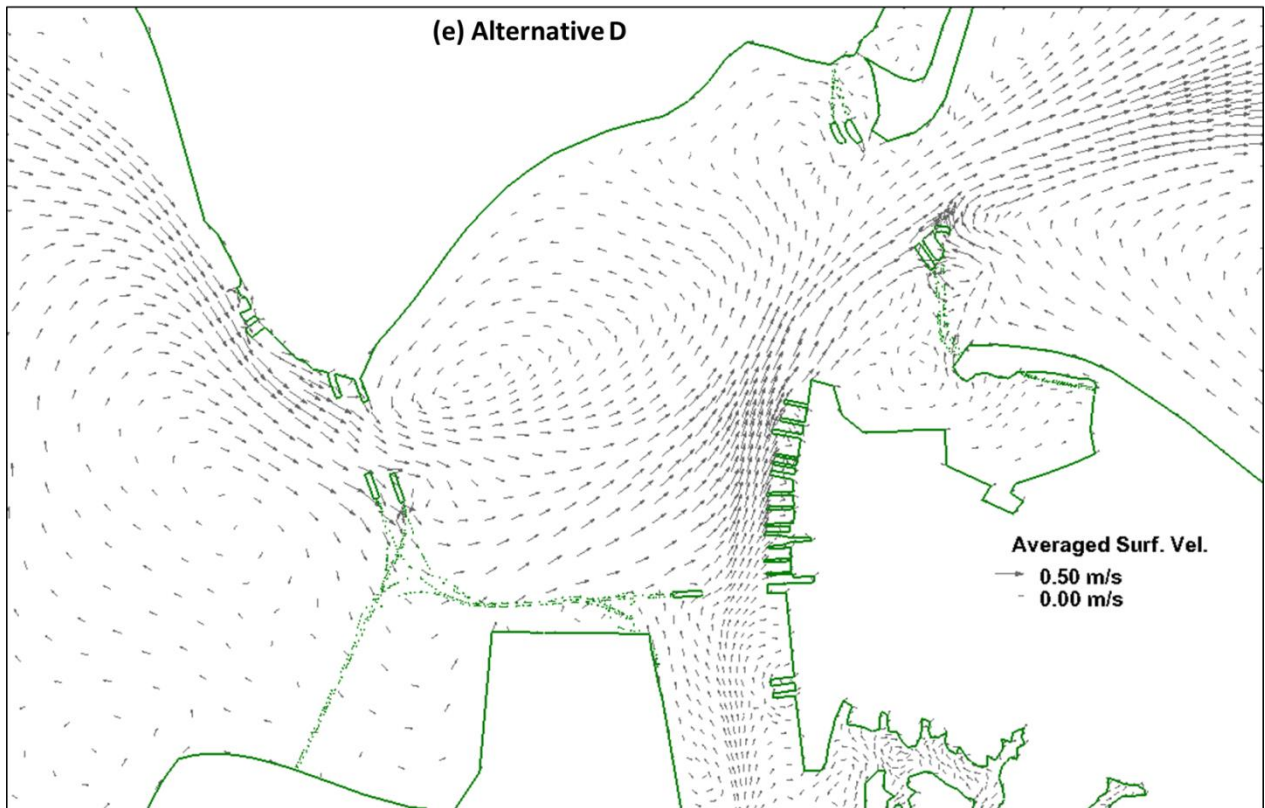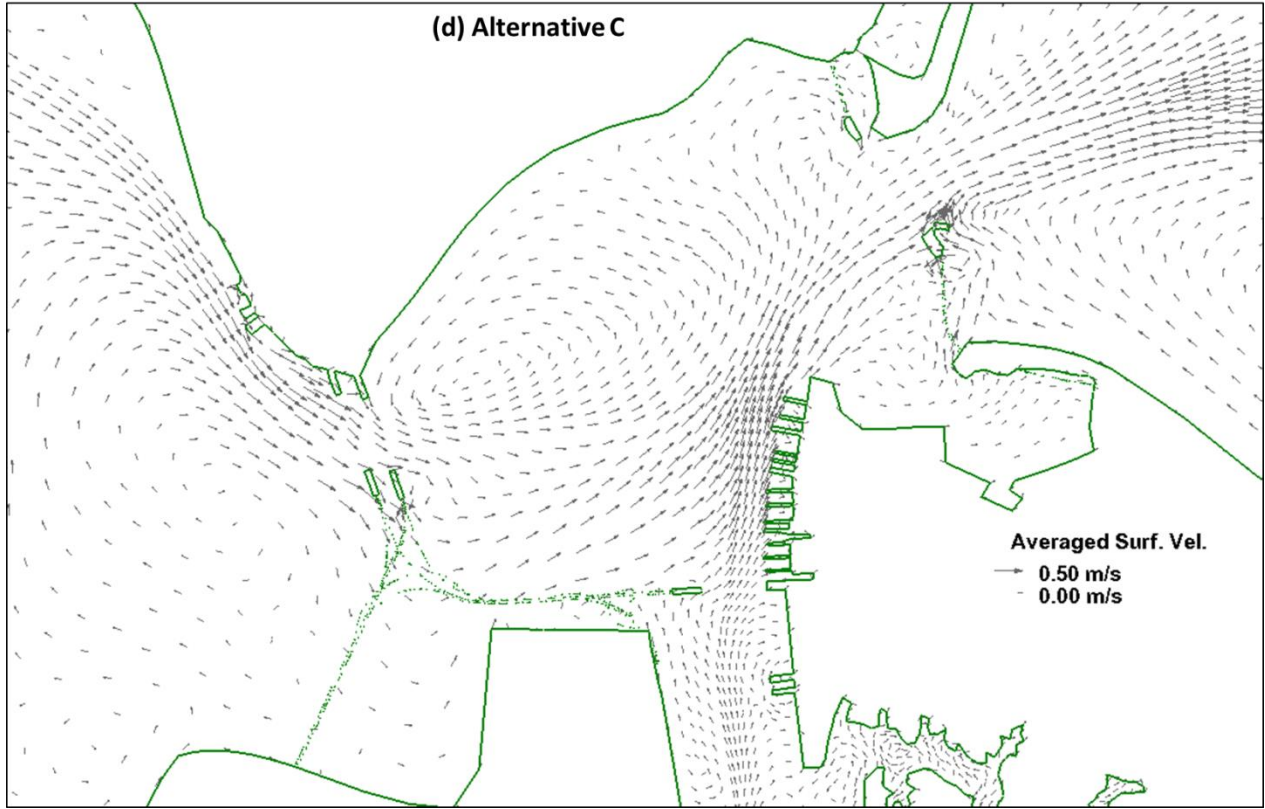
Figure 20: Surface velocity comparison between Base and 4 alternatives. The vectors have been interpolated onto a common coarser grid to clearly show the eddy structure.

(a) Base

Vorticty (S^-1)
0.15
0.09
0.03
-0.03
-0.09
-0.15

(b) Alternative A

Vorticty (S^-1)
0.15
0.09
0.03
-0.03
-0.09
-0.15

(c) Alternative B

Vorticty (S^-1)
0.15
0.09
0.03
-0.03
-0.09
-0.15

(d) Alternative C

Vorticty (S^-1)
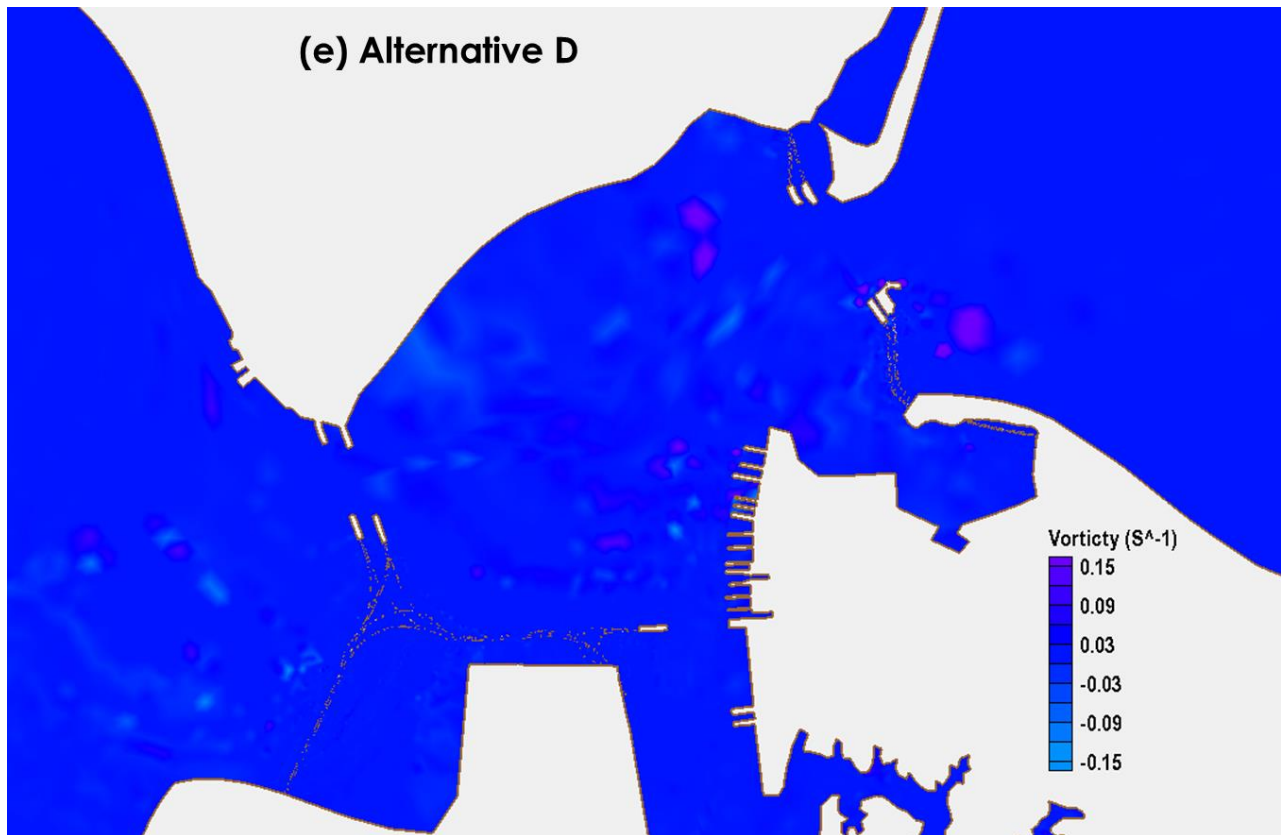0.15
0.09
0.03
-0.03
-0.09
-0.15
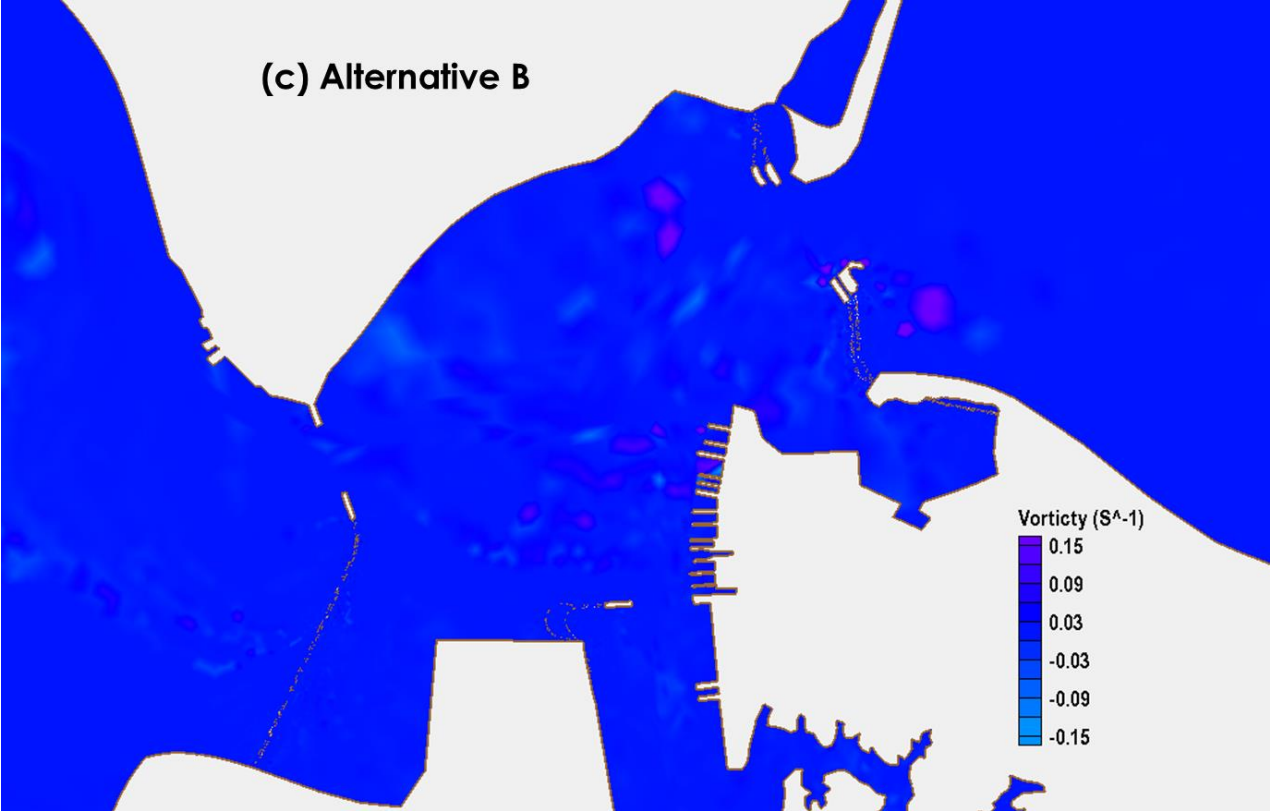
Figure 21: Surface vorticity comparisons between Base and 4 alternatives.

Figure 23 through **Figure 26** show the age differences between the 4 alternatives and the Base. In general, the differences are small and localized near new bridge structures and in the semi-enclosed areas. Most increase in the water age (~0.3 days) in Alternative A is found in Mill Creek and near the southern tunnel island (**Figure 23**). A similar increase is also found in Alternative B, as well as an ~0.3-day increase near the tunnel island of I564 Connector (**Figure 24**). The age increase in the Mill Creek is not seen in Alternative C, where the most prominent increase is in the newly created semi-enclosed area north of Craney Island (**Figure 25**). The increase in Alternative D is again approximately the sum of Alternatives B&C (**Figure 26**). The maximum increase of ~1 day is found near the entrance of Elizabeth River near the new Tunnel Island. Most of the lower James River experiences an increase of ~0.1 days. The results suggest that the impact from the new pilings on the water quality may be fairly localized in the project area.

Finally, the erosion and deposition potential is quantified using the bottom shear stress (**Figure 27**). The change in the latter is mostly confined near the new pilings. The bottom shear stress generally decreases both upstream and downstream of the pilings but increases between the pilings. The decreases (~0.1 Pa) occur mostly near the tunnel islands of I64 in Alternative A due to reduced flow there (**Figure 27a**). The addition of I564 and I664 Connectors in Alternative B only causes a small decrease locally (~0.02Pa),
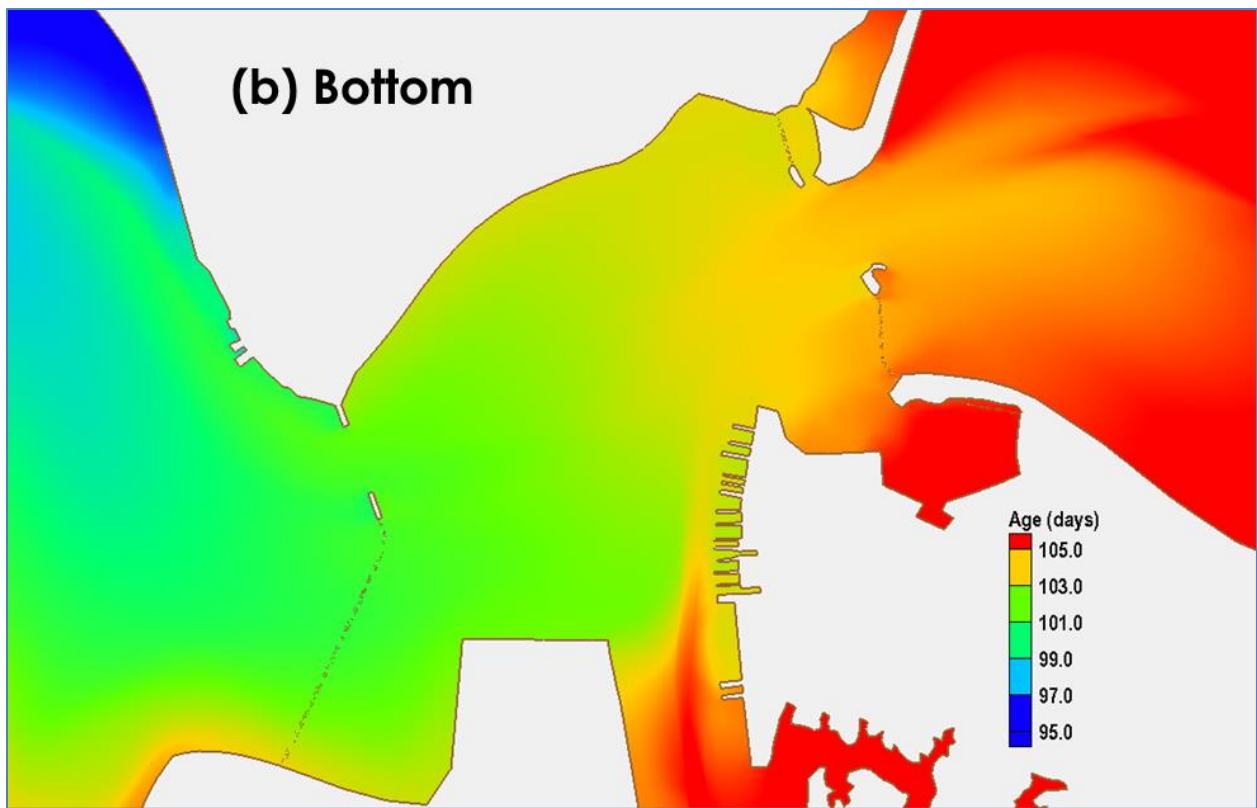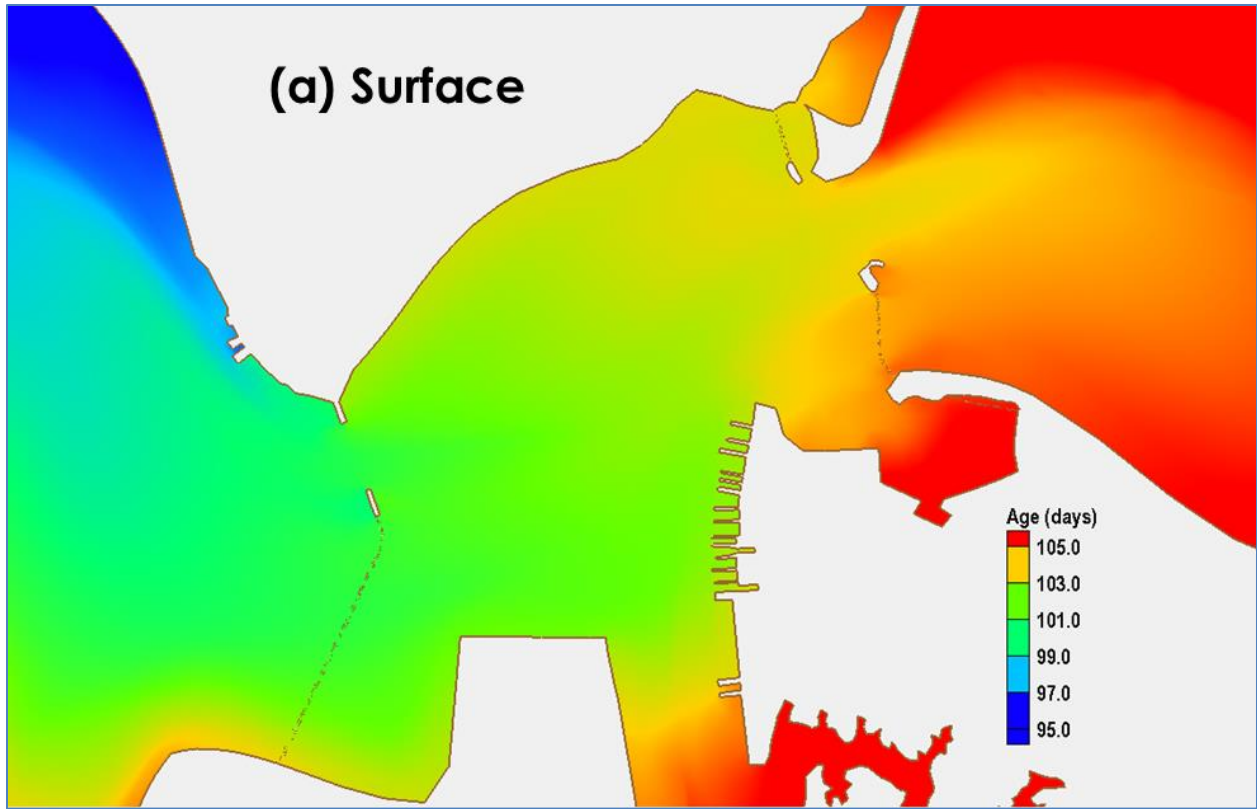
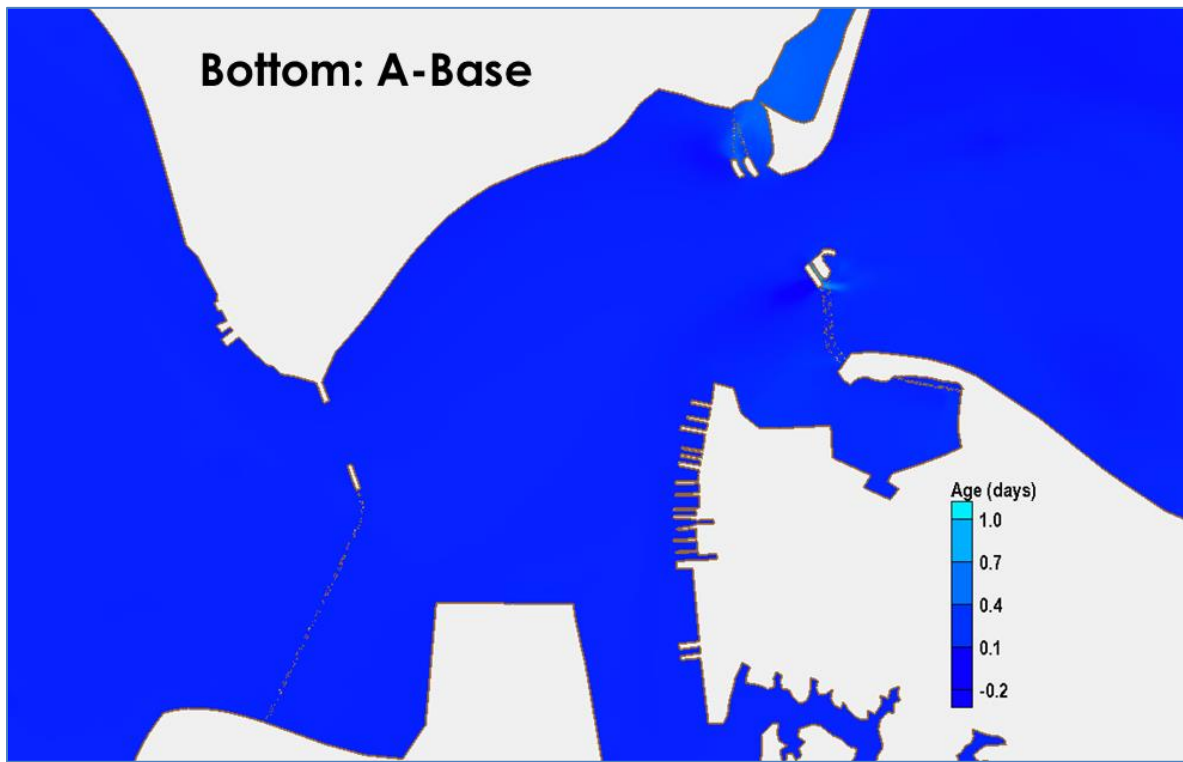Figure 22: Age distributions near the project area at (a) surface and (b) bottom from Base.
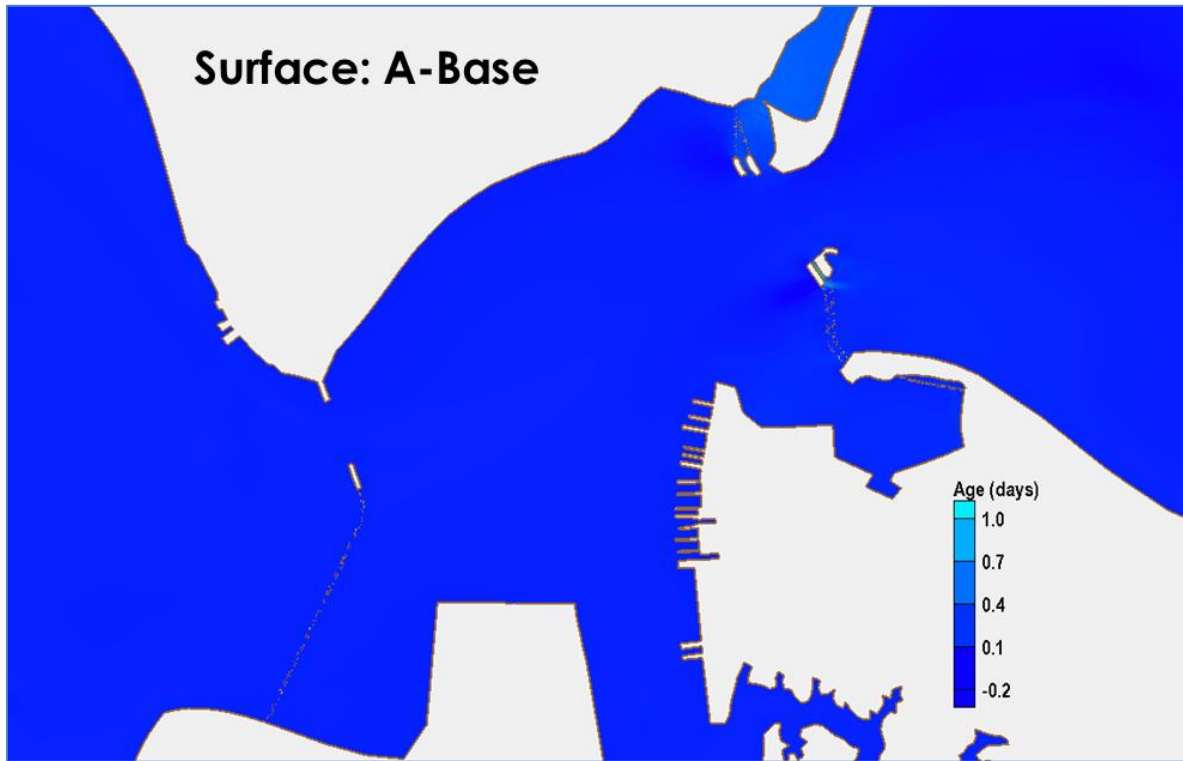
Figure 23: Age differences at surface and bottom, between Alternative A and Base.
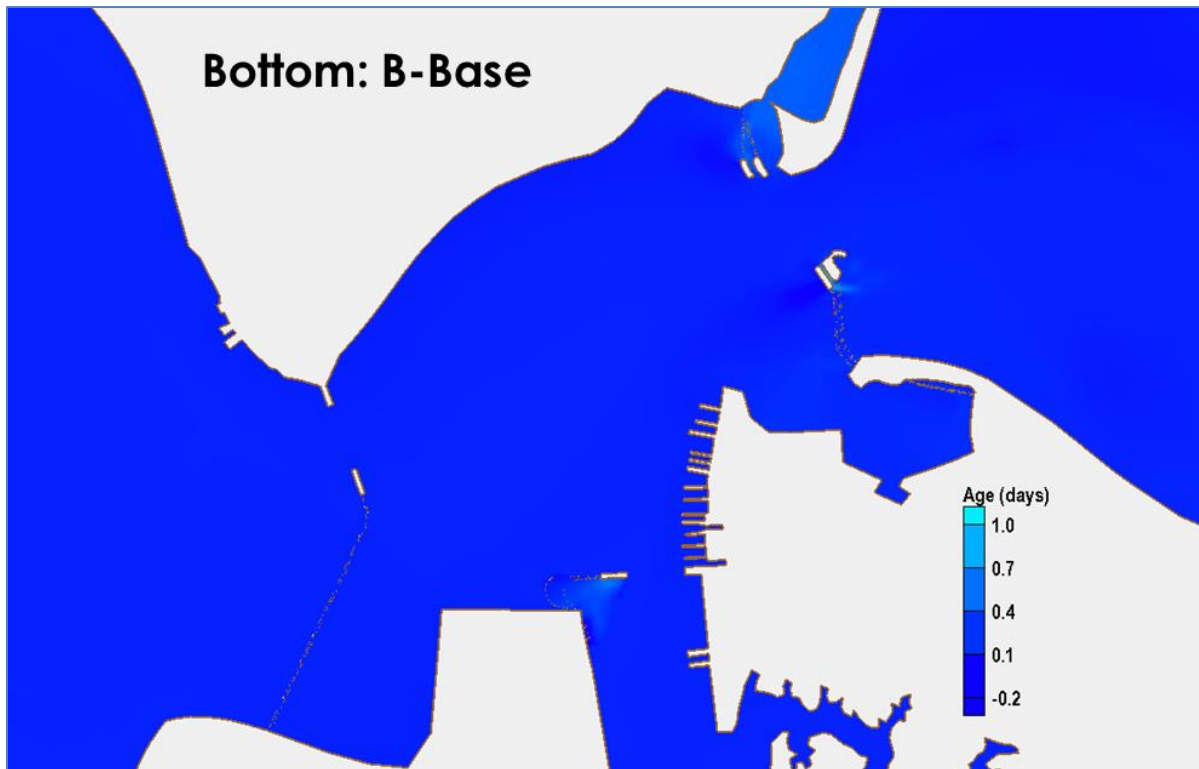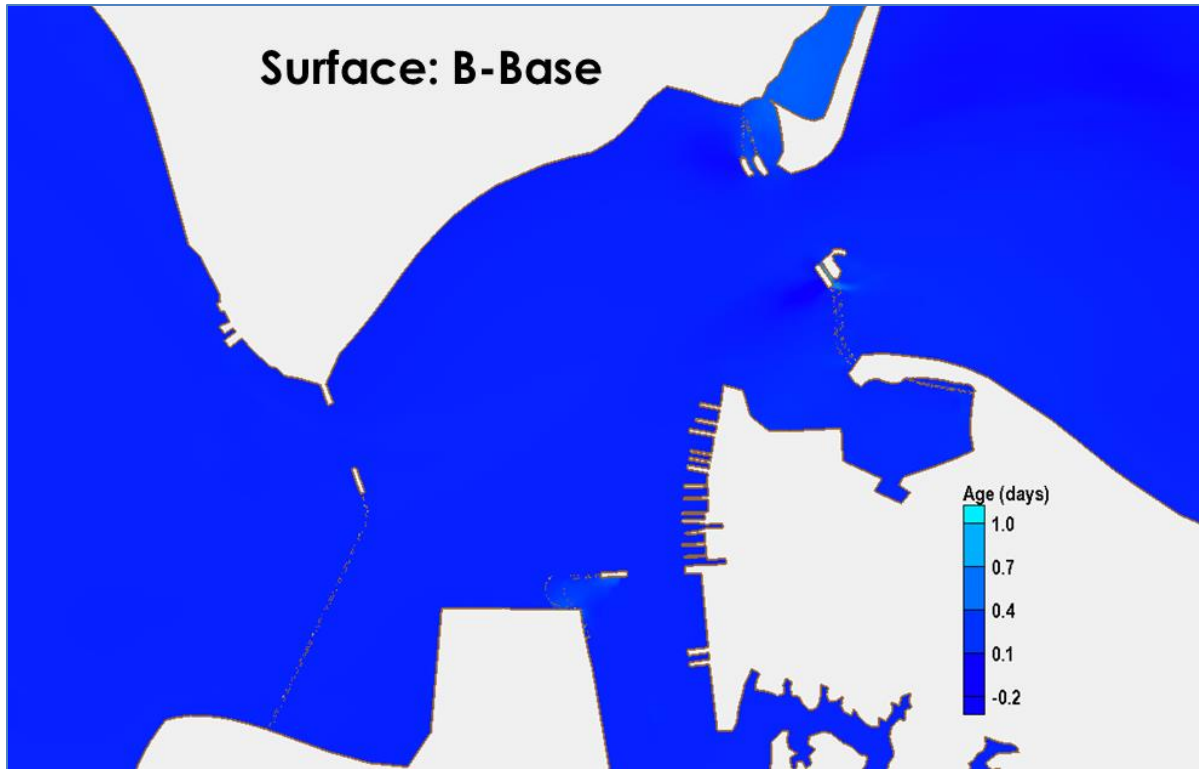
Figure 24: Age differences at surface and bottom, between Alternative B and Base.

Figure 25: Age differences at surface and bottom, between Alternative C and Base.

Figure 26: Age differences at surface and bottom, between Alternative D and Base.
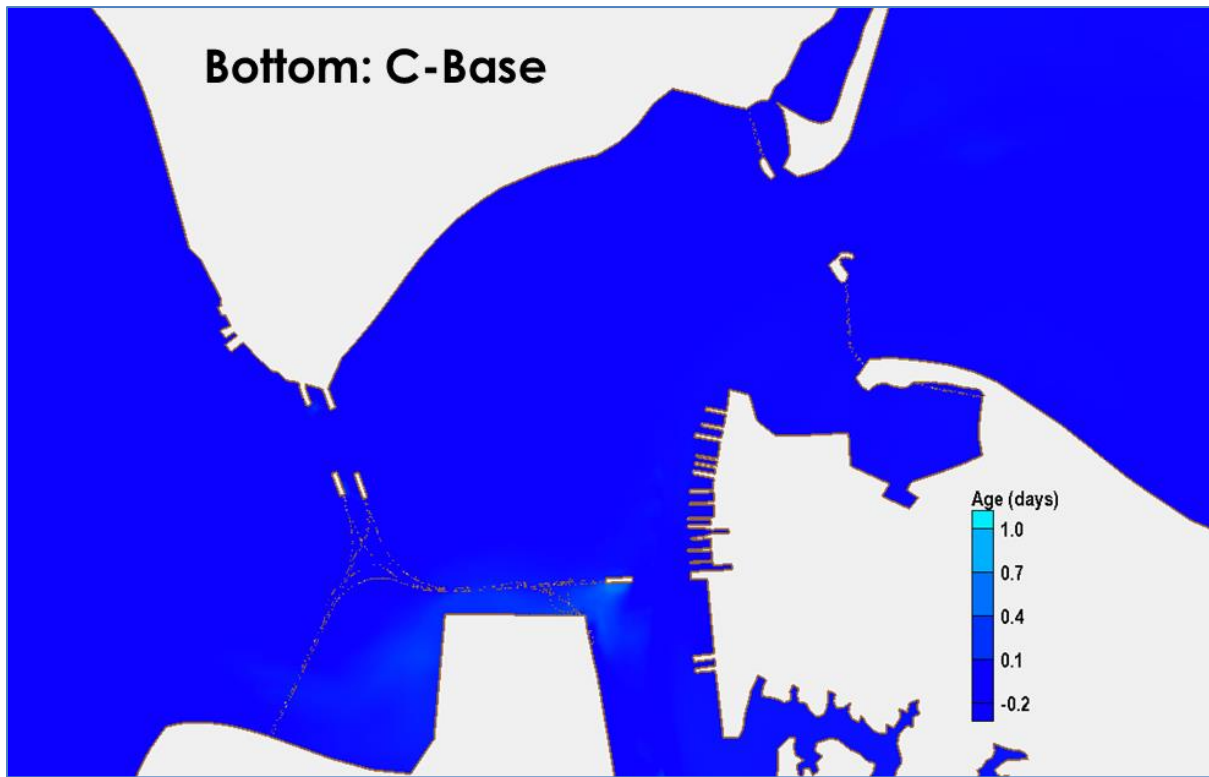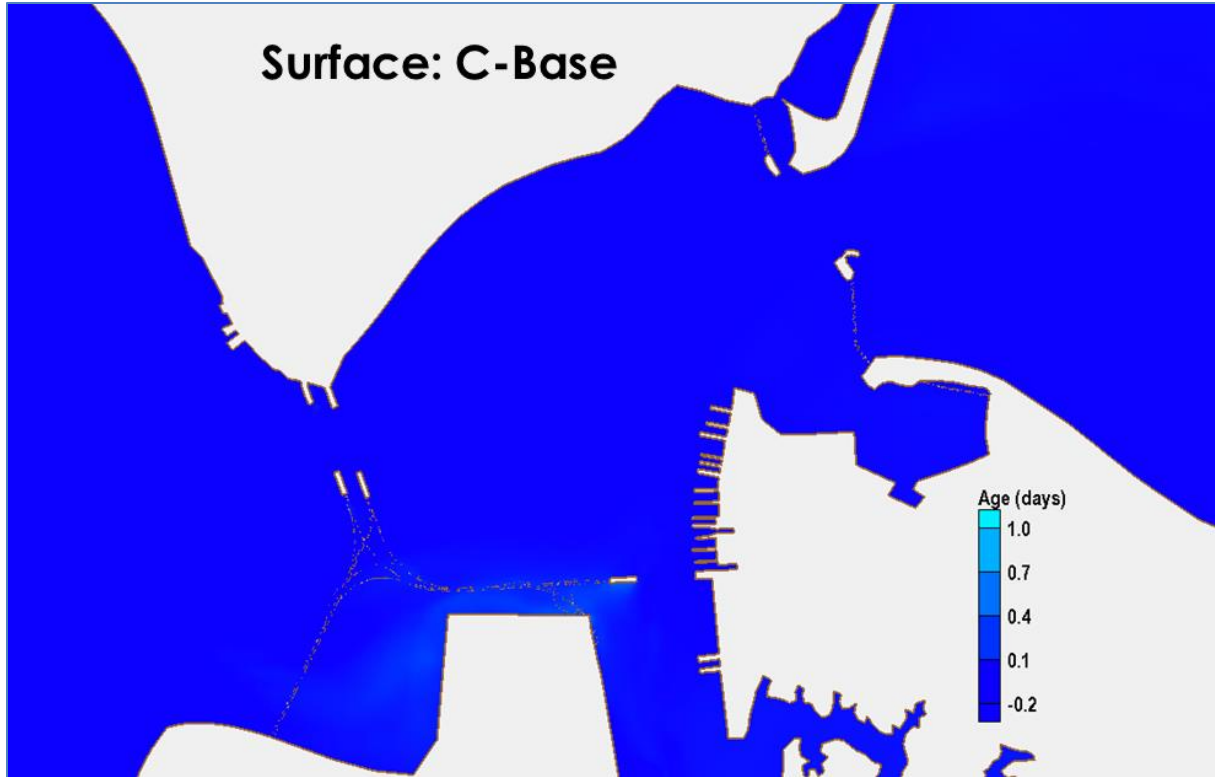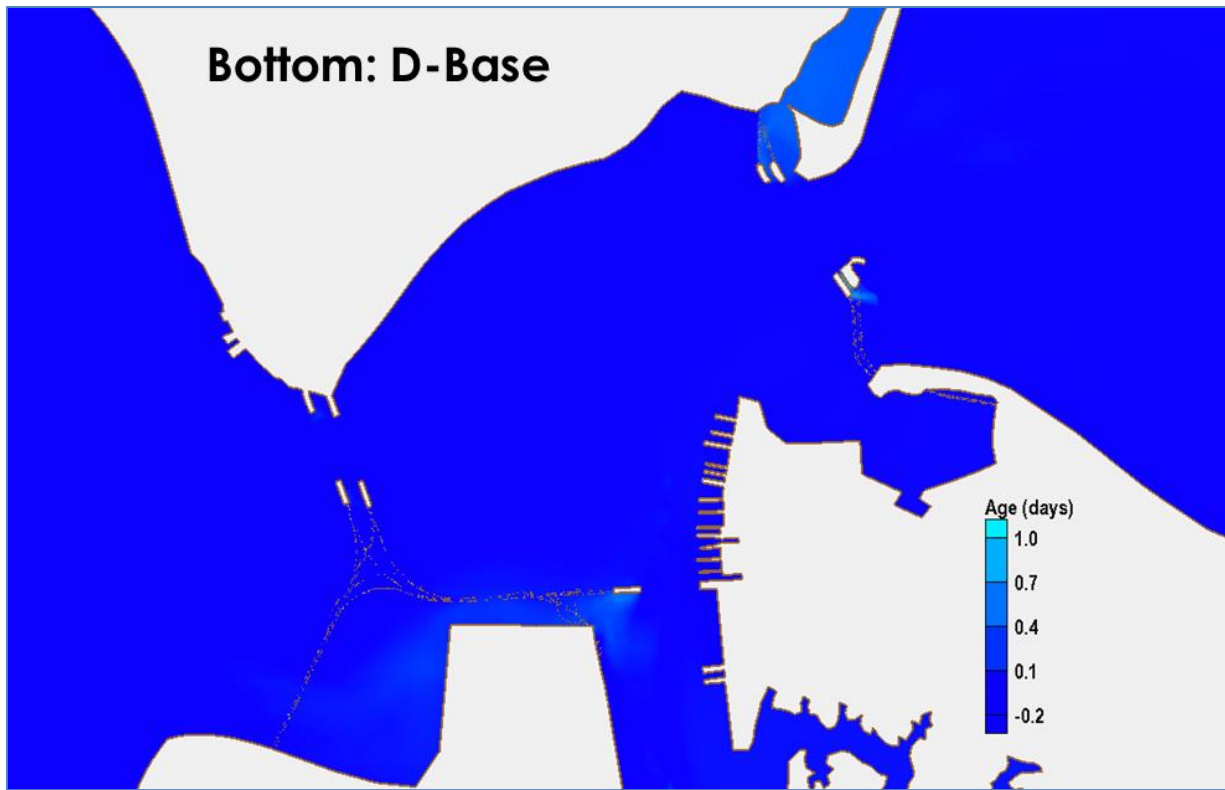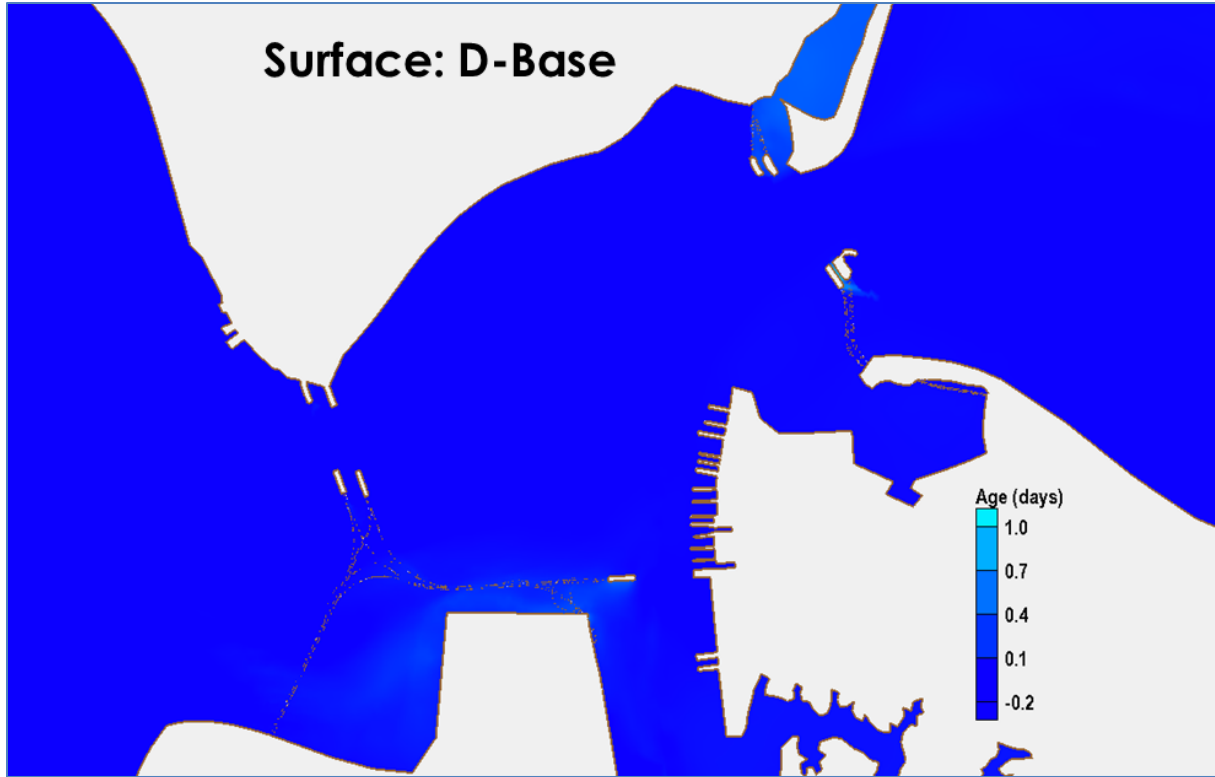
because the flow near the entrance of Elizabeth River is not as strong as that in James River (**Figure 27**b). More blocking of flow by the I664 expansion in Alternative C leads to similar decreases in the bottom stress (~0.06Pa) near the tunnel islands, but significant increases (~0.06 Pa) on the north and west sides of the southern tunnel are also observed (**Figure 27**c). The changes in Alternative D are approximately the sum of changes in Alternatives B&C (**Figure 27**d). The changes are mostly correlated to those in the averaged flow: the flow tends to slow down both upstream and downstream due to the blocking effects of the pilings, but tends to increase between pilings due to more constriction there (**Figure 27**e-h). The movement of sediment on the bed begins when the shear stress becomes sufficiently great to overcome the frictional and gravitational forces holding the grains. The value is the critical shear stress. Based on the measurement by Maa et al. (1993), the critical bed shear stress is about 0.23 – 0.25 Pa depending on the grain size distribution. A 3D sediment transport model is available to explicitly simulate the sediment movement in this system, but requires detailed information such as the initial grain size distribution, as well as sediment concentration from the river inflow and from the bank erosion. Since this analysis is done at a planning level, it does not assume full design and construction details. Based on the model results, although some appreciable changes can occur at the pier scale, when the entire project site in the lower James River are considered, the changes in sediment erosion and deposition are likely to be small and localized, and thus its impact on the existing shipping channels will be minimal. This integral approach for the impact analysis will be discussed in the next section.
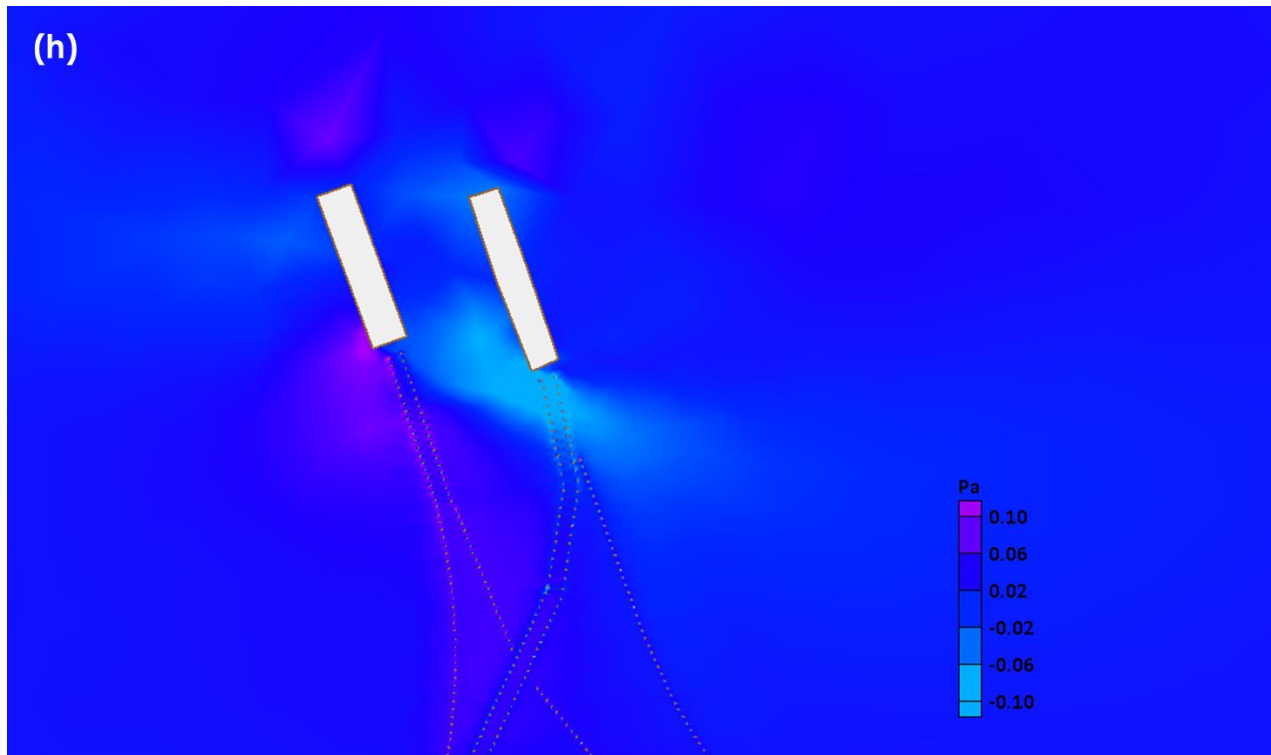
(b) B - Base

(c) C - Base

(d) D - Base

(e)
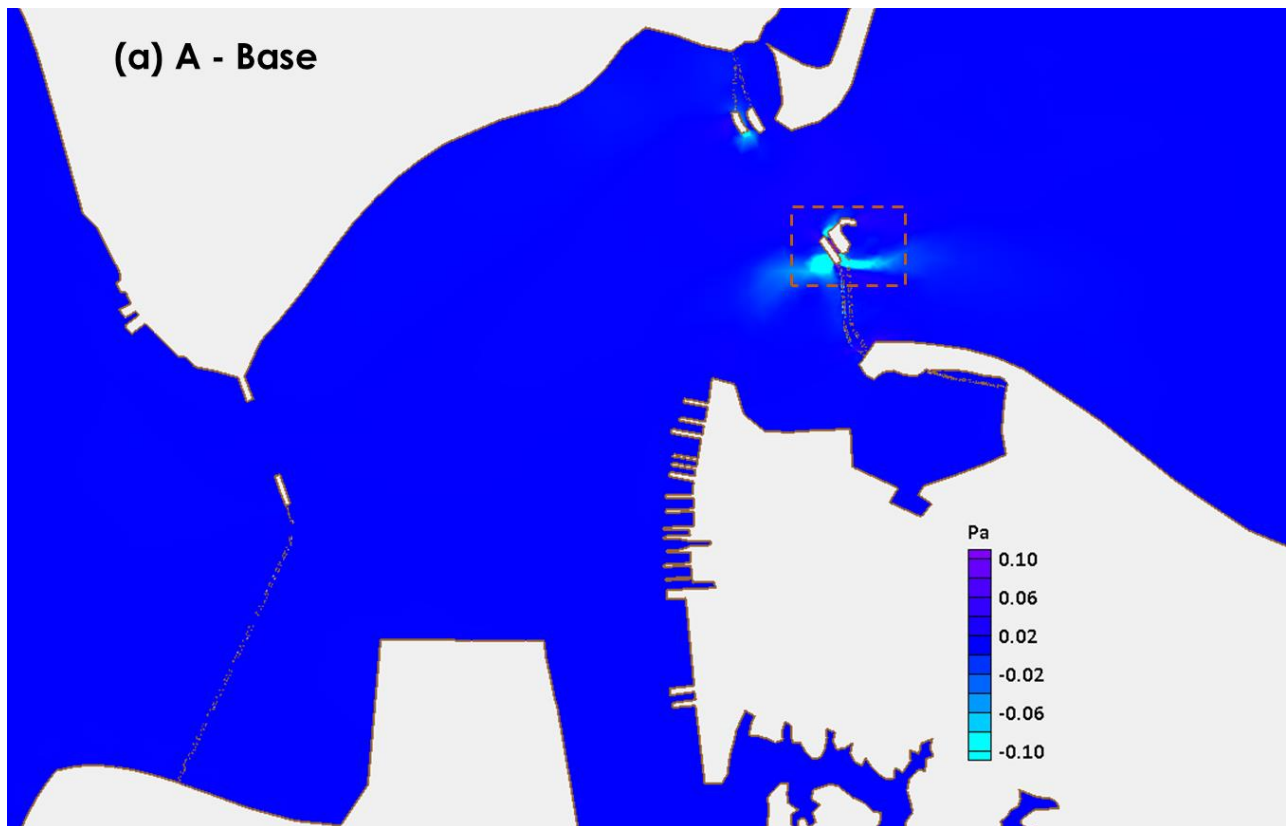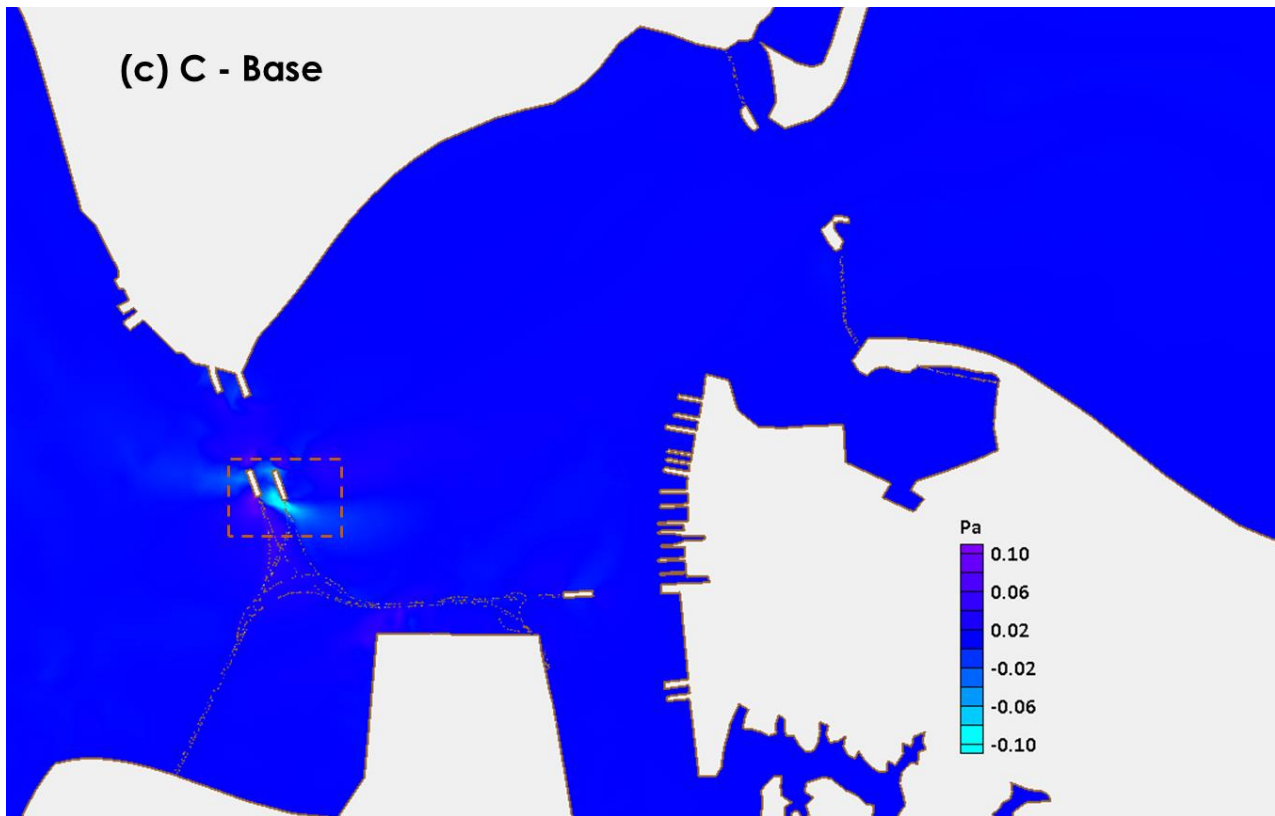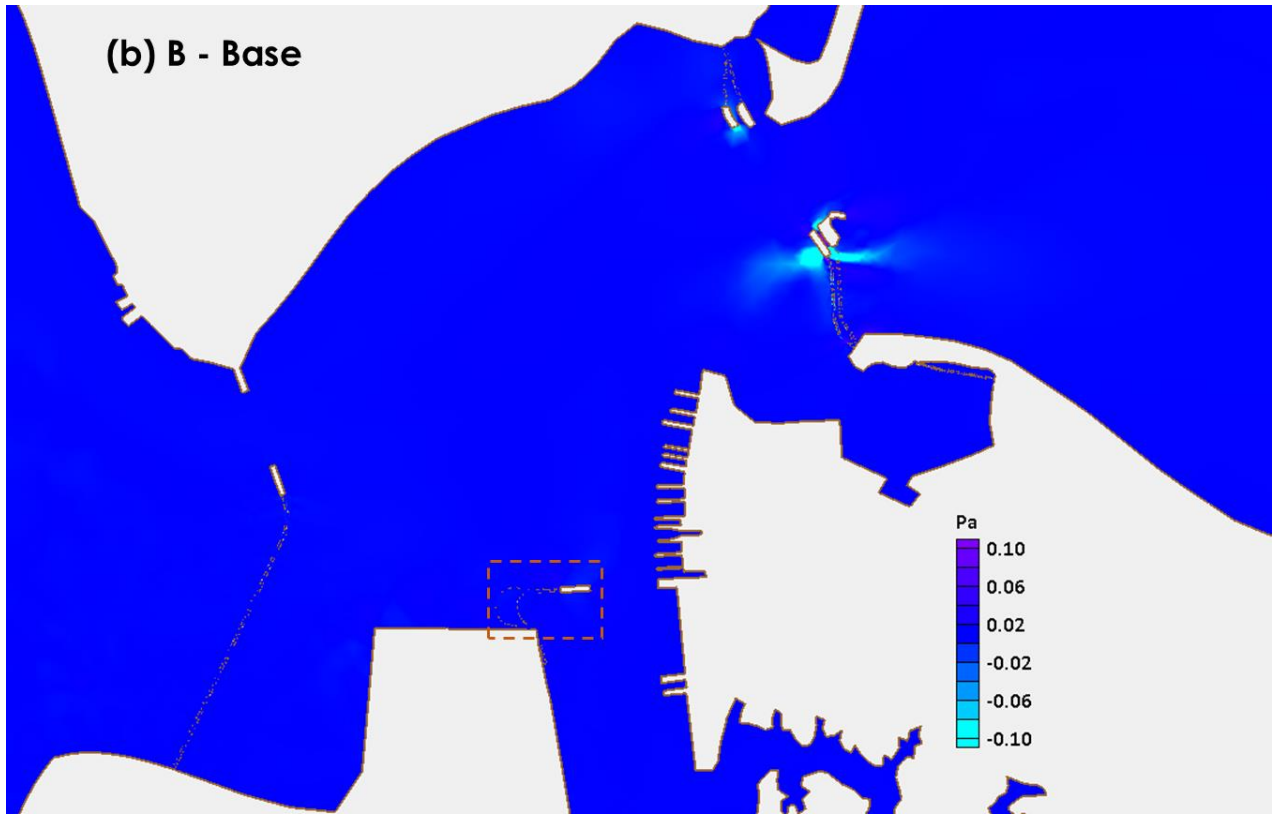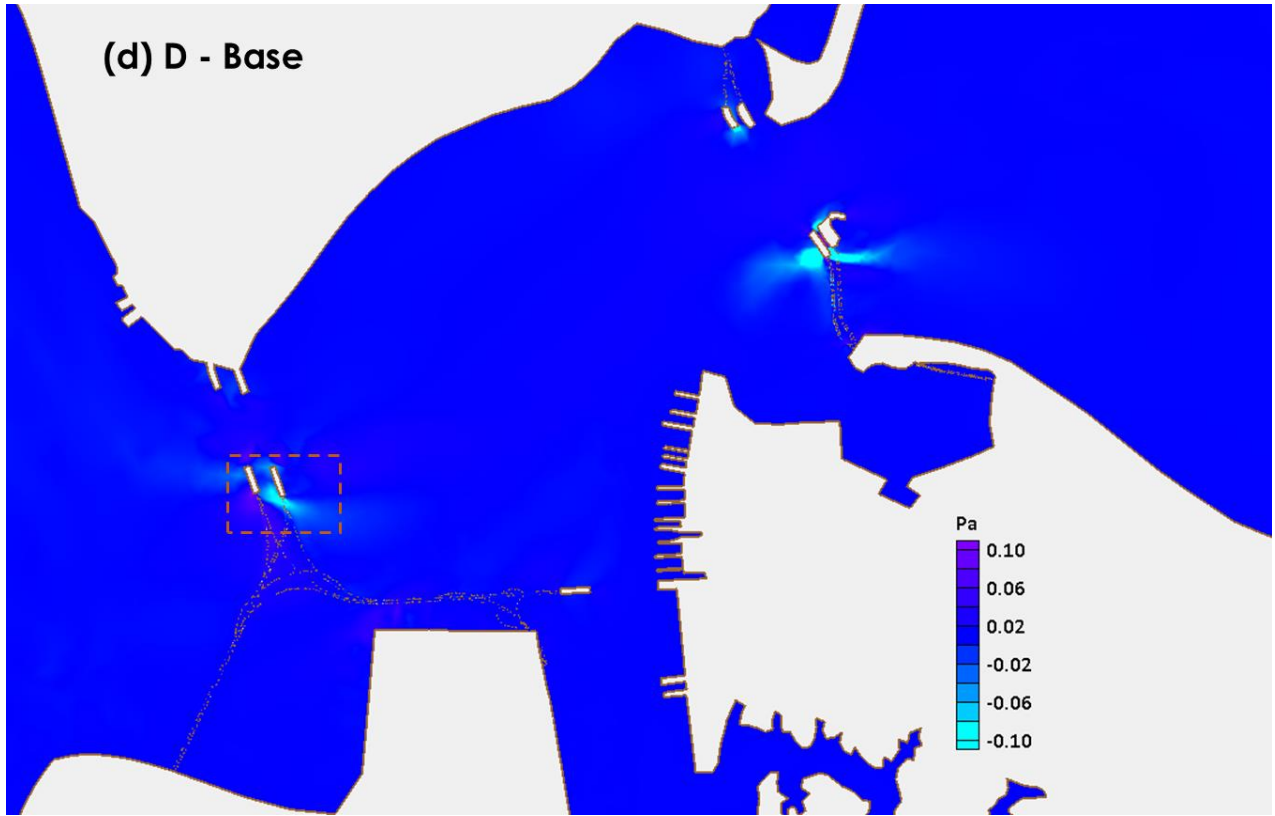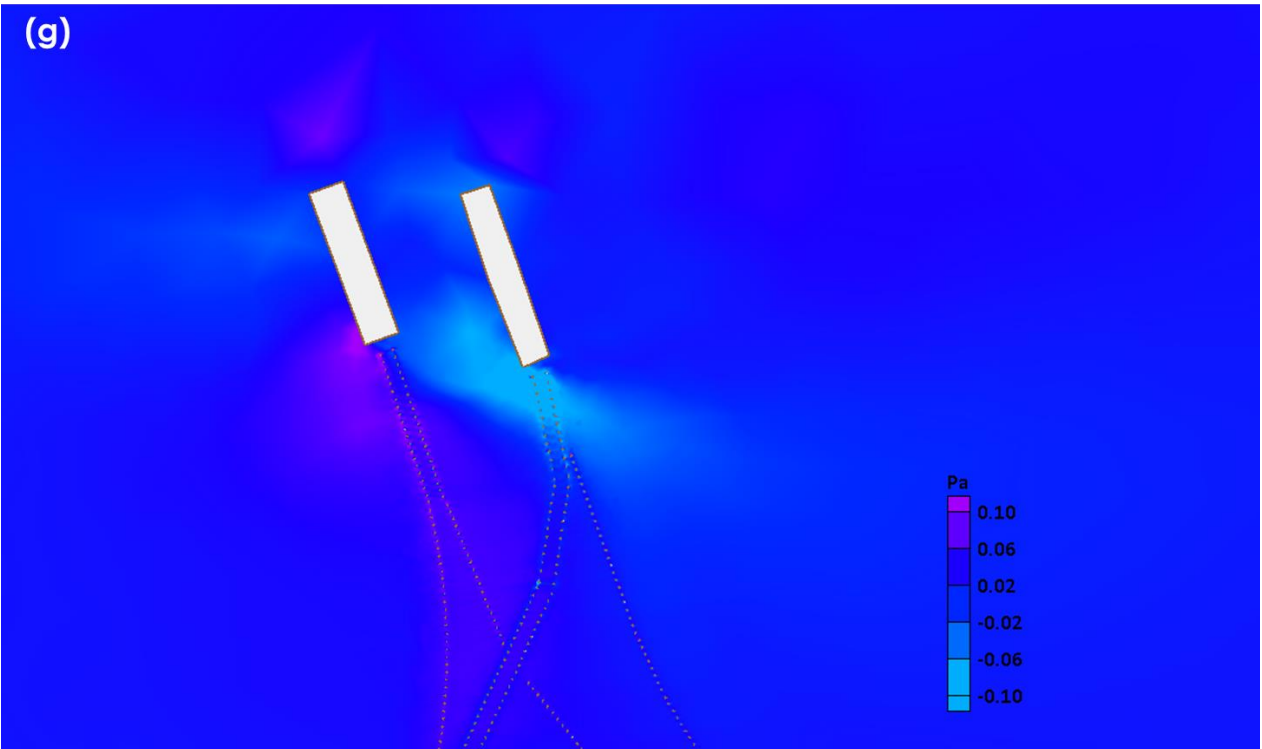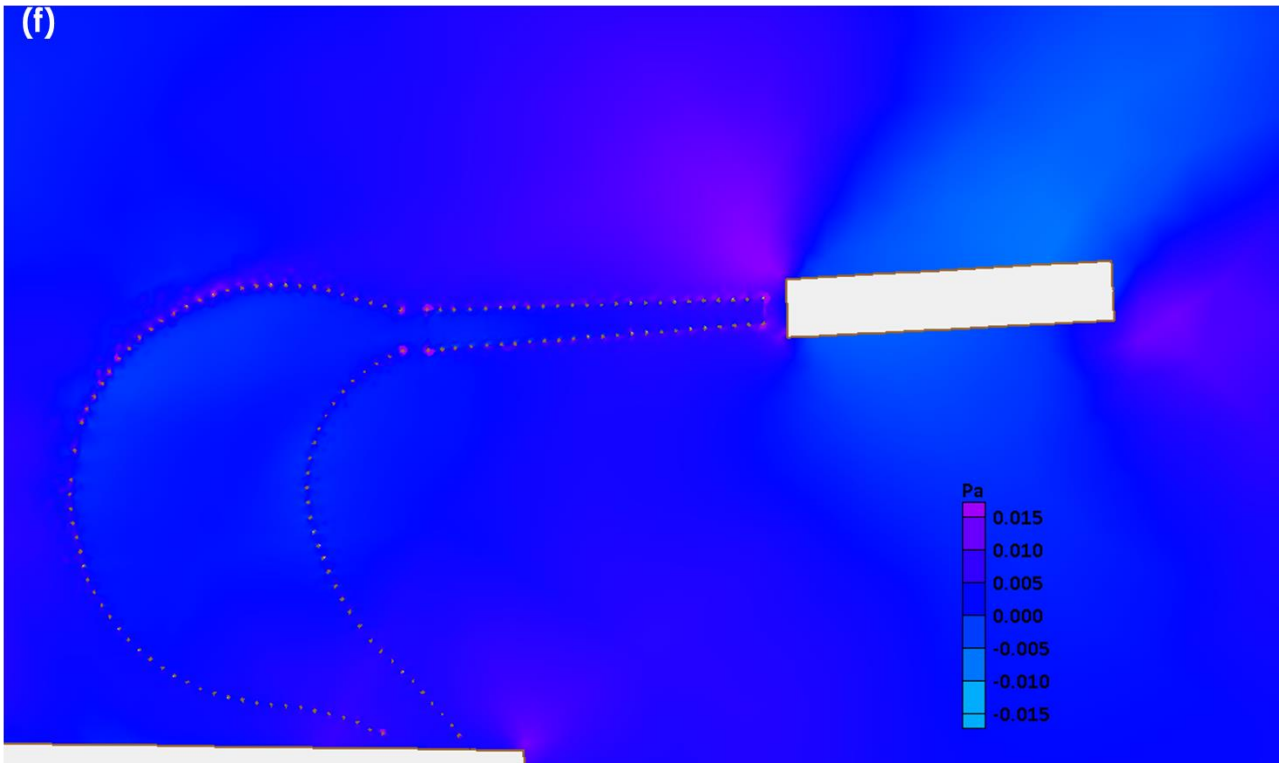
Figure 27: Changes in the averaged bottom shear stress between 4 alternatives and Base. (e-h) are zoom-ins of the dashed boxes shown in (a-d).

4.2 Global analysis

In the previous chapters, we discussed the capability of the SCHISM model in resolving many small scale fluid dynamics features induced by the bridge piling and the terminal island. For the environmental flow including estuarine circulation in the James River, it is not uncommon to have eddies occur in the water. The large eddies can be generated by flow passing through large structure or vessels and extract energy from the mean field, which in turn cascades into smaller eddies. The smaller eddies are strained by the velocity field of the largest eddies and continue to down-scaling. The small eddies do not, in general, interact with the large eddies or the mean field, but continue to feed into even smaller eddies until reaching the Kolmogorov microscale, the smallest scale on the order of 0.01 mm, and then dissipating into the heat eventually. In the proposed alternatives in the James River, it is comprehensible that the eddies can be generated by the proposed pilings and tunnel islands in the local area. However, the existence of the eddy does not automatically equate to an appreciable impact on the mean flow fields such as tidal, wind-driven and gravitational generated circulation. Whether the eddies can pose impacts on the important parameters of the flow including water level, salinity, temperature, current and the bottom shear stress will need to be assessed holistically, taking into account the aerial percentage of the change over the entire area. Our view through inspecting the spatial plots is that the scale of the eddies is very small compared to the water body of the James River and that their influence may only be confined to a very small localized area primarily in the vicinity of the piling and tunnel island.

In order to incorporate the factor of the area into the impact analysis, a global analysis that includes the area-weighted mean will be conducted. Here, the term *'global'* is used to refer to the region from *the*

50

mouth of the James River to the Route 17 James River Bridge where the transportation infrastructure preside. The global technique described in this section involves the generation of a frequency histogram distribution and percentile analysis of the mean time-average comparison of parameters predicted by the model for the Base Case and the 4 alternatives.

A. Frequency distribution

The frequency distribution is made possible by virtue of the fact that all model output from the 53,781 grid cells in the global domain of the SCHISM is saved hourly for 365 days (equivalent to a time series with 8760 data points for each cell). This allows us to compare, for each location in the model domain, time series of the Base Case versus the 4 alternatives. The general formula used has two steps:

$$MAD_i = \sum_{k=1}^{8760} \left\| MP_{alternative,k} - MP_{base,k} \right\|_i \qquad \text{............} \quad (1)$$

followed by

$$wMAD = \sum_{i=1}^{53781} MAD_i \ \frac{area_i}{\sum_{i=1}^{53781} area_i} \qquad \text{...............}(2)$$

where k is the counter for time variation and i is the counter for individual cell in space; MAD_i is the mean absolute deviation for each cell; wMAD is the area weighted mean absolute deviation; $MP_{alternative,k}$ is the model prediction for alternative; $MP_{base,k}$ is the base result at each cell; $area_i$ is individual area of each cell.

To assess the global impact of the alternatives on the base case, it is important to know the distribution of the deviation weighted by the percentage of area impacted to the total area. This can be accomplished by plotting the frequency histogram for class intervals between minimum to maximum deviation. In plotting the frequency distribution, since we are interested in both the positive and negative of the difference between the base case and the alternative, rather than the absolute value, the positive and negative class values were preserved. Examples of the frequency and cumulative distribution function for the surface velocity, bottom velocity, surface salinity, bottom salinity and the bottom shear stress under alternative D are shown in Figure 28 to Figure 32 respectively. (The similar results with all other alternatives, A, B, and C can be found in Appendix A) By examining the frequency distribution of the deviation when the area size of variation was taken into consideration, it was found that all variables have a central tendency toward zero deviation. For the surface velocity, bottom velocity, and bottom shear stress the distribution are nearly symmetric but for the salinities, it is skewed to the positive. It is also worth noting that the spread of the distribution, representing moving away from the central mean, were the largest for surface salinity under the Alternative C and D, as shown in A-11(of the Appendix) and Figure 30, respectively.

B. Percentile Analysis

From the previous analysis, it is clear that when the size of the area of the variation is taken into consideration, the deviation for the alternatives from the base tend to be clustered in the center of the distribution with small values. This is not unexpected. However, it is also important to look at the spread of the distribution, which will give us an idea how the mean values in the center of distribution represent the data. One way to quantify the measure of the spread is to quantile the data by breaking into quarters, just like the median breaks the data in half. To do so, the following steps were taken:

(a). Obtaining the MAD_i from equation (1) and find MIN = min (MAD_i) and MAX = max (MAD_i).

(b) Adding 0.001 interval from MIN to MAX and order them from the smallest to the largest as: [MIN, MIN+0.0001], [MIN+0.0001, MIN+ 1*0.0001] …. [MIN+(k-1)0.0001, MIN+k*0.0001]…….

[MAX - 0.0001, MAX]

In a tabulated form and using a counter g from 1 to T, it reads:

Intervals	[MIN, MIN+0.0001]	[MIN+0.0001, MIN+0.0002]	…	[MAX-0.0001, MAX]
Interval counter g	1	2	…	T

(c) For each interval g (from 1 to T), calculate the total area of the elements in which MAD_i fall

(d) Calculate the percentage of the area for each g as: $$PER_g = \frac{\sum_{i=1}^{n_g} area_i}{\sum_{j=1}^{N} area_j}$$

where N is the number of elements in the global region, which is 53,781, and n_g is the number of elements that fall in the interval of g. It should be noted that PER_g has a value from $0 - 1$.

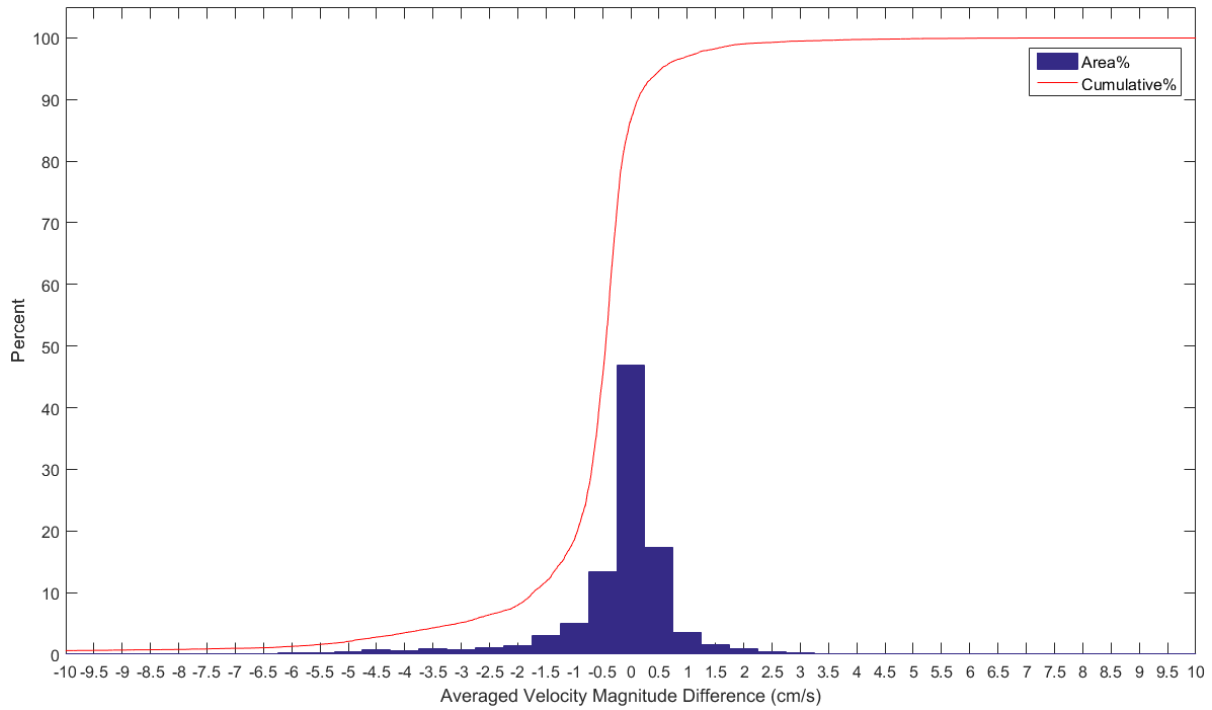
Figure 28: **The frequency distribution bar diagram of surface velocity difference for Alternative D versus the base case. The red line is the cumulative frequency function.**
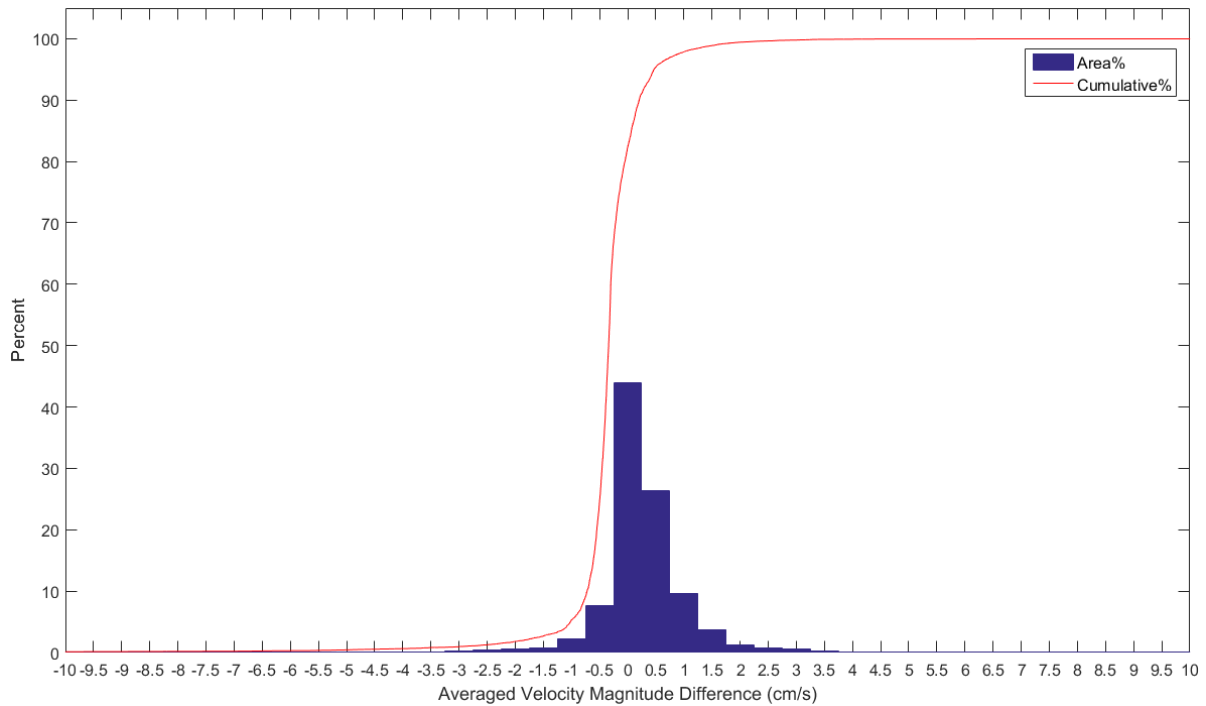

Figure 29: The frequency distribution bar diagram of bottom velocity difference for Alternative D versus the base case. The red line is the cumulative frequency function.
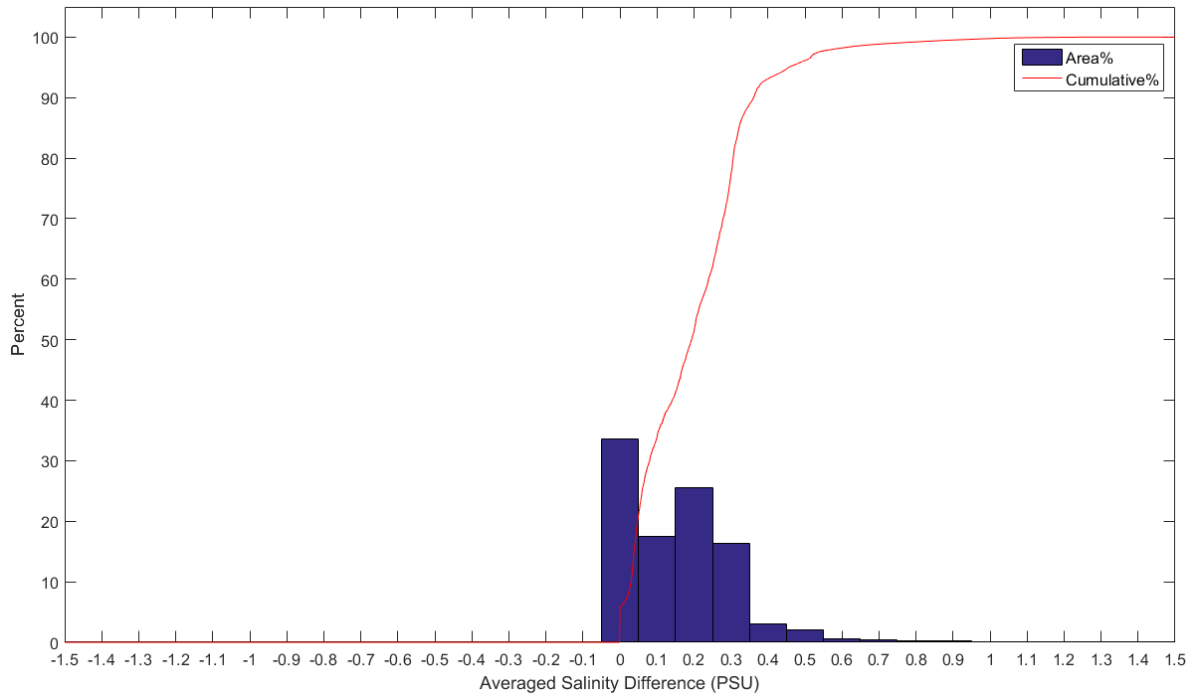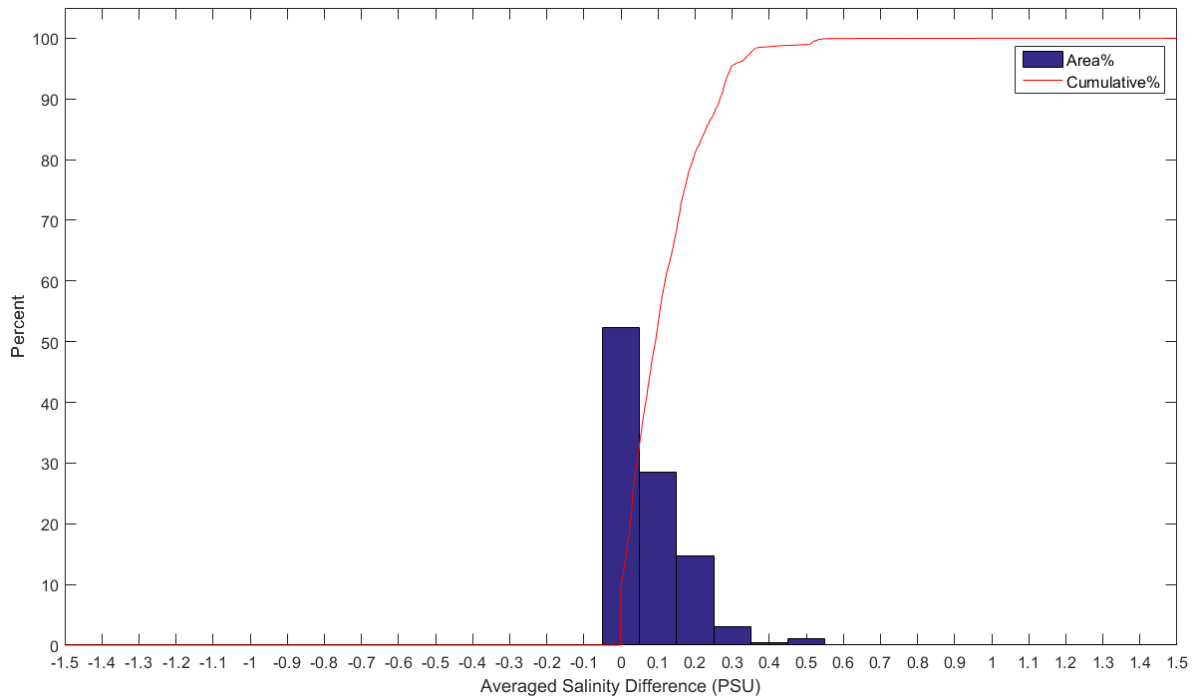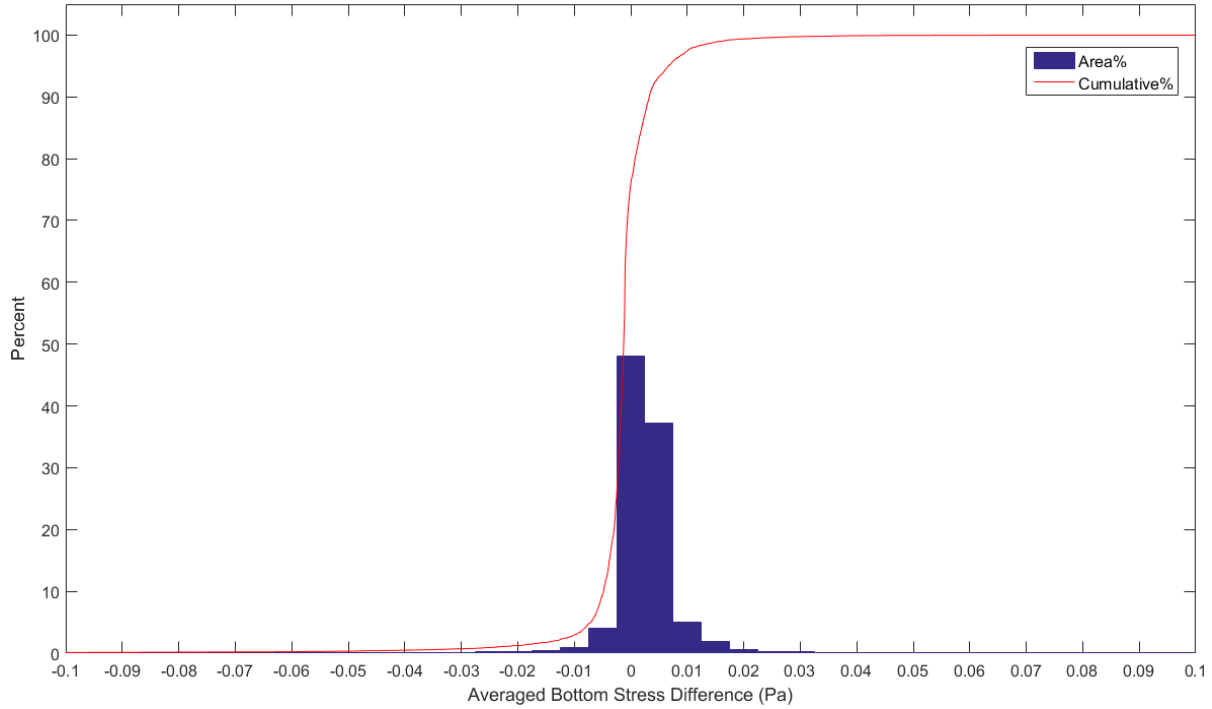
Figure 30: The frequency distribution bar diagram of surface salinity difference for Alternative D versus the base case. The red line is the cumulative frequency function.

Figure 31: The frequency distribution bar diagram of bottom salinity difference for Alternative D versus the base case. The red line is the cumulative frequency function.

Figure 32: The frequency distribution bar chart of bottom shear stress difference for Alternative D versus the base case. The red line is the cumulative frequency function.

Having finished above 4 steps, we further define *S(k)* as a summation of PER_g: $S(k) = \sum_{g \leq k} PER_g$

This is a function also called cumulative frequency function, which will allow one to find the values of MAD_g in certain quantile. For example, if one wants to find the MAD_g at the 1/4 quantile, one should make the summation until $S(k) = 0.25$. The very *K* th value corresponding to the 1/4 quantile will be chosen to find the interval [MIN+(K-1)*0.001, MIN+K*0.001] in which the MAD_K is located.

In the environmental risk assessment, using a 95th percentile value as a threshold is a conservative approach to ensure that 95 percent of the data are well represented and the outliers in the data are not overly-smoothed, as it does by mean and median (US EPA HHRA Program). For the first phase of the James River alternative assessment, the 95th percentile was chosen for worst-case scenario assessment (Boon et al. 1999). Using the step-by-step method outlined above, the 95th percentile threshold value for the parameters including surface velocity, bottom velocity, surface salinity, bottom salinity, and the bottom shear stress were found for alternative A, B, C, and D, as shown in Table 11 (a). Also listed in the column 6 is the reference values from base case, which were chosen from the 90th and 95th percentiles of the base case value of *MP base, i* , used by equation (1). This table shows the absolute value of the deviation of the alternatives to the base case. The unit used for velocity is cm/s, for salinity is psu and for bottom shear stress is Pascal. Using the values listed in Table 11(a), the percentage of impact of alternative relative to the base case was also calculated, as shown in Table 11(b). For the difference of impacts from various alternatives, all the relative impacts under Alternatives A and B are below 1%, and Alternative D clearly has the biggest impact, but still under 2%. Among the difference of impacts from parameters, velocity has the relatively lowest relative impact, followed by bottom salinity, surface

salinity, and the bottom shear stress has the largest impact with 1.95%. Overall the impacts are below 1 - 2%, depending on which alternative is chosen.

Table 11 (a): The total absolute deviation of alternatives from the base case using 95th percentile global analysis

Global Change – 95th Percentile (Total absolute deviation of alternatives from the base case)					
Cumulative Impact of Bridge Piling and Terminal Island from HRCS SEIS Alternatives					
Difference from Base Case	**Alternative A**	**Alternative B**	**Alternative C**	**Alternative D**	**Reference values** from Base Case (95th | 90th)
Surface Velocity	0.10 cm/s	0.11 cm/s	0.15 cm/s	0.15 cm/s	28 cm/s | 24 cm/s
Bottom Velocity	0.05 cm/s	0.05 cm/s	0.10 cm/s	0.11 cm/s	12 cm/s | 10 cm/s
Surface Salinity	0.17 psu	0.21 psu	0.32 psu	0.33 psu	24 psu | 22 psu
Bottom Salinity	0.14 psu	0.18 psu	0.26 psu	0.28 psu	26 psu | 24 psu
Bottom Shear Stress	0.002 Pa	0.002 Pa	0.003 Pa	0.0045 Pa	0.25 Pa | 0.23 Pa

Table 11 (b): The total percentage deviation of alternatives from the base case using 95th percentile global analysis

Global Change – 95th Percentile (Total percentage deviation of alternatives from the base case)					
Cumulative Impact of Bridge Piling and Terminal Island from HRCS SEIS Alternatives					
Difference from Base Case	**Alternative A (%)**	**Alternative B (%)**	**Alternative C (%)**	**Alternative D (%)**	**Reference values** from Base Case (95th | 90th)
Surface Velocity (% of impact relative to the base case)	0.36| 0.42	0.39 | 0.46	0.54 | 0.63	0.54 | 0.63	28 cm/s | 24 cm/s
Bottom Velocity (% of impact relative to the base case)	0.42 | 0.5	0.42 | 0.5	0.83 | 1.0	0.92 |1.1	12 cm/s | 10 cm/s
Surface Salinity (% of impact relative to the base case)	0.71 | 0.77	0.88 | 0.95	1.33 | 1.45	1.38| 1.50	24 psu | 22 psu
Bottom Salinity (% of impact relative to the base case)	0.54 | 0.58	0.69 | 0.75	1.0 | 1.08	1.08 | 1.17	26 psu | 24 psu
Bottom Shear Stress (% of impact relative to the base case)	0.80 | 0.87	0.80 | 0.87	1.2 | 1.3	1.80 | 1.95	0.25 Pa | 0.23 Pa

5. Conclusions

The effect of new bridge crossing structures on the lower James River water movement has been studied using a high-resolution unstructured-grid model SCHISM. Using SCHISM's superior capability, the bridge pilings and the tunnel island were explicitly resolved by the locally refined modeling grid (note: The effects of bridge's above-water-payments and the underground tunnels are not part of this study as they do not directly impact the hydrodynamics.) Model calibration under the existing condition compared well with the observation with good model skills. The modeled elevation when compared with the observation data has an average RMSE of no more than 5.4 cm, salinity of 1.4 PSU, and temperature of 0.8 ℃. The model was able to accurately capture the gravitational circulation including periodic stratification and de-stratification.

On the local level, the comparison of results from the existing conditions and 4 alternatives A-D (with D being the 'sum' of A-C) revealed that, in general, the impact of these alternatives is relatively minor and concentrated near the new bridge pilings, and the largest impact, unsurprisingly, was associated with Alternative D. Of major hydrodynamic variables, the tidal amplitudes and phases of elevation and total outflow are only marginally affected (~1mm for elevation or a few m^3/s for flow). The residual velocity shows increased vorticity near and away from the new pilings, due to horizontal transport of turbulence. The surface salinity is increased up to ~1.5 PSU near the new structures and less than 0.1 PSU in all areas 4 km away from the structures. The change in the bottom salinity is smaller, and the largest change is located in the semi-enclosed areas in Mill Creek as the relatively stagnant water in these areas prevents it from blending with the adjacent moving water and are thus more sensitive to the blocking effects by new pilings. The turbulence mixing is enhanced near the structures and, as a result, the density stratification is generally reduced. The impact on the residence time is also small and fairly localized, with a maximum value of 1 day found near Elizabeth River. The changes in the bottom shear stress are mostly correlated to those with the flow: the flow velocity tends to slow down both upstream and downstream due to the blocking effects of the pilings, but tends to increase between pilings due to more constriction there. Therefore, the changes in bottom shear stress are likely to be small and localized.

On the global level, a global analysis was conducted to assess overall impact, whereby the changes in the entire region from the mouth of the James River to the Route 17 James River Bridge were taken into consideration. From the frequency histogram and cumulative distribution function, it was found all the examined variables (surface velocity, bottom velocity, surface salinity, bottom salinity, and bottom shear stress) have a central tendency toward zero deviation from the base case. Most of the distributions are symmetric except salinities are skewed to the positive deviation. The percentile analysis was also conducted in which the 95th percentile value was selected to conservatively estimate the deviation of the 4 alternatives from the base. A table showing the absolute deviation value for the alternatives from the base case has already been highlighted in the execute summary. Here we emphasize the percentage of impact of alternative relative to the base case, presented in Table 11(b). For the difference of impacts from various alternatives, all the relative impacts under Alternatives A and B are below 1%, and for the Alternatives C and D, the impacts are larger, but still under 2%. Among the difference of impacts from parameters, velocity has the lowest relative impact, followed by bottom salinity, surface salinity and the bottom shear stress, which has the impact with 1.95% under Alternative D. For 4 alternatives, the percentage impact are all less than 2 % (1% for Alternatives A and B), which, from environmental risk assessment point of view, are considered to be small.

In all, the modeling analyses, conducted under VDOT planning level which does not assume full design/construction details, confirm the results from the previous investigation results that the changes due to the projects are largely localized in nature and the overall impacts of transportation infrastructure on the lower James are relatively small compared to the 'no-build' base case.

6. References

Boon, J.D., Wang, H.V., Kim, S.C., Kuo, A.Y. and Sisson, G.M. (1999). Three-dimensional Hydrodynamic-Sedimentation Modeling Study, Special Report #354 for Virginia Department of Transportation, Virginia Institute of Marine Science.

Burchard, H., and Hetland, R.D. (2010). Quantifying the contributions of tidal straining and gravitational circulation to residual circulation in periodically stratified tidal estuaries. J. Phys. Oceanogr., 40, 1243–1262, doi:10.1175/2010JPO4270.1.

Cho, K.H. Wang, H.V., Shen, J., Valle-Levinson, A. and Teng, Y.C. (2012). A modeling study on the response of the Chesapeake Bay to Hurricane Events of Floyd and Isabel. Ocean Modeling, vol. 49-50, pp. 22-46.

Fischer, H.B., E.J. List, J. Imberger, R.C.Y. Koh, and N. H. Brooks (1979). Mixing in Inland and Coastal Waters, Academic Press.

Le Roux, D.Y., C.A. Lin, and A. Staniforth (1997). An accurate interpolating scheme for semi-Lagrangian advection on an unstructured mesh for ocean modelling. Tellus, 49A, pp. 119-138.

Maa, J.P.-Y, L. D. Wright, C.-H. Lee and T. W. Shannon (1993). VIMS Sea Carousel: A field instrument for studying sediment transport.   Marine Geology, 115., p271-287.

Monismith, S.G., W. Kimmerer, M.T. Stacey, and J.R. Burau (2002). Structure and Flow-Induced Variability of the Subtidal Salinity Field in Northern San Francisco Bay. J. Phys. Ocean, 32(11): 3003-3019.

NTHMP (2012). Proceedings and results of the 2011 NTHMP (National Tsunami Hazard Mitigation Program) model benchmarking workshop. Boulder: US Depart. of Commerce/NOAA/NTHMP, NOAA Special Report 436p.

Shen, J. and L. Haas (2004). Calculating age and residence time in the tidal York River using three-dimensional model experiments, Estuarine, Coastal and Shelf Science, 61, 449–461.

Simpson, J.H., Brown, J., Matthews, J. and Allen, G. (1990). Estuaries, 13: 125.

Umlauf, L. and H. Burchard (2003). A generic length-scale equation for geophysical turbulence models. J. Mar. Res., 6, pp. 235-265.

US Environmental Protection Agency, National Center for Environmental Assessment, Human Health Risk assessment research (HHRA) program. https://www.epa.gov/aboutepa/about-human-health-risk-assessment-research-hhra-program.

Zeng, X., M. Zhao and R.E. Dickinson (1998). Intercomparison of bulk aerodynamic algorithms for the computation of sea surface fluxes using TOGA COARE and TAO

 data. J. Clim., 11, pp. 2628-2644.

Zhang, Y. and Baptista, A.M. (2008a). SELFE: A semi-implicit Eulerian-Lagrangian finite-element model for cross-scale ocean circulation, Ocean Modelling, 21(3-4), 71-96.

Zhang, Y., and Baptista, A.M. (2008b). An Efficient and Robust Tsunami Model on Unstructured Grids. Part I: Inundation Benchmarks. Pure and Applied Geophysics: Topical issue on Tsunamis, vol. 165, pp. 1-20. pdf .

Zhang, Y., Witter, R.W. and Priest, G.P. (2011). Tsunami-Tide Interaction in 1964 Prince William Sound Tsunami, Ocean Modelling, 40, 246-259.

Zhang, Y., Ateljevich, E., Yu, H-C., Wu, C-H., and Yu, J.C.S. (2015). A new vertical coordinate system for a 3D unstructured-grid model, Ocean Modelling, 85, 16-31.

Zhang, Y., Ye, F., Stanev, E.V., and Grashorn, S. (2016). Seamless cross-scale modeling with SCHISM, Ocean Modelling, 102, 64-81. doi:10.1016/j.ocemod.2016.05.002.

Appendix A: Frequency distribution bar diagrams and cumulative frequency functions for various parameters under Alternatives A, B, C, and D.
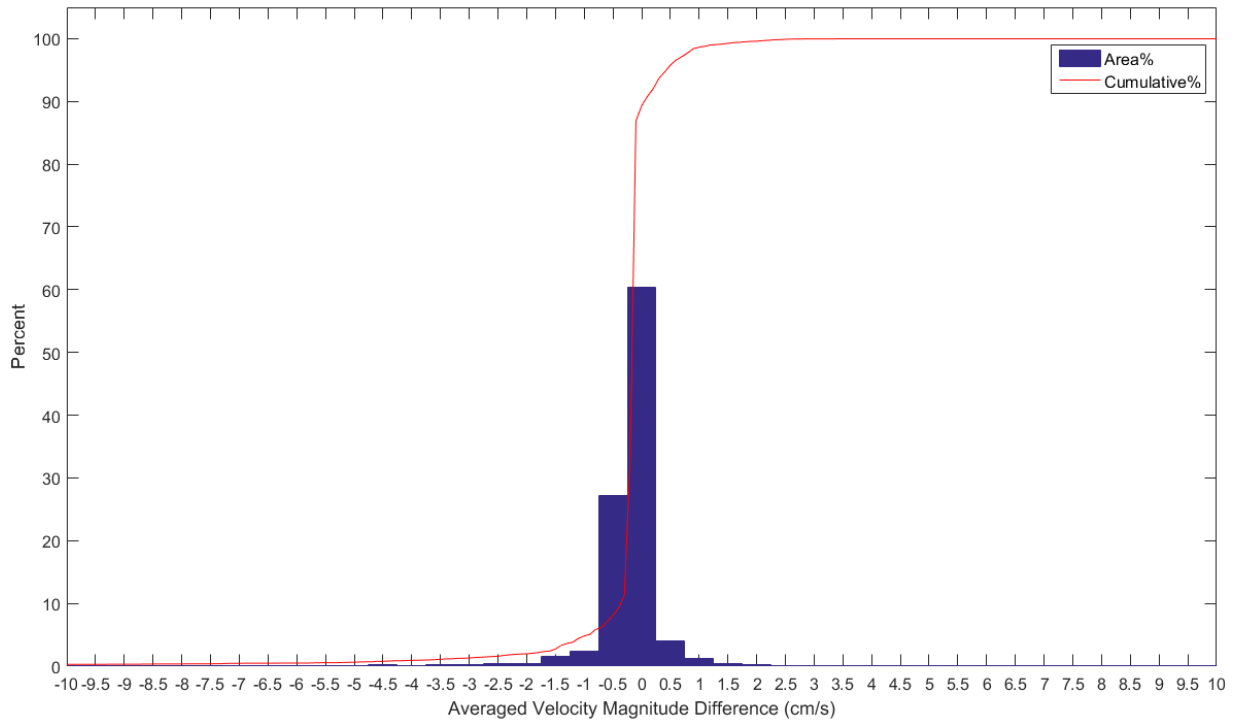
Figure A-1: The frequency distribution bar diagram of surface velocity difference for Alternative A versus the base case. The red line is the cumulative frequency function.
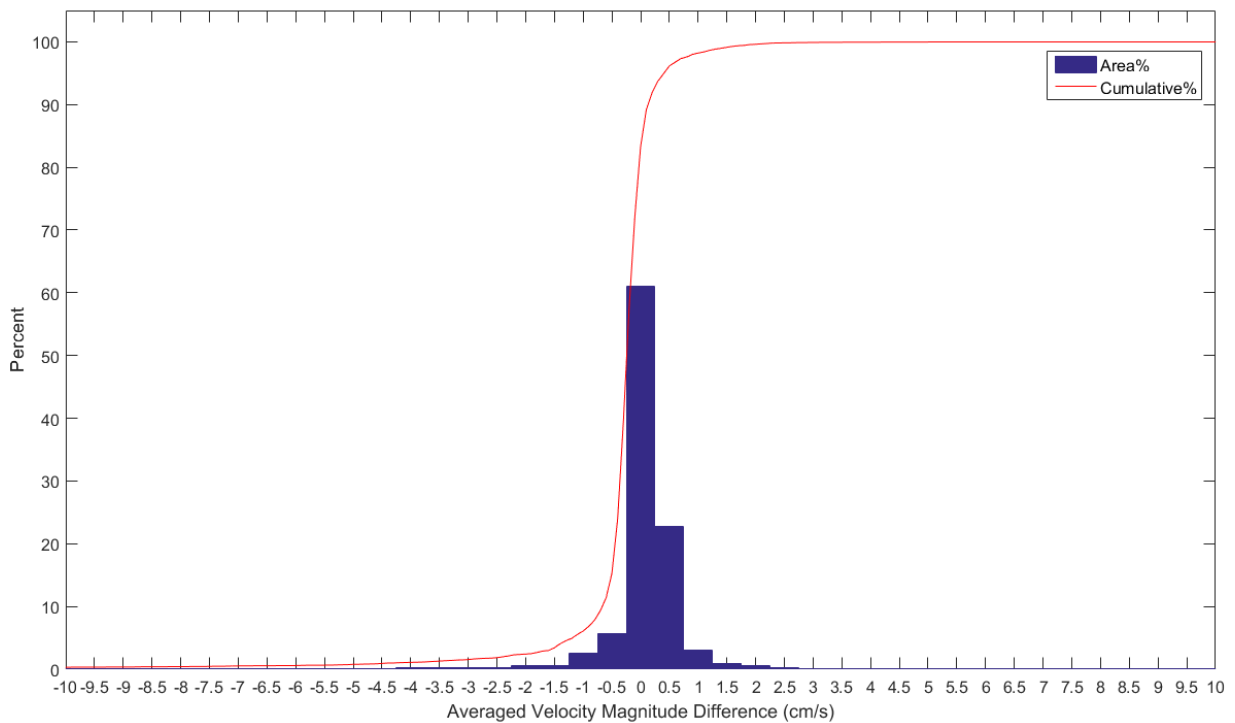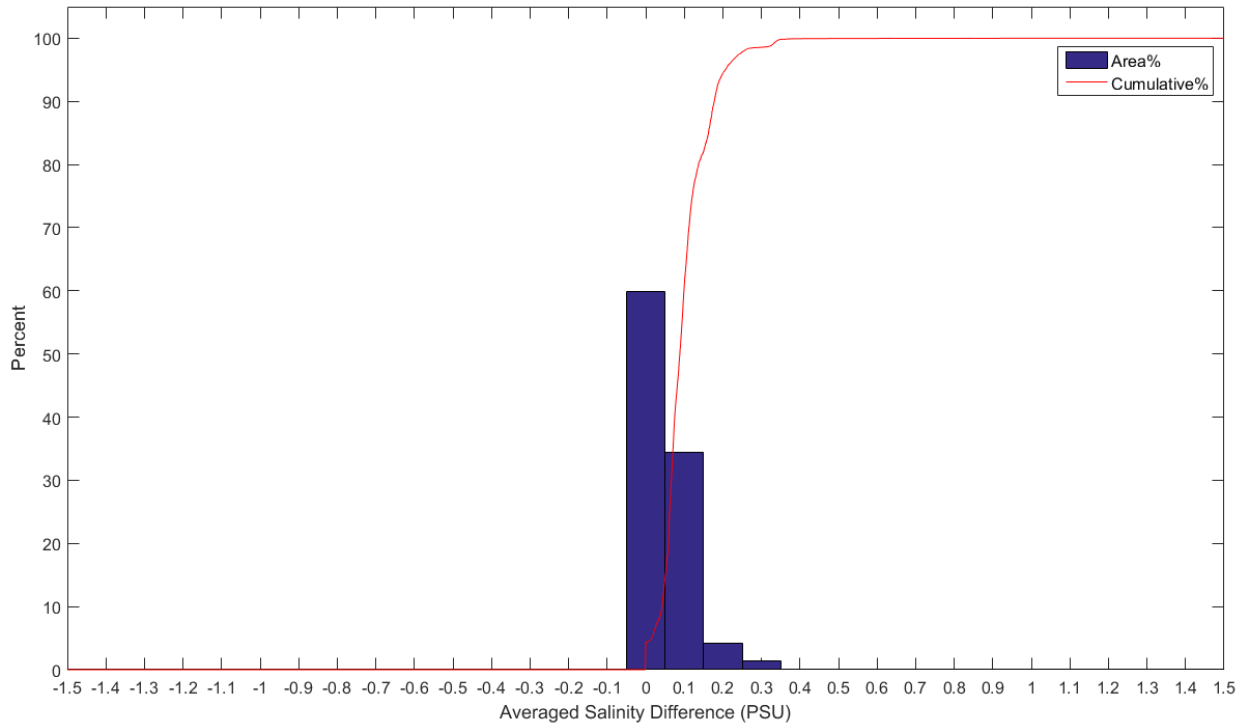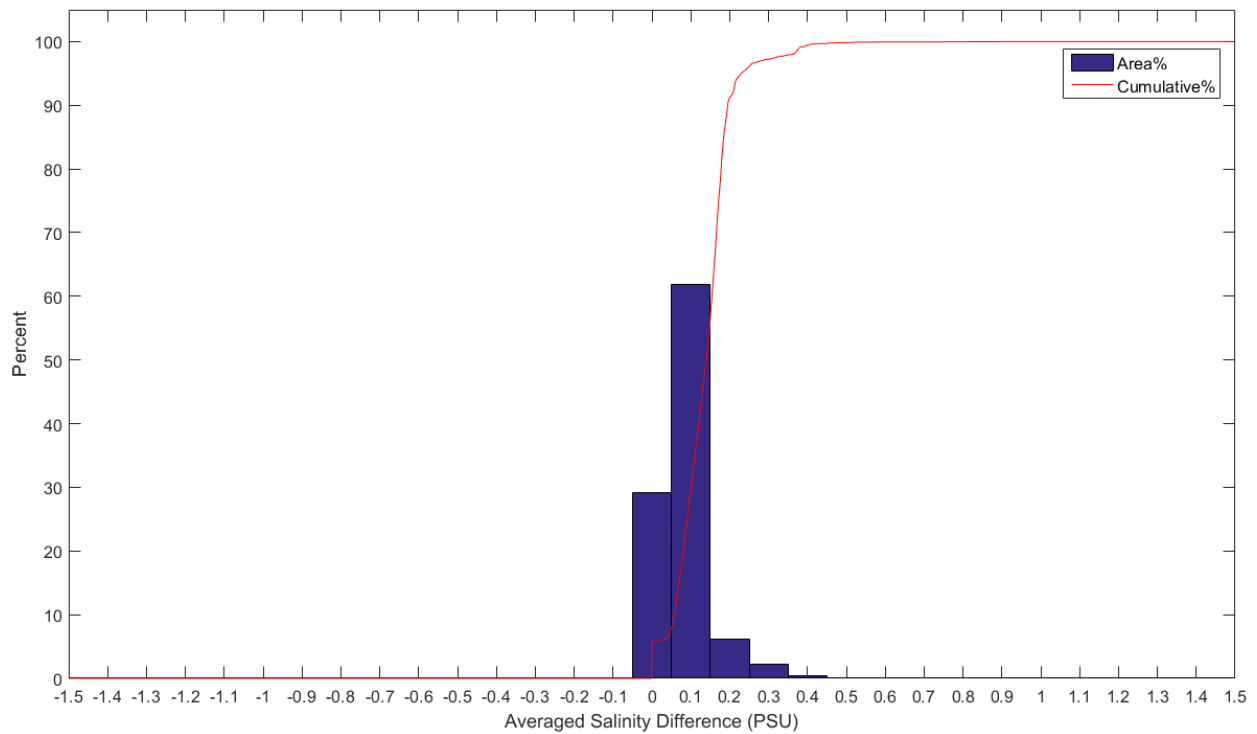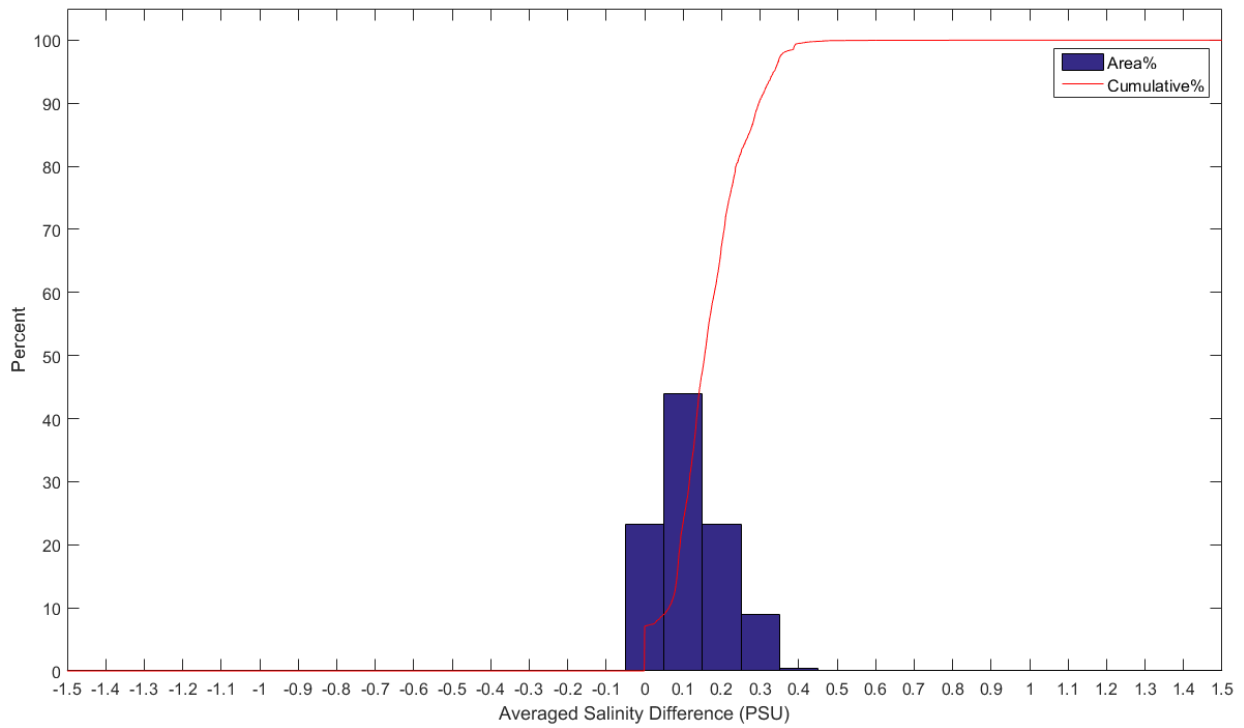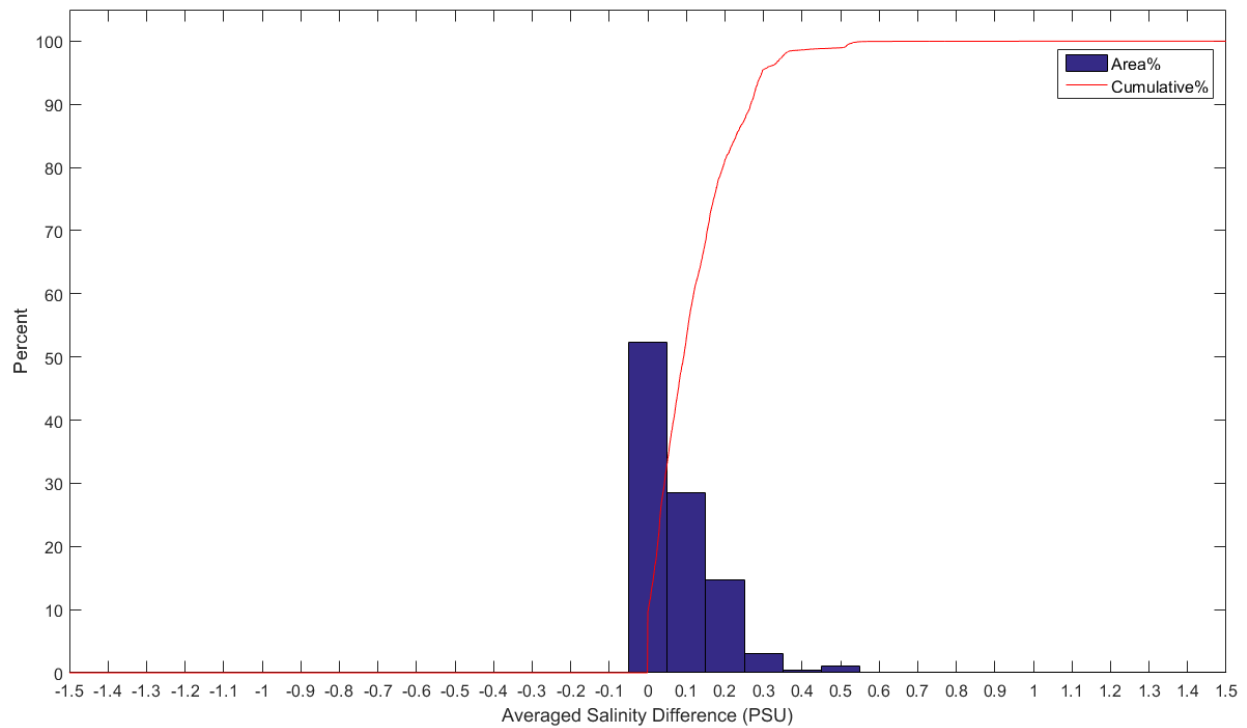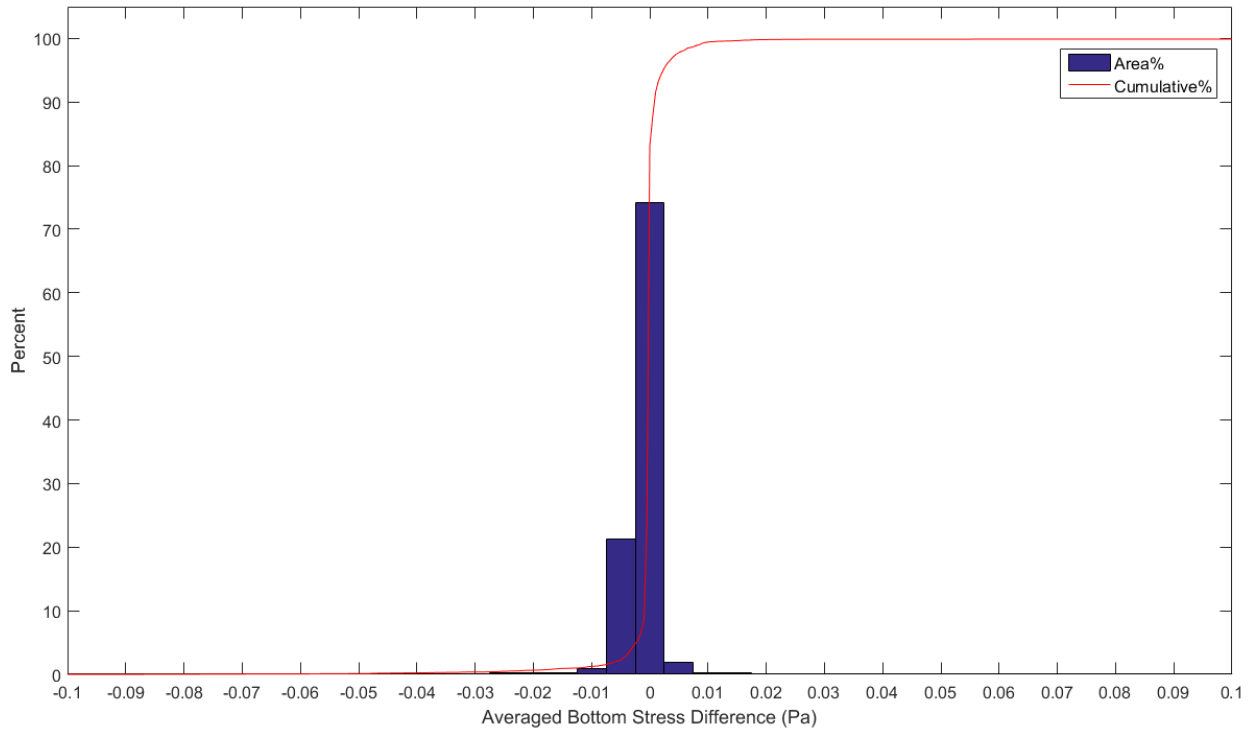

Figure A-2: The frequency distribution bar diagram of surface velocity difference for Alternative B versus the base case. The red line is the cumulative frequency function.
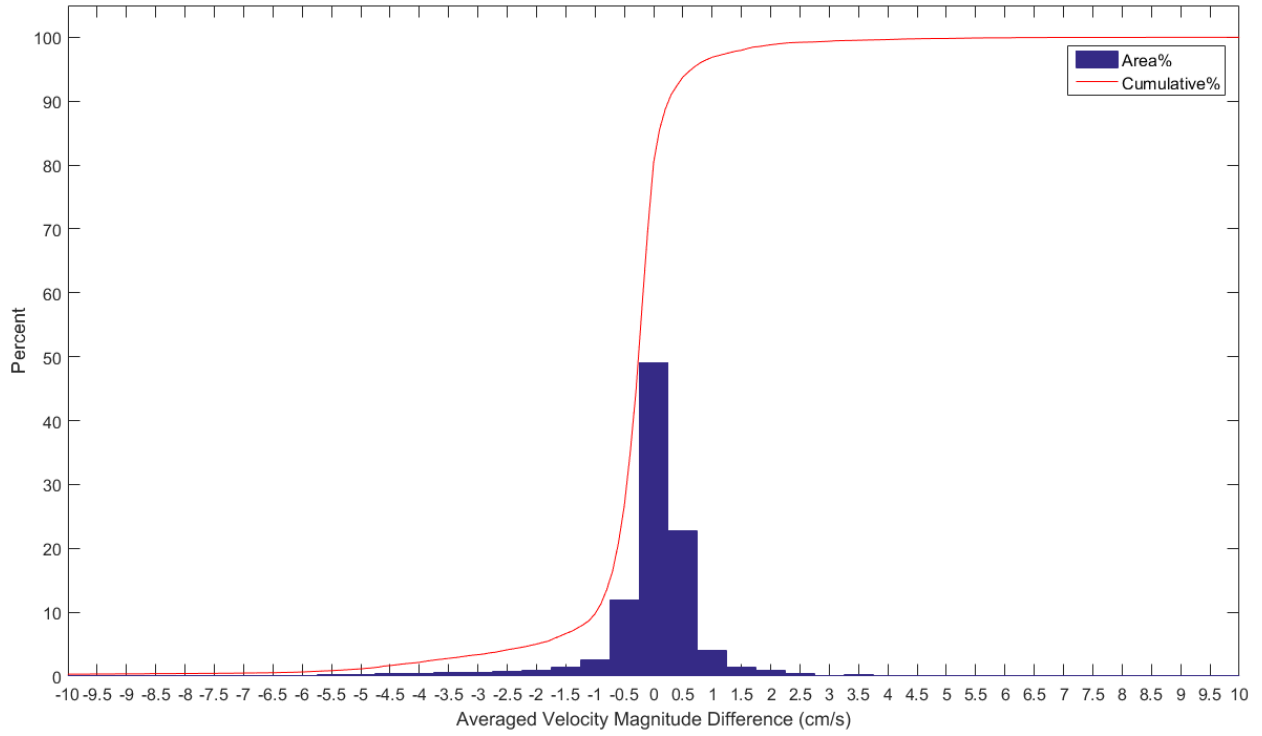
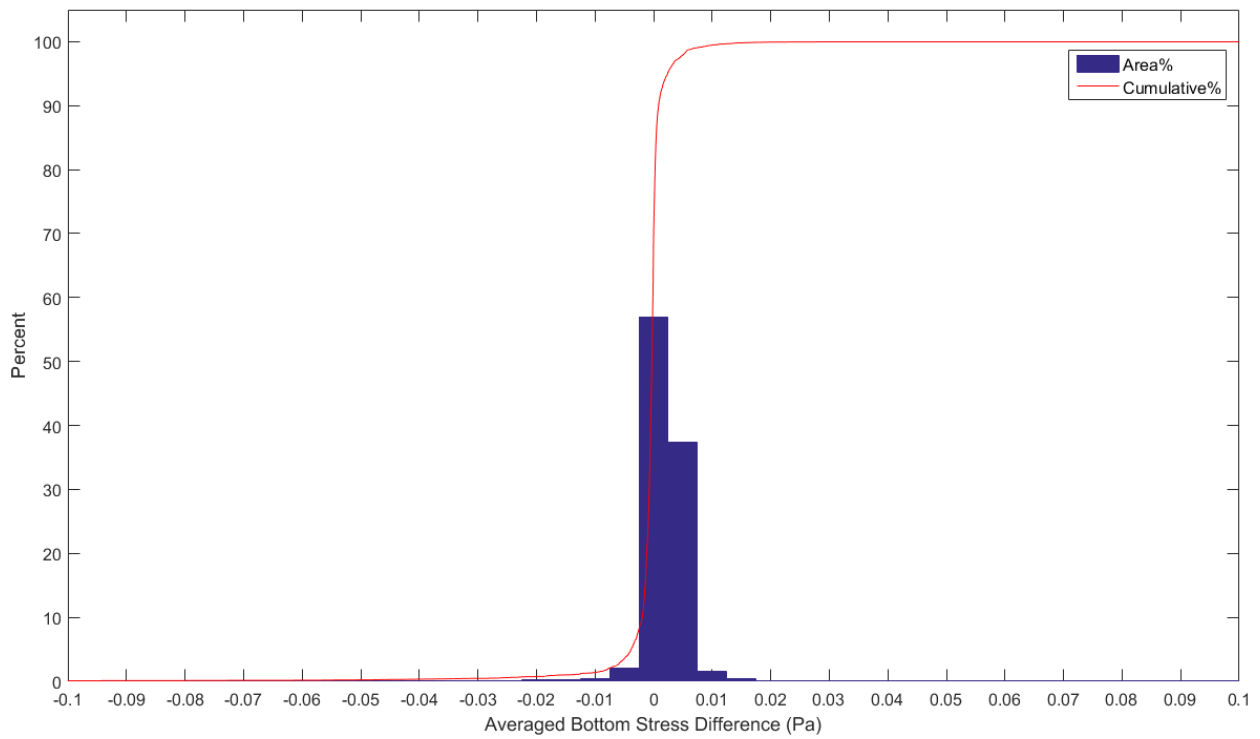Figure A-3: The frequency distribution bar diagram of surface velocity difference for Alternative C versus the base case. The red line is the cumulative frequency function.
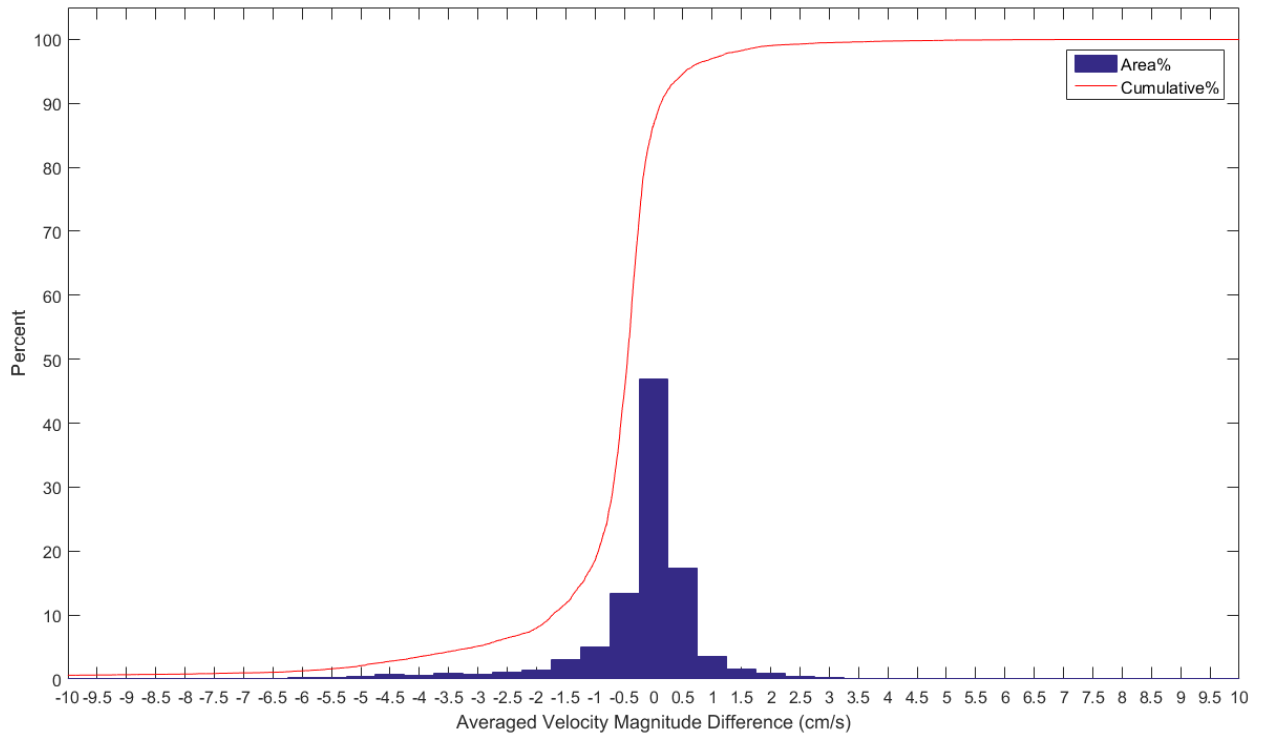
Figure A-4: The frequency distribution bar diagram of surface velocity difference for Alternative D versus the base case. The red line is the cumulative frequency function.

A2
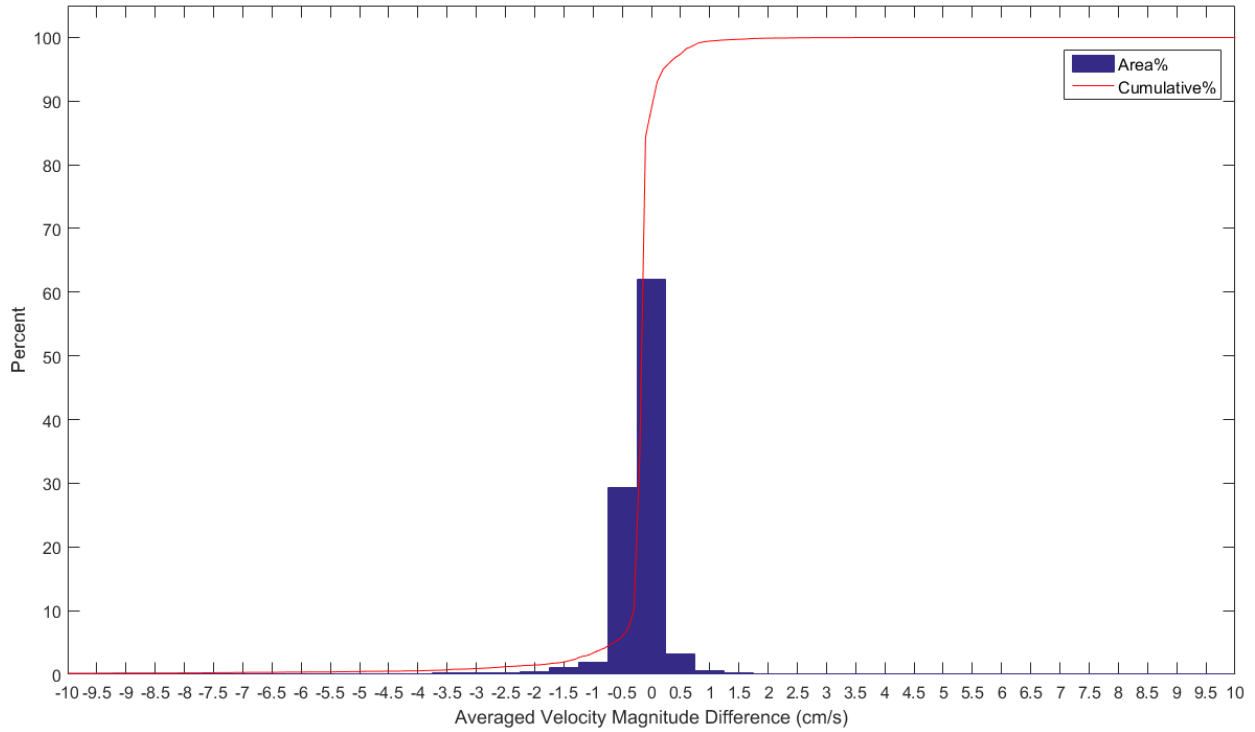
Figure A-5: The frequency distribution bar diagram of bottom velocity difference for Alternative A versus the base case. The red line is the cumulative frequency function.
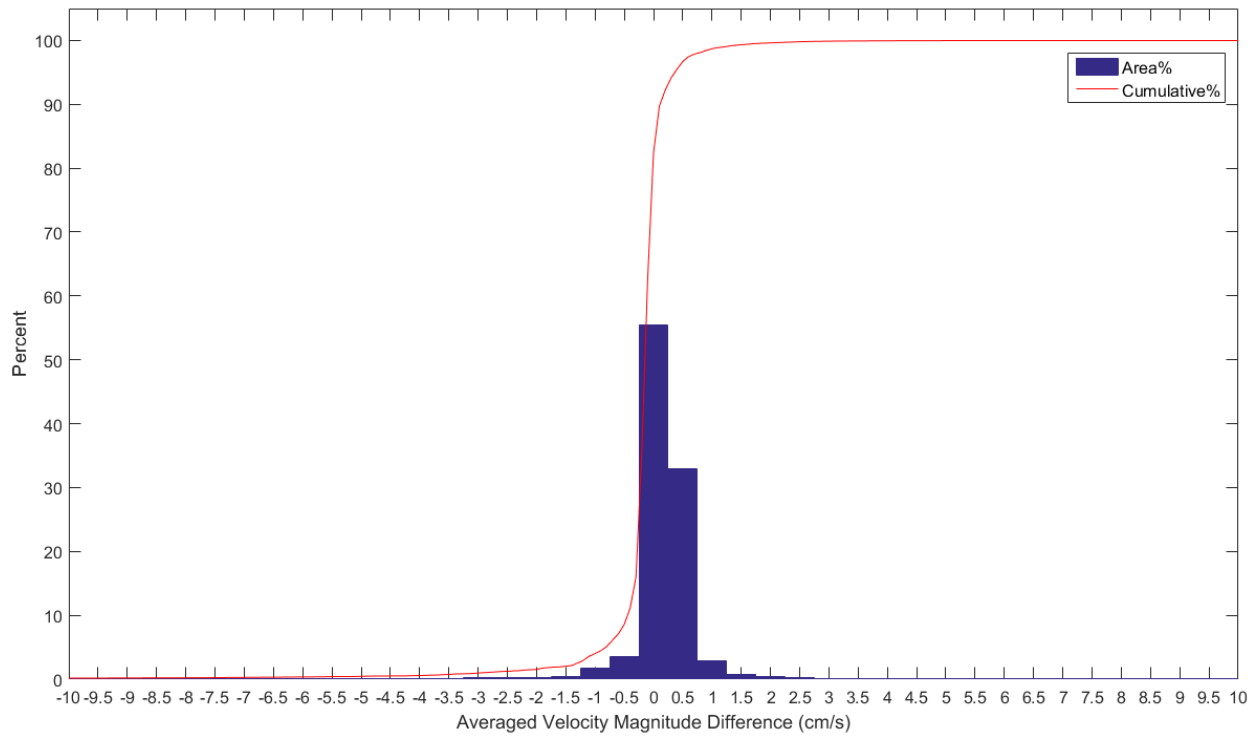
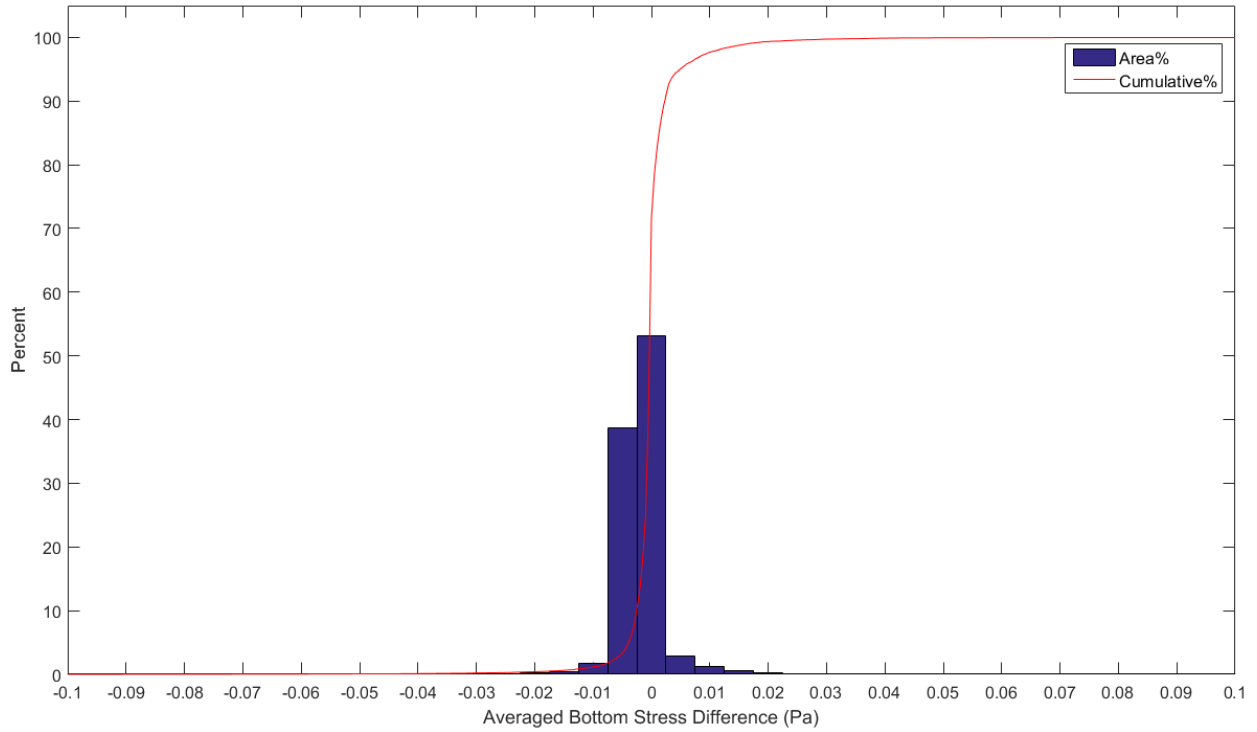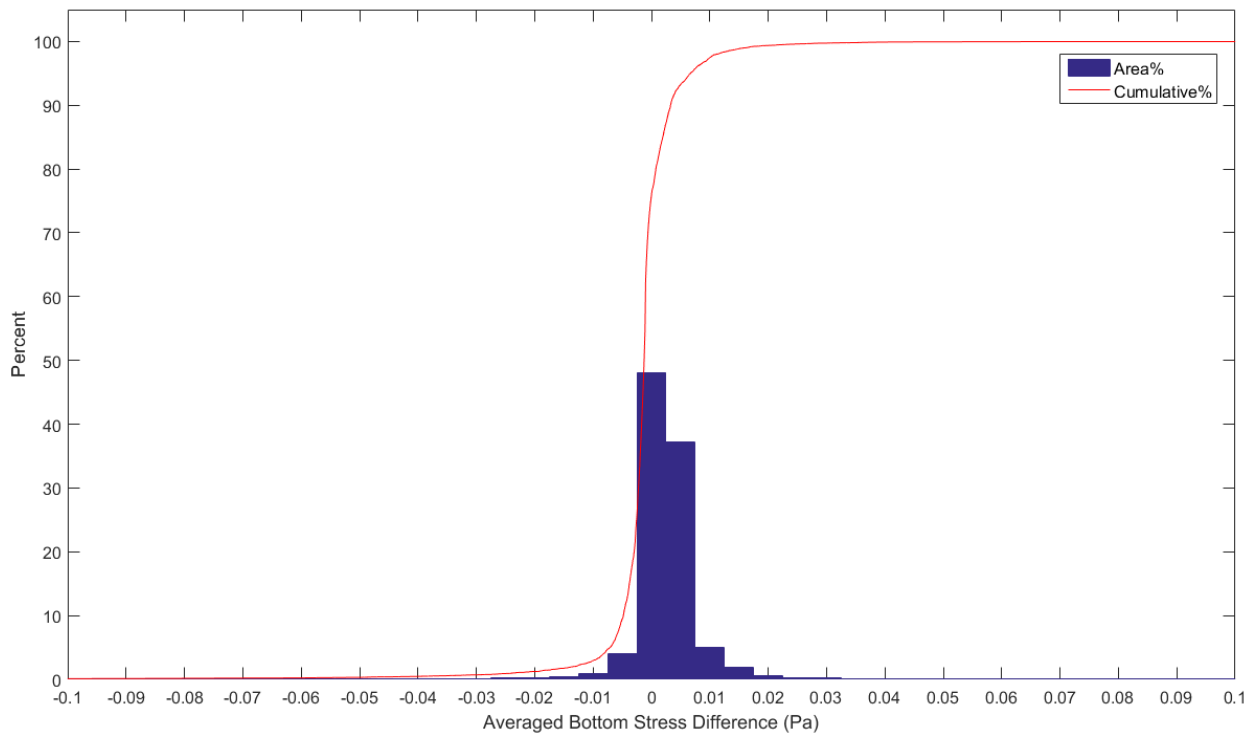Figure A-6: The frequency distribution bar diagram of bottom velocity difference for Alternative B versus the base case. The red line is the cumulative frequency function.
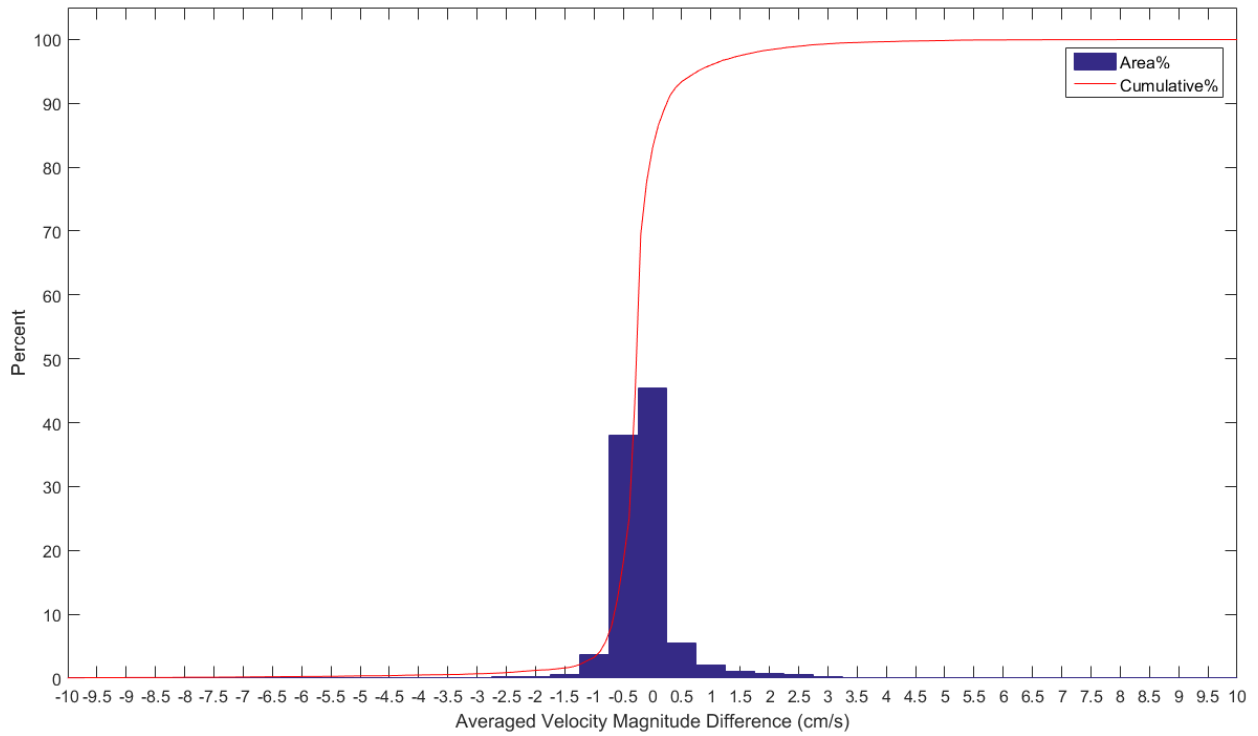
Figure A-7: The frequency distribution bar diagram of bottom velocity difference for Alternative C versus the base case. The red line is the cumulative frequency function.
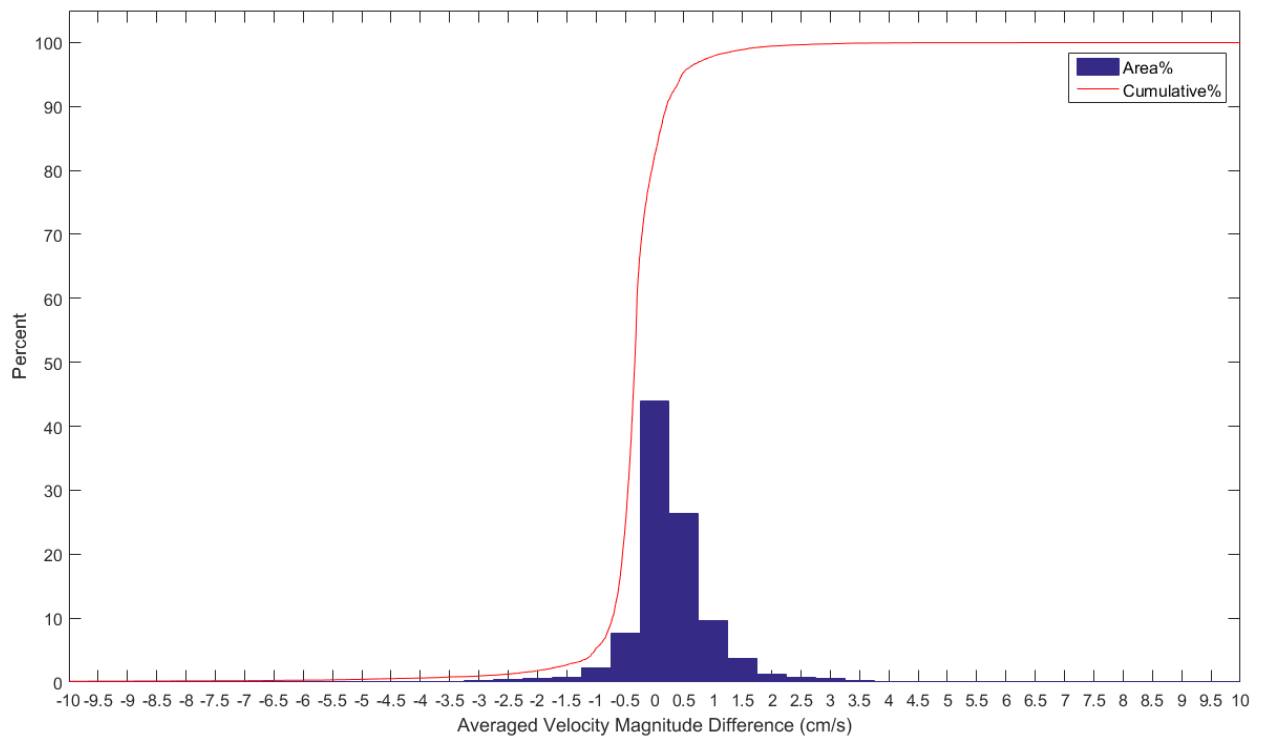
Figure A-8: The frequency distribution bar diagram of bottom velocity difference for Alternative D versus the base case. The red line is the cumulative frequency function.
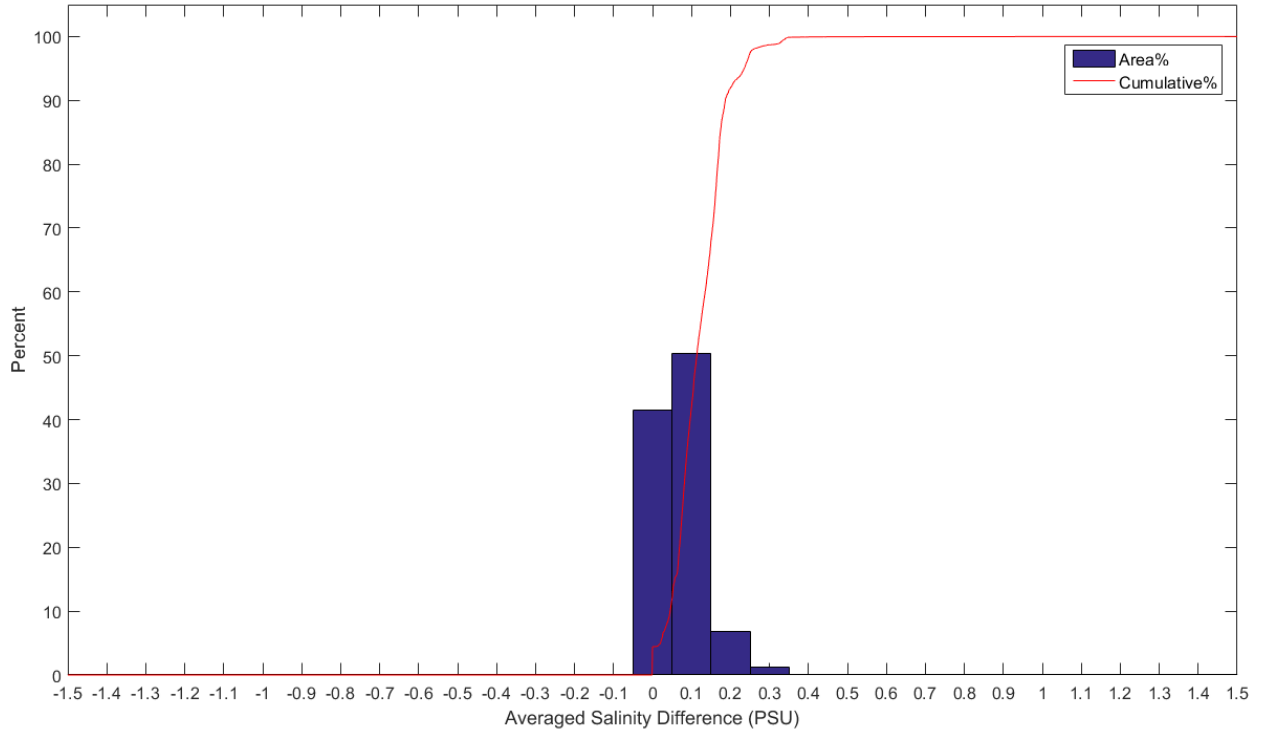
Figure A-9: The frequency distribution bar diagram of surface salinity difference for Alternative A versus the base case. The red line is the cumulative frequency function.
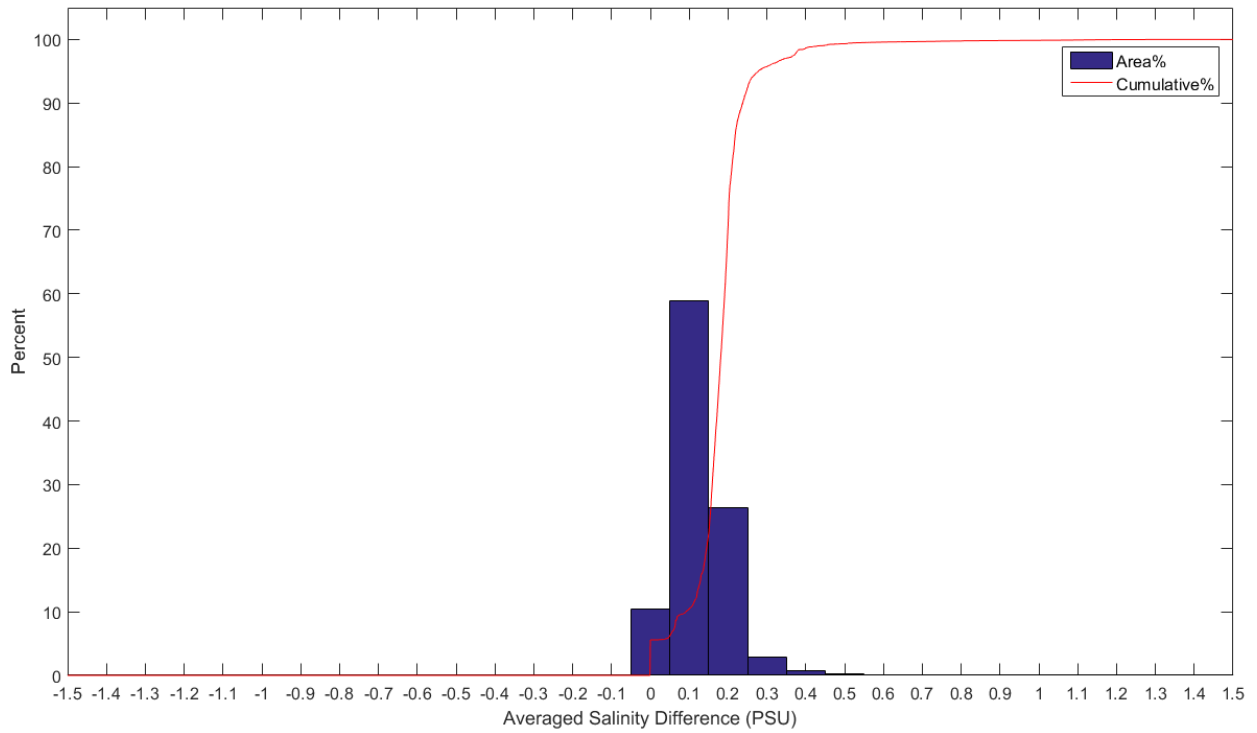
Figure A-10: The frequency distribution bar diagram of surface salinity difference for Alternative B versus the base case. The red line is the cumulative frequency function.
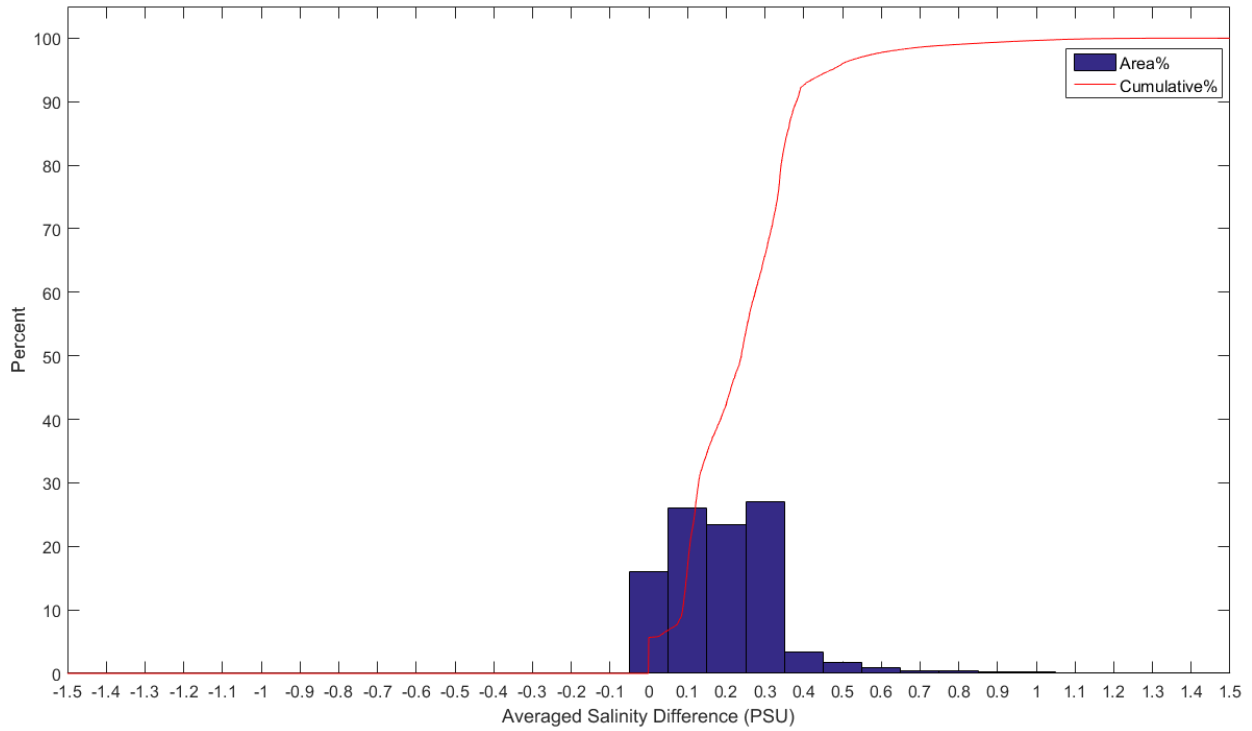
Figure A-11: The frequency distribution bar diagram of surface salinity difference for Alternative C versus the base case. The red line is the cumulative frequency function.
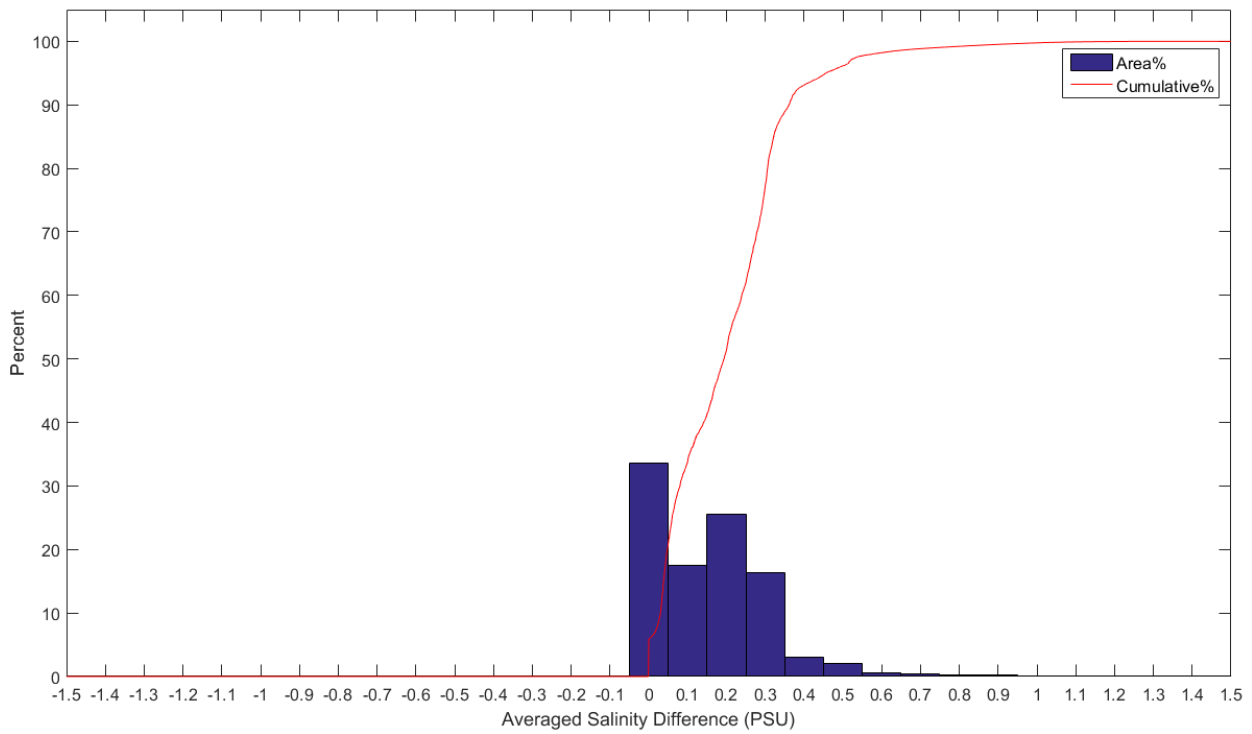
Figure A-12: The frequency distribution bar diagram of surface salinity difference for Alternative D versus the base case. The red line is the cumulative frequency function.

Figure A-13: The frequency distribution bar diagram of bottom salinity difference for Alternative A versus the base case. The red line is the cumulative frequency function.

Figure A-14: The frequency distribution bar diagram of bottom salinity difference for Alternative B versus the base case. The red line is the cumulative frequency function.

Figure A-15: The frequency distribution bar diagram of bottom salinity difference for Alternative C versus the base case. The red line is the cumulative frequency function.

Figure A-16: The frequency distribution bar diagram of bottom salinity difference for Alternative D versus the base case. The red line is the cumulative frequency function.

Figure A-17: The frequency distribution bar diagram of bottom shear stress difference for Alternative A versus the base case. The red line is the cumulative frequency function.

Figure A-18: The frequency distribution bar diagram of bottom shear stress difference for Alternative B versus the base case. The red line is the cumulative frequency function.

Figure A-19: The frequency distribution bar diagram of bottom shear stress difference for Alternative C versus the base case. The red line is the cumulative frequency function.

Figure A-20: The frequency distribution bar diagram of bottom shear stress difference for Alternative D versus the base case. The red line is the cumulative frequency function.
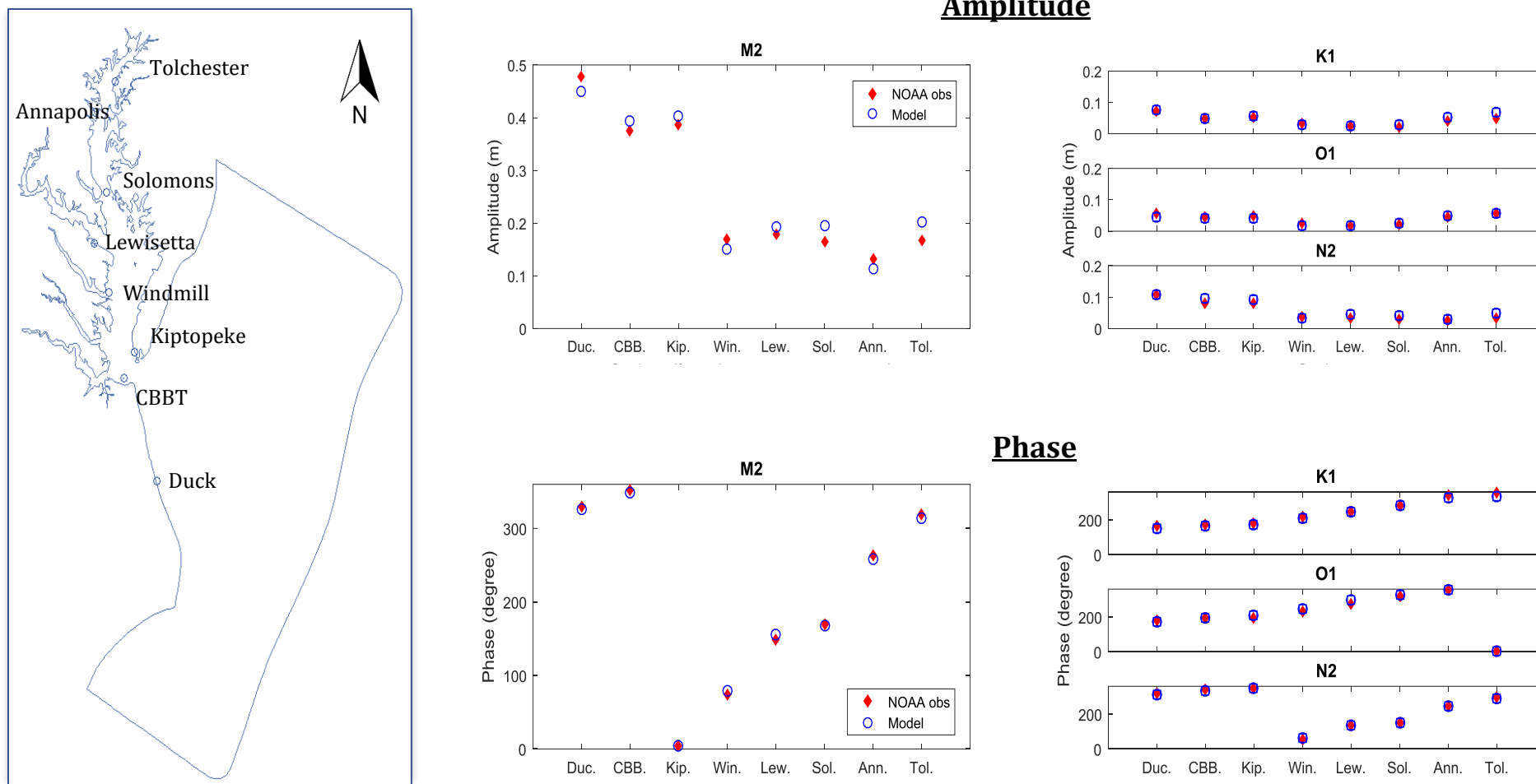
Figure B-1: The harmonic analysis of 2010 water level for NOAA stations located in the Chesapeake Bay and Duck, NC.
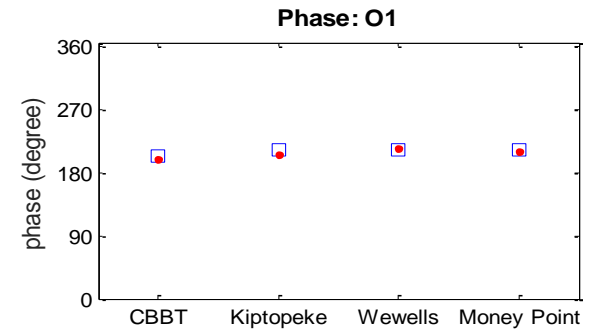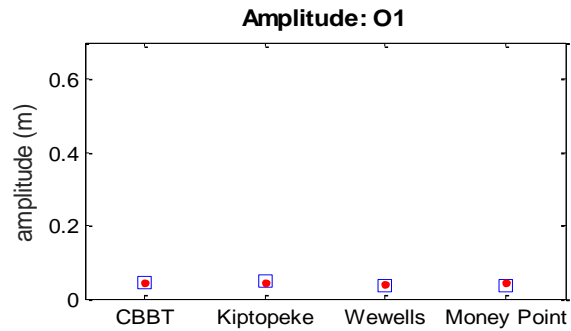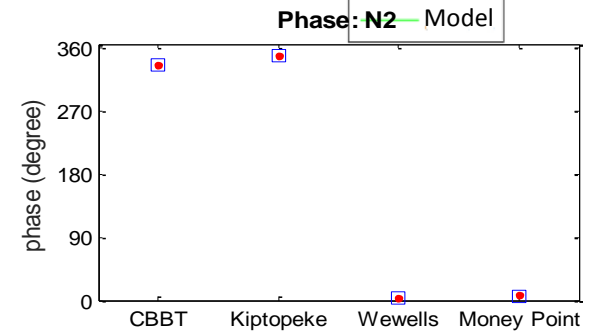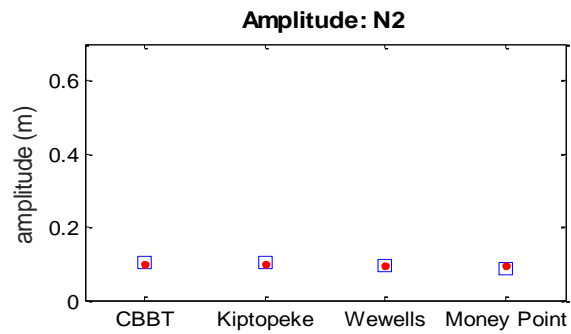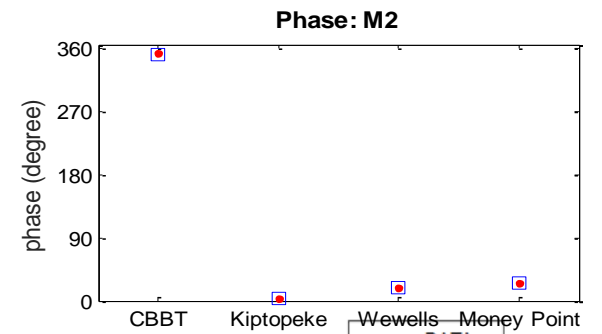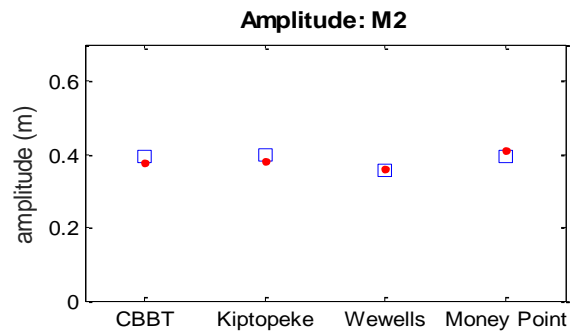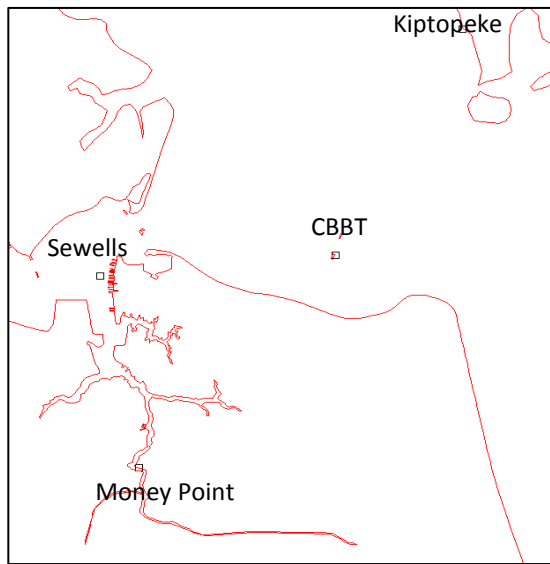
Figure B-2: The harmonic analysis of 2010 water level for NOAA stations in the lower Chesapeake Bay
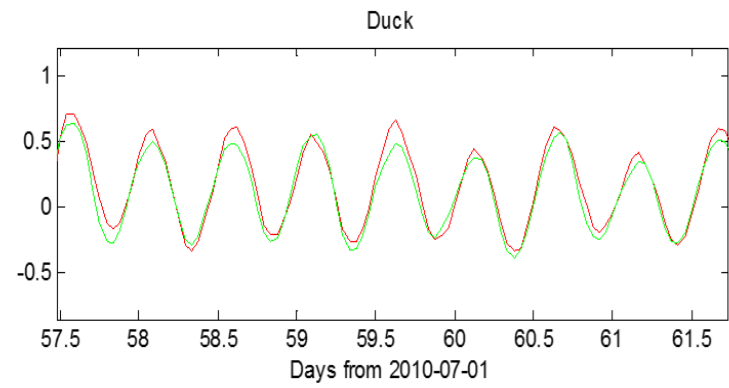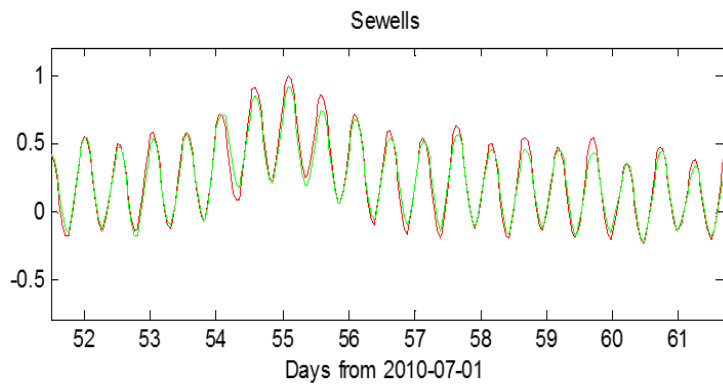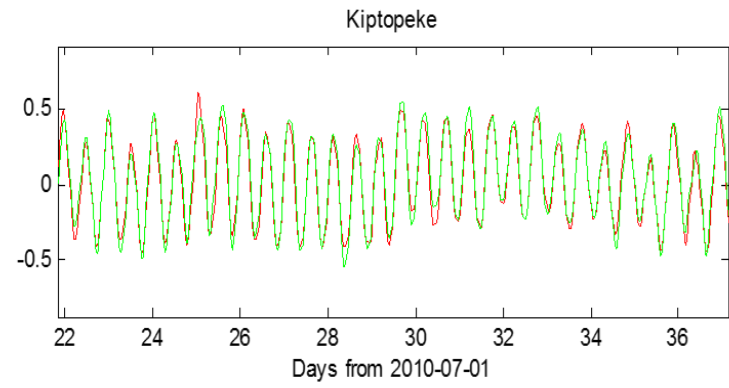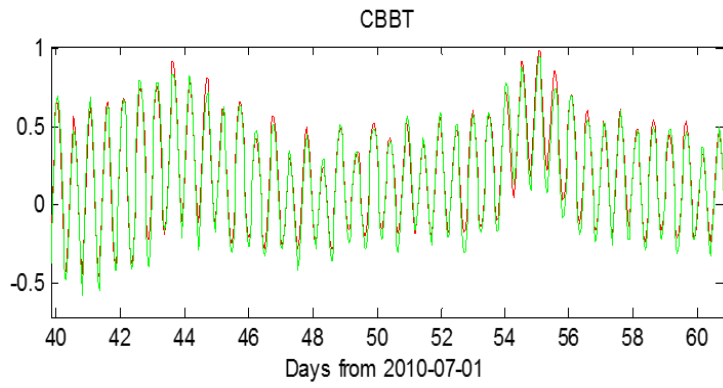
Figure B-3: The comparison between modeled versus observed real water level in the lower Chesapeake Bay and Duck, NC, summer 2010.
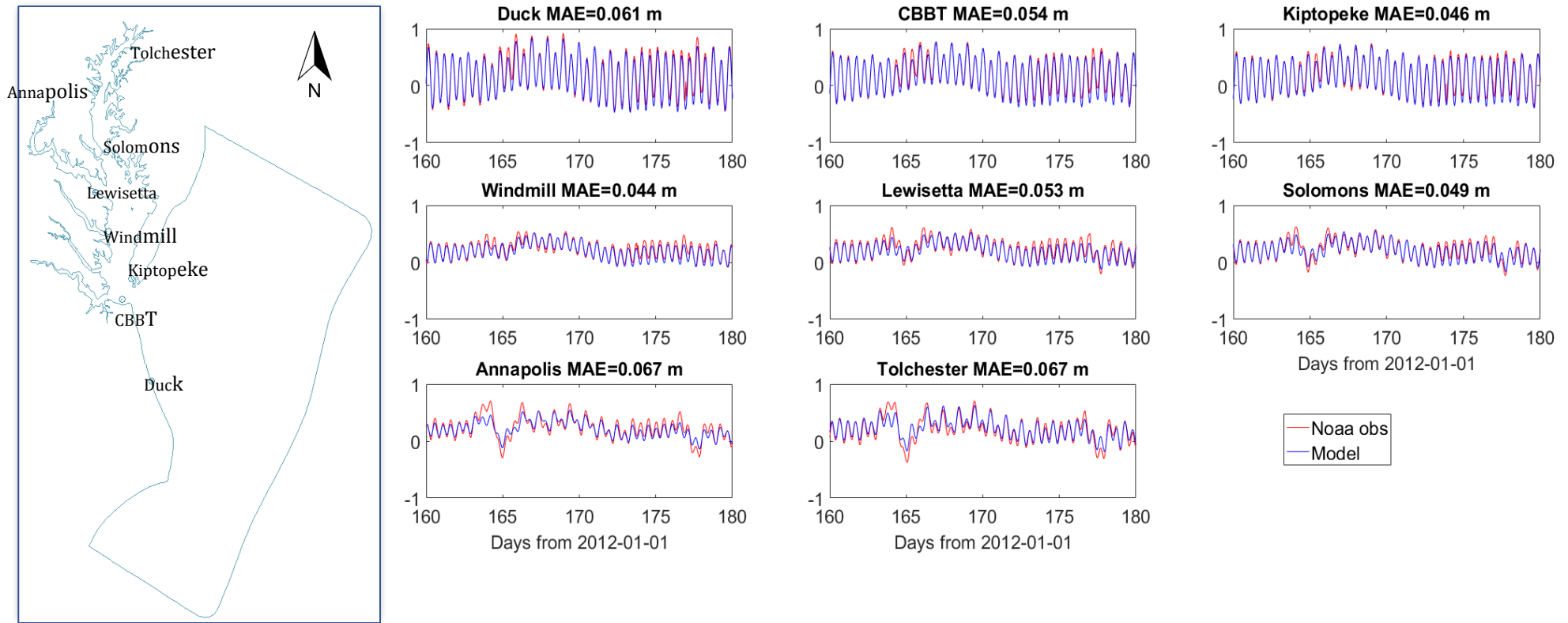
Figure B-4: The comparison between modeled versus observed real water level in the Chesapeake Bay and Duck, NC, spring 2012

ADCP velocity measurements

(Station location)
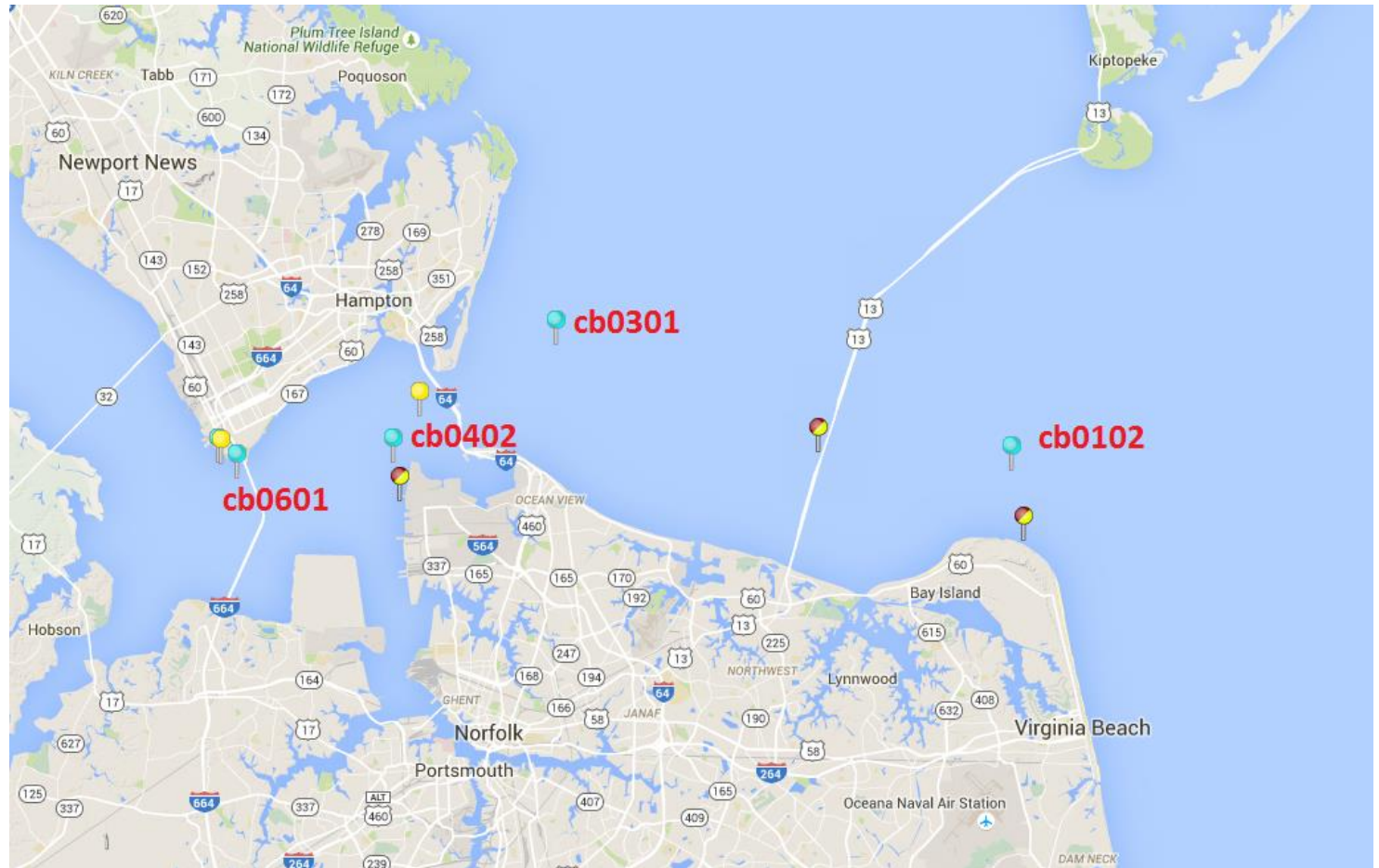
Figure B-5:   The NOAA ADCP current profile station locations in the lower Chesapeake Bay
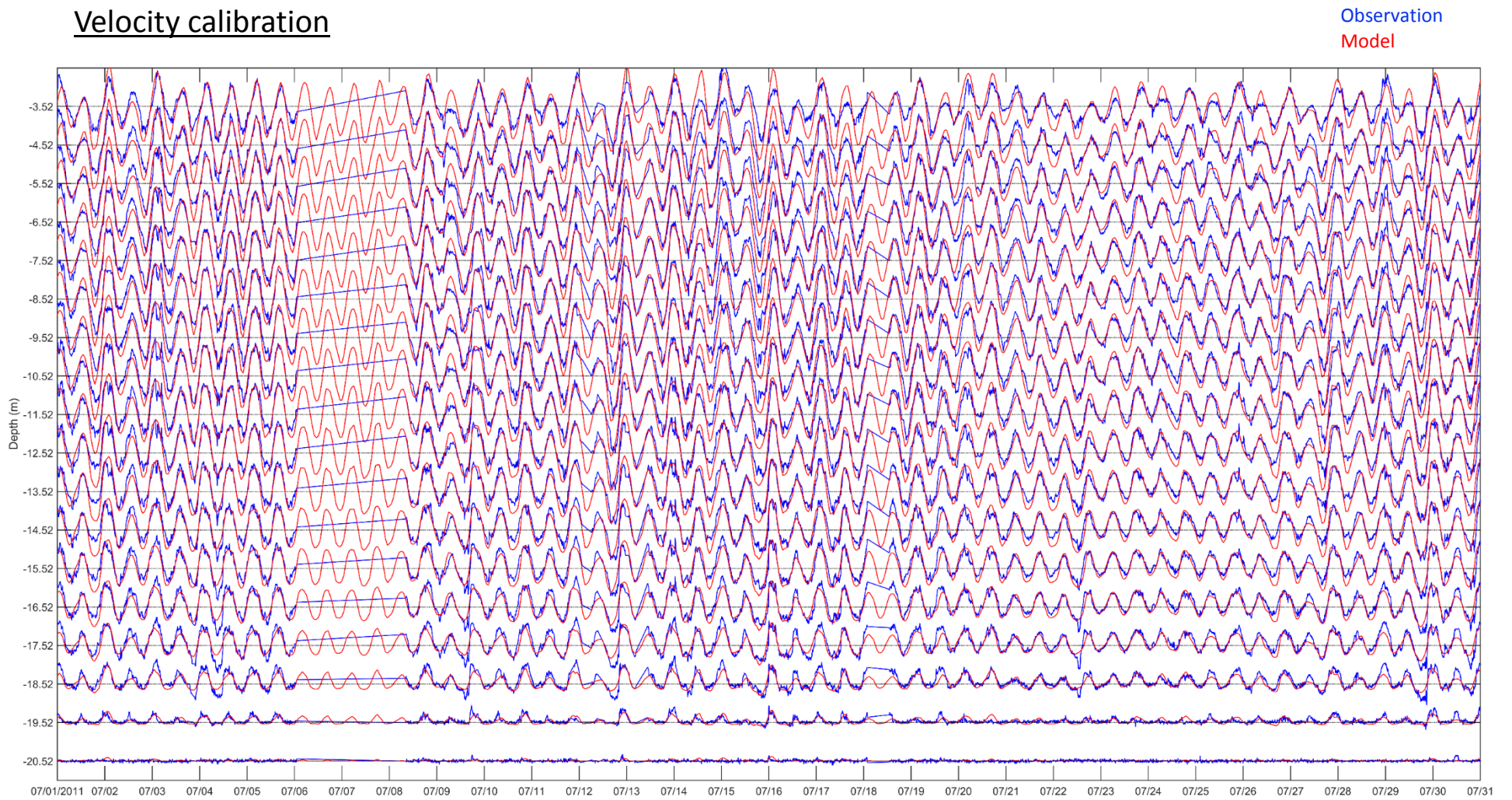
Figure B-6: Modeled versus observed velocity profile in July, 2011 at station CB0102
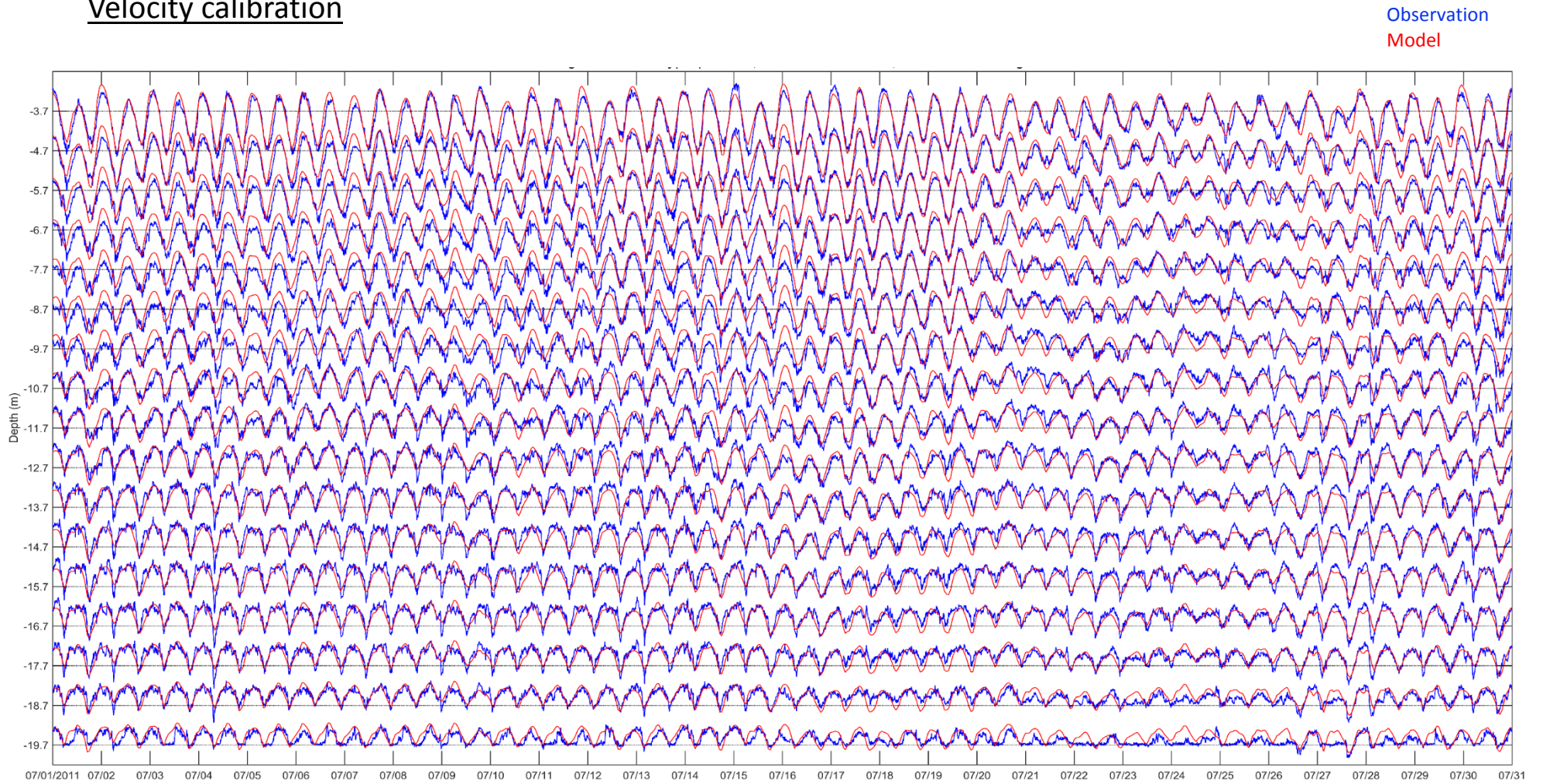
Figure B-7: Modeled versus observed velocity profile in July, 2011 at station CB0301

Velocity calibration
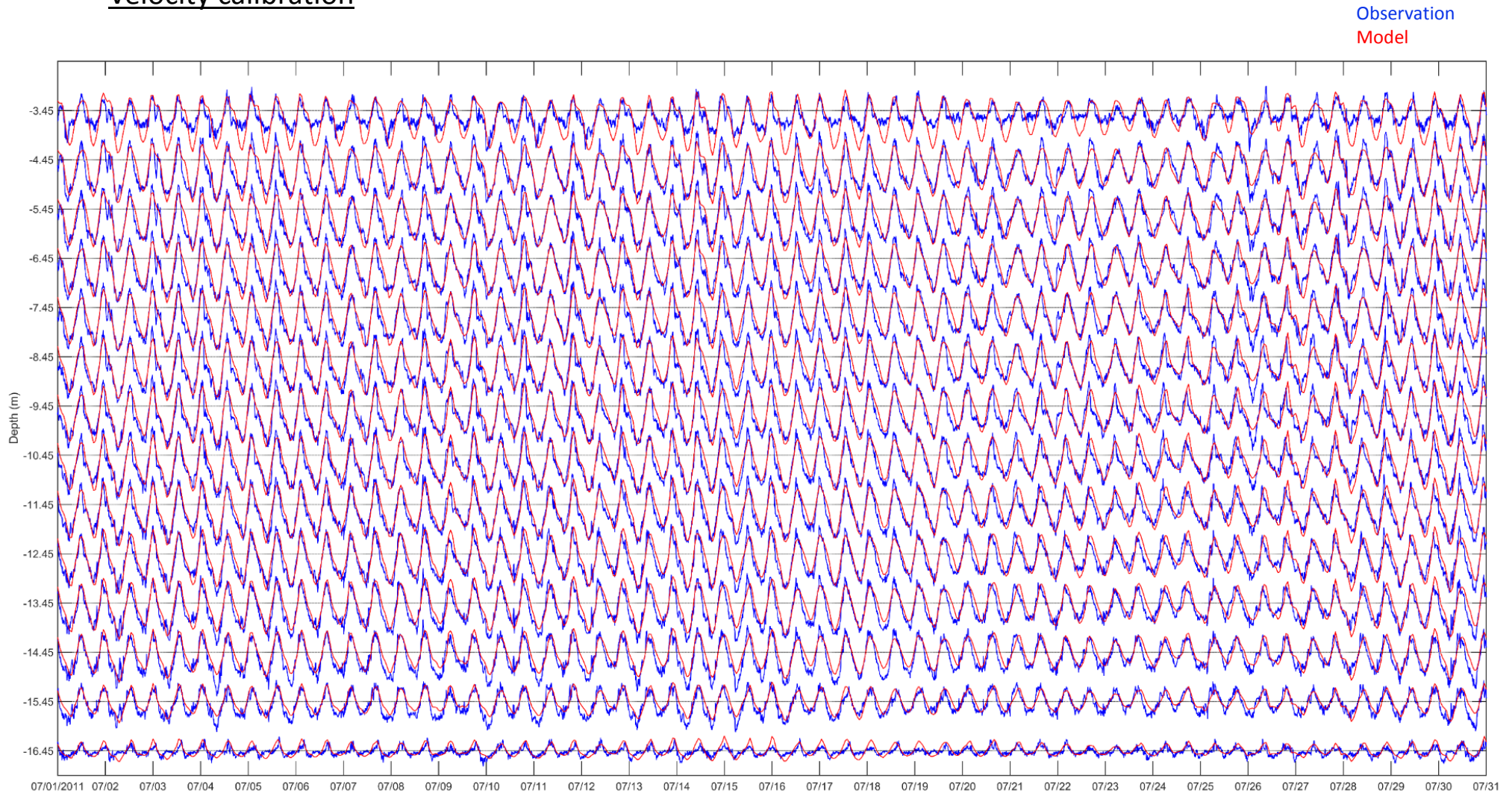
Figure B-8:   Modeled versus observed velocity profile in July, 2011 at station CB0402

Velocity calibration
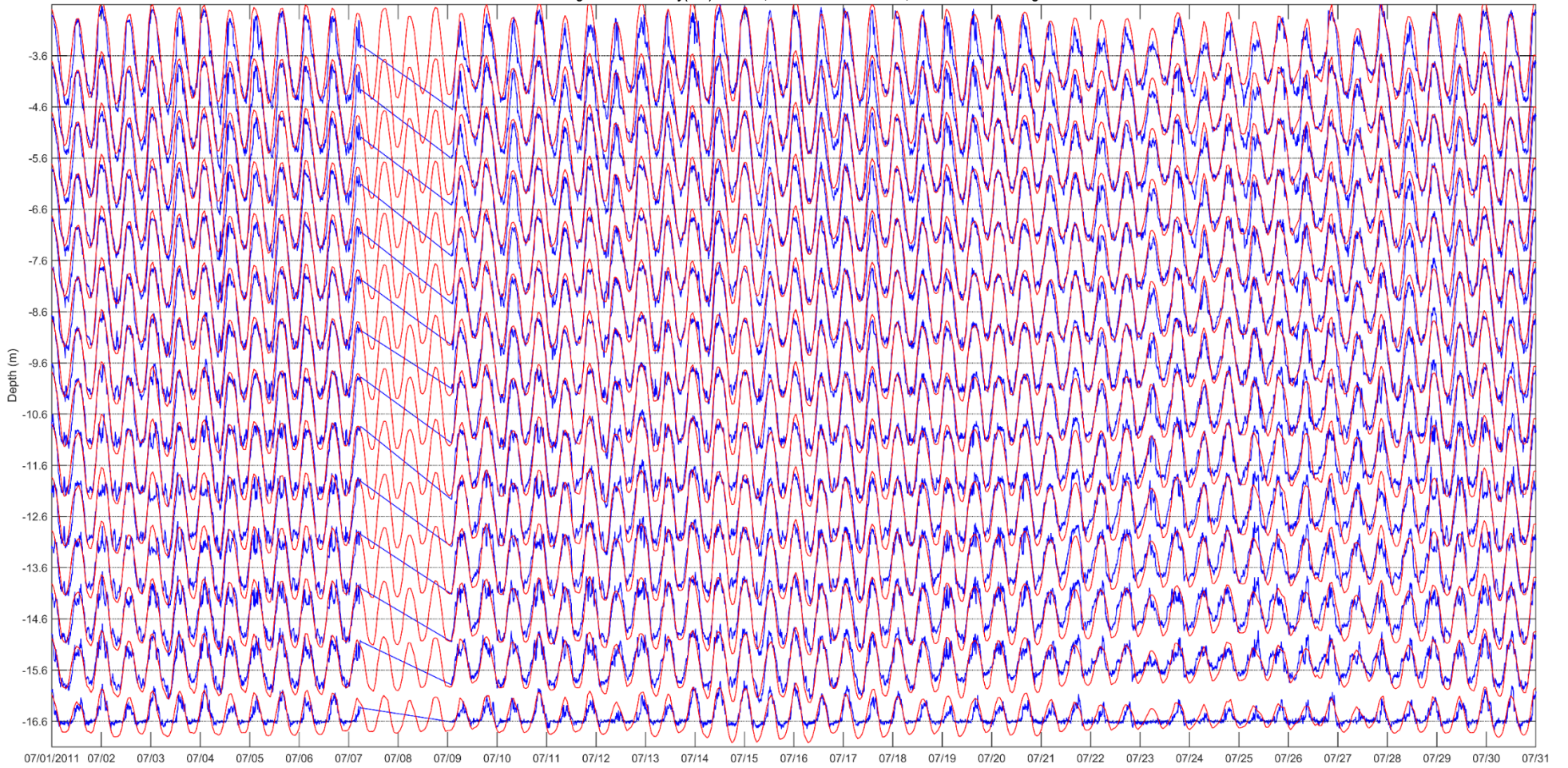
Figure B-9:   Modeled versus observed velocity profile in July, 2011 at station CB0601
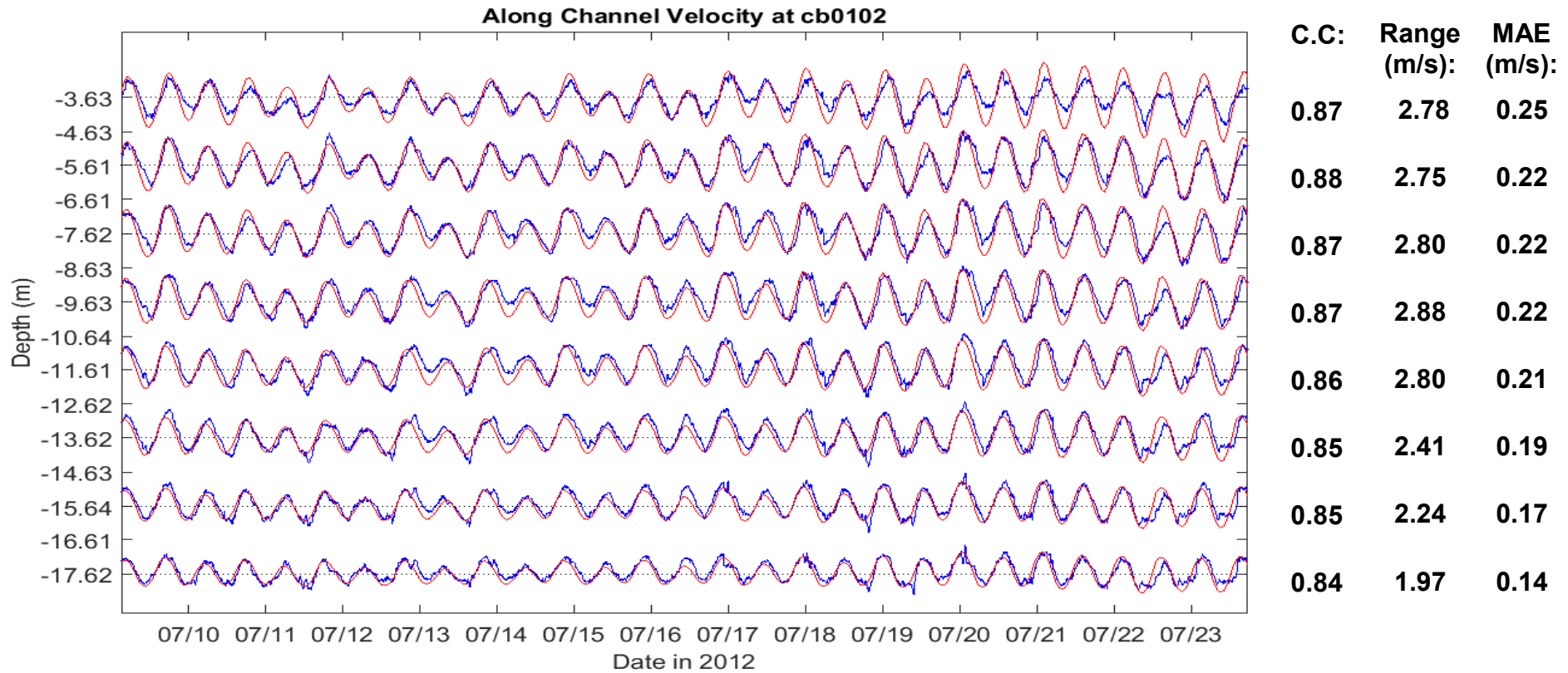
Velocity calibration

Statistics (July, 2012)

Along Channel Velocity at cb0102

C.C:	Range (m/s):	MAE (m/s):
0.87	2.78	0.25
0.88	2.75	0.22
0.87	2.80	0.22
0.87	2.88	0.22
0.86	2.80	0.21
0.85	2.41	0.19
0.85	2.24	0.17
0.84	1.97	0.14

Figure B-10: The modeled versus observed velocity profile in July, 2012 at station CB0102 and the statistical comparison in CC (correlation coefficient) and MAE (mean absolute error).

B10

Salinity and temperature measurement

(Station location)
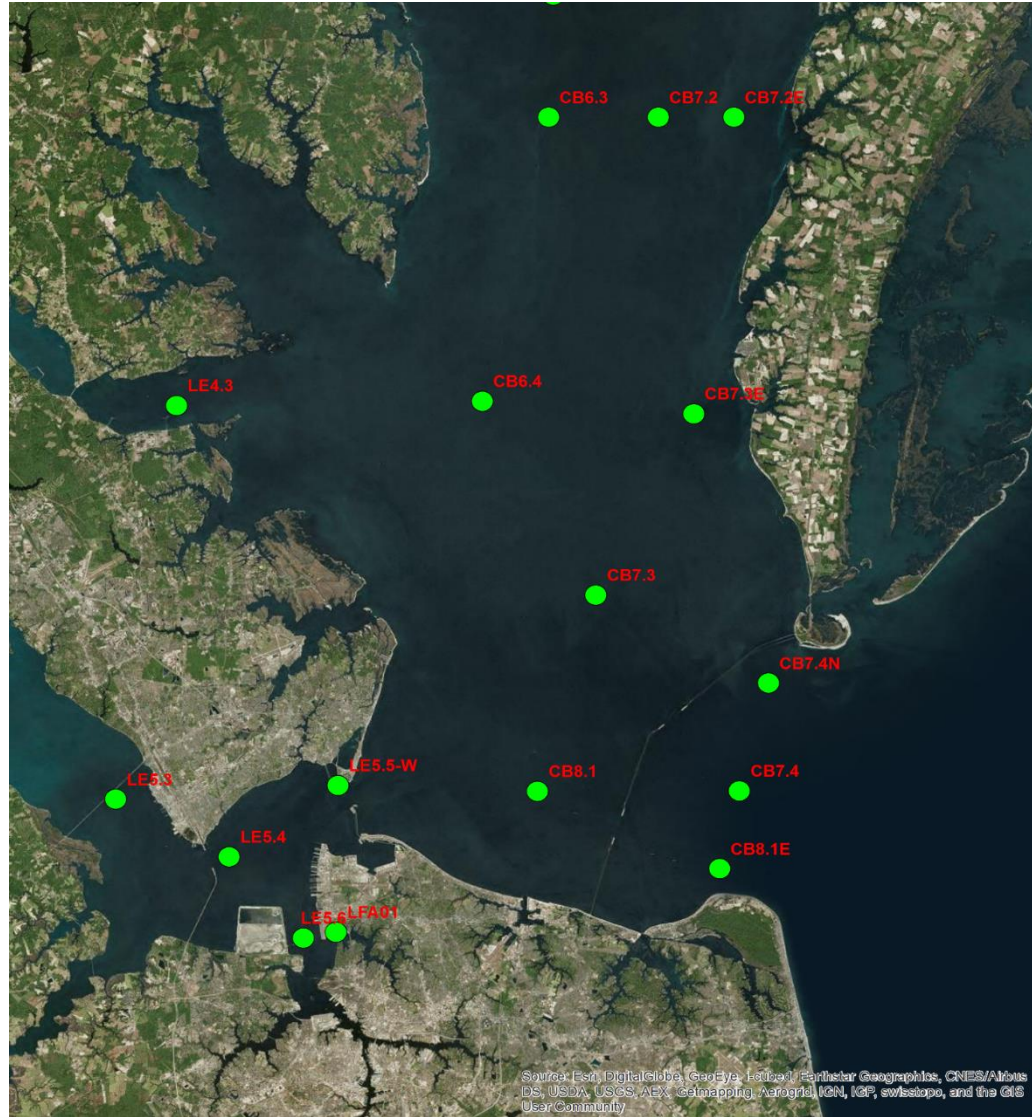
Figure B-11: The station locations for EPA Chesapeake Bay Program salinity and temperature monitoring program in the lower Chesapeake Bay
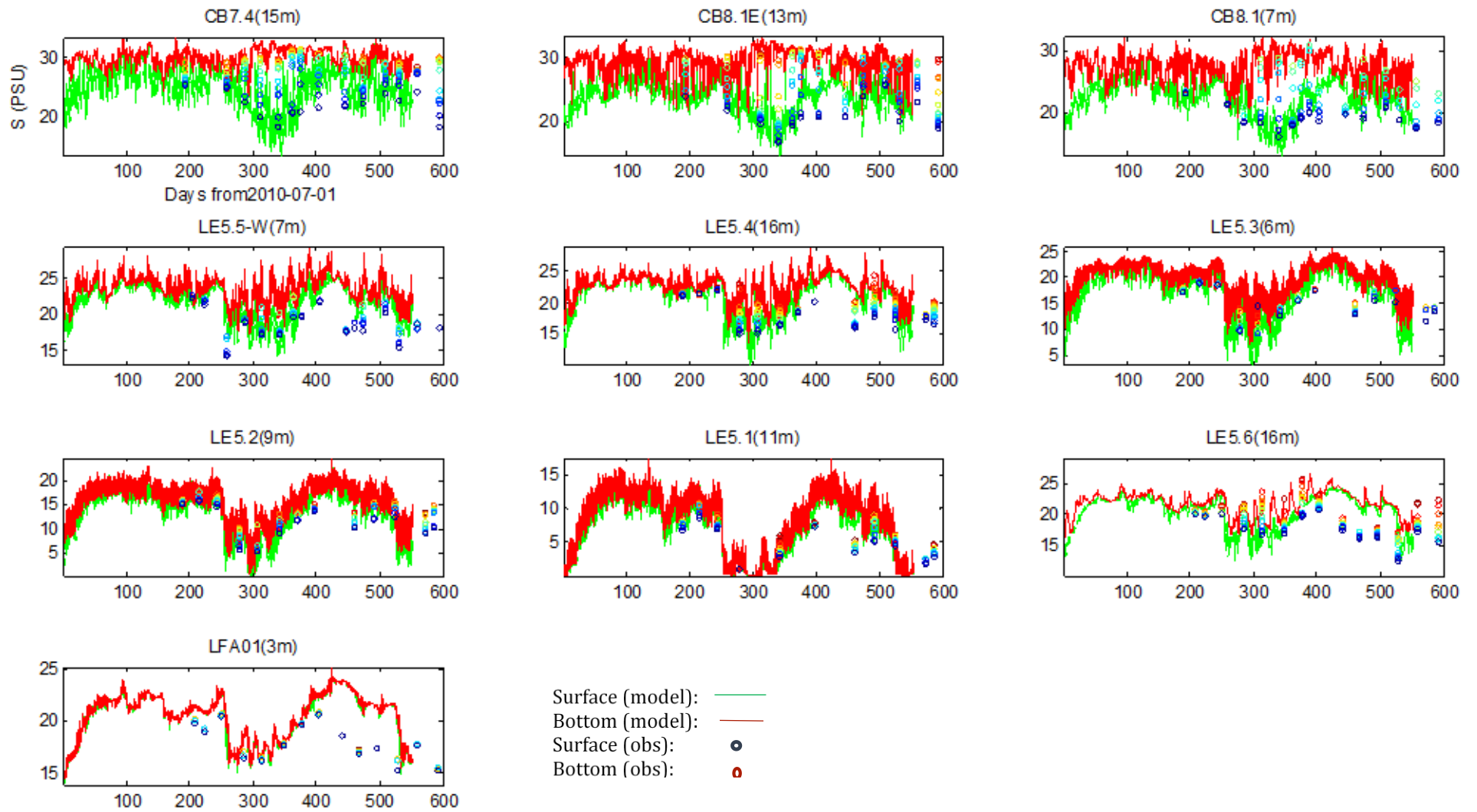
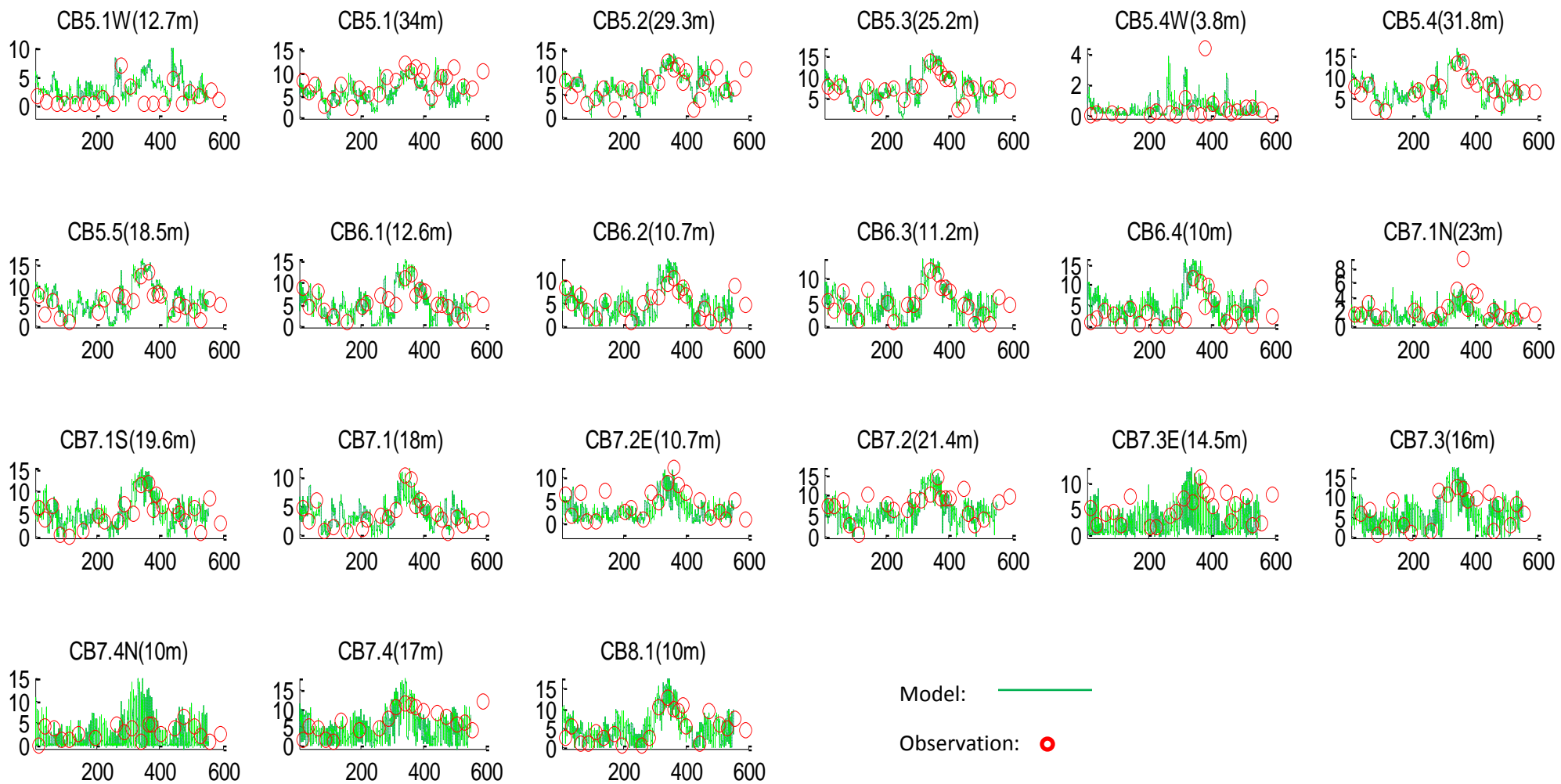Figure B-12: Comparison of modeled versus observed surface and bottom salinity from July, 2010 to December 2011

Figure B-13: Comparison of modeled versus observed salinity vertical stratification from July, 2010 to December 2011
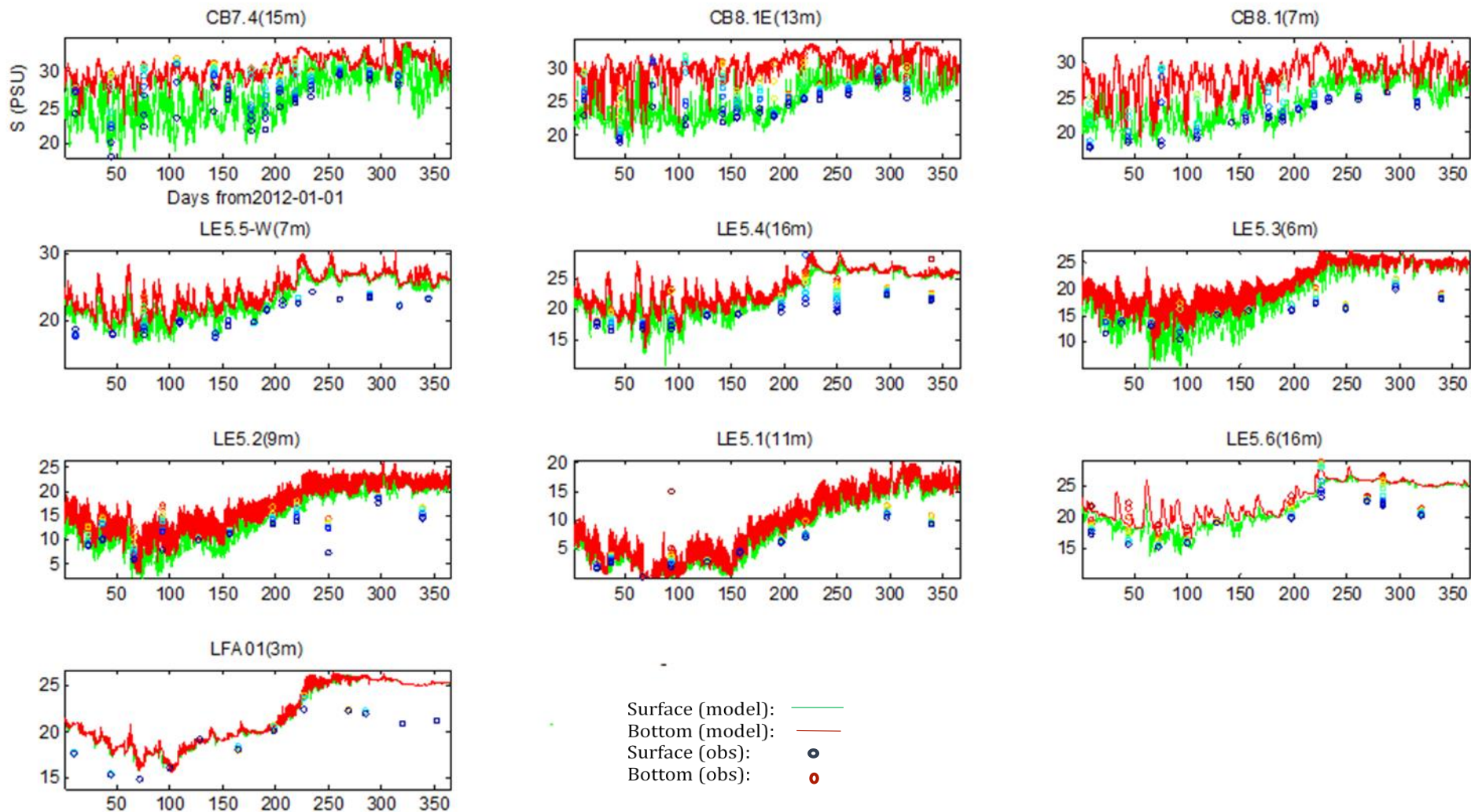
Figure B-14: Comparison of modeled versus observed surface and bottom salinity from January, 2012 to December 2012 at lower Chesapeake Bay stations
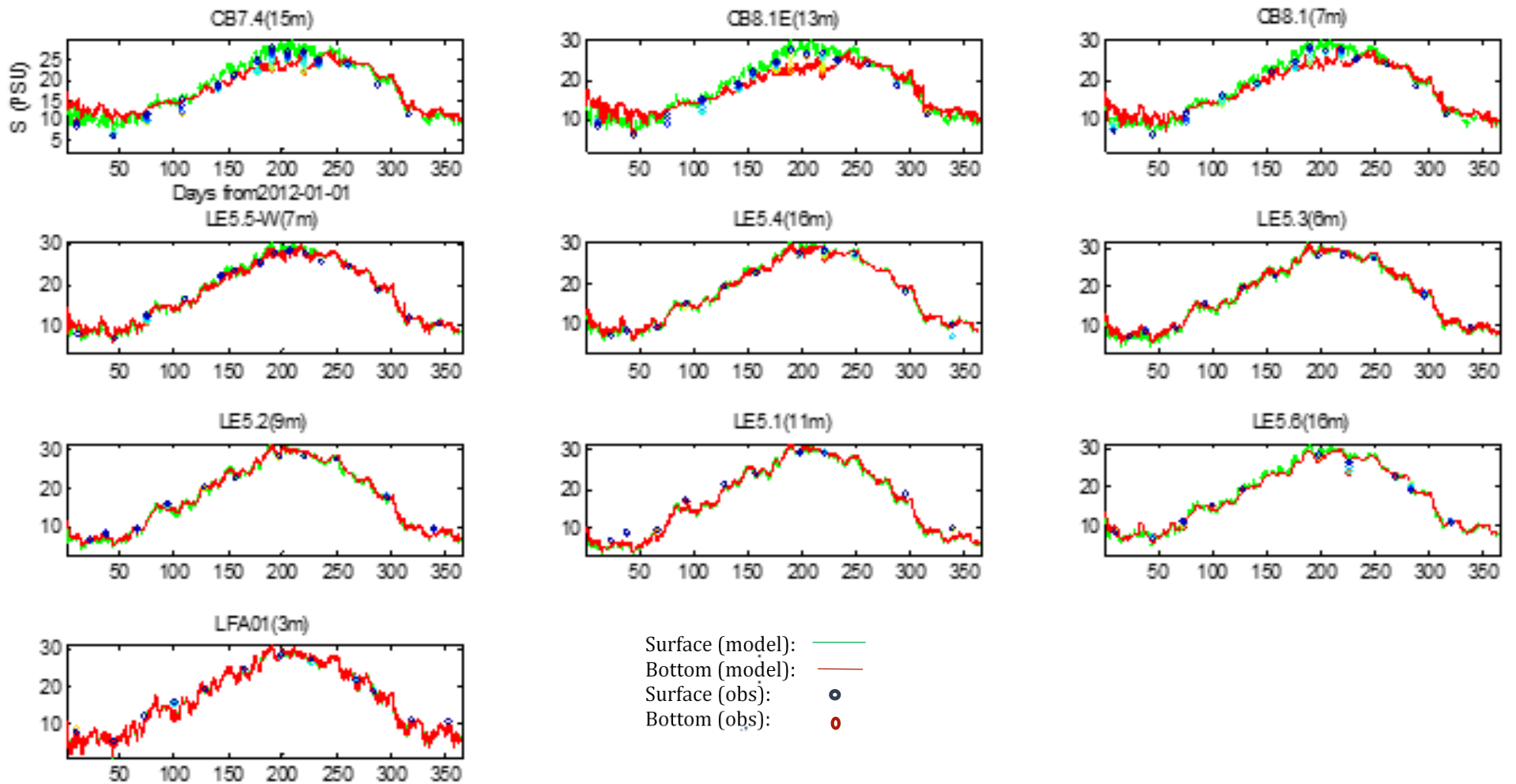
Figure B-15: Comparison of modeled versus observed surface and bottom temperature from January, 2012 to December 2012 at lower Chesapeake Bay stations
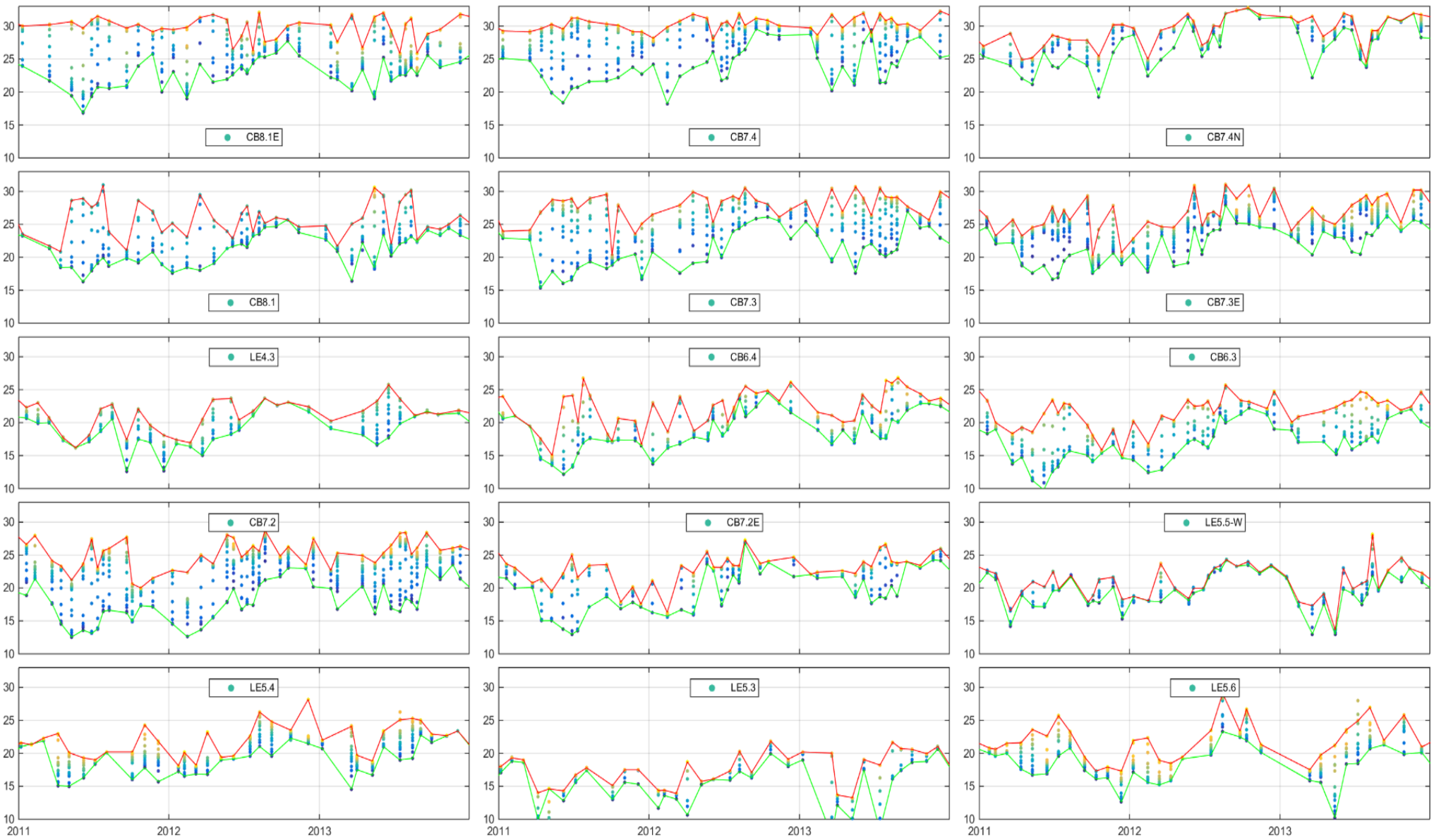
Figure B-16: Comparison of modeled versus observed surface and bottom monthly salinity from January, 2011 to December, 2013 at lower Chesapeake Bay stations
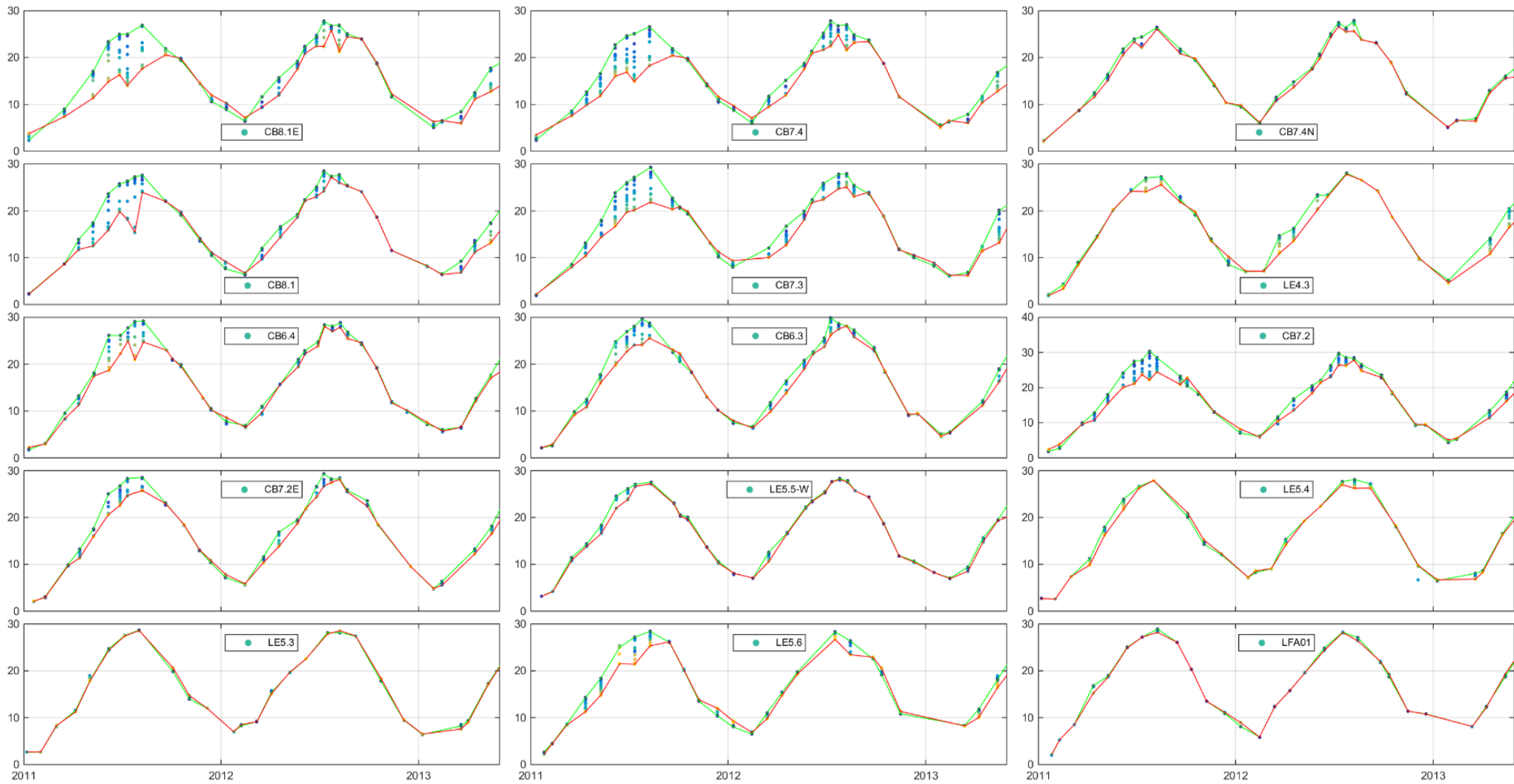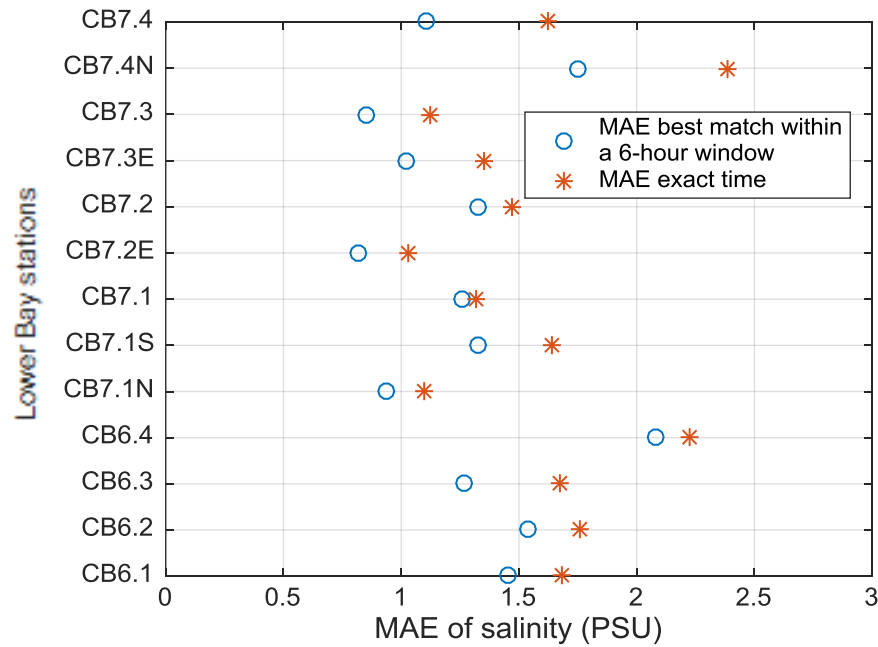
Figure B-17: Comparison of modeled versus observed surface and bottom monthly temperature from January, 2011 to December, 2013 at lower Chesapeake Bay

Statistical comparison for salinity and temperature

Lower Bay salinity at all sampling depths, 2011-2013

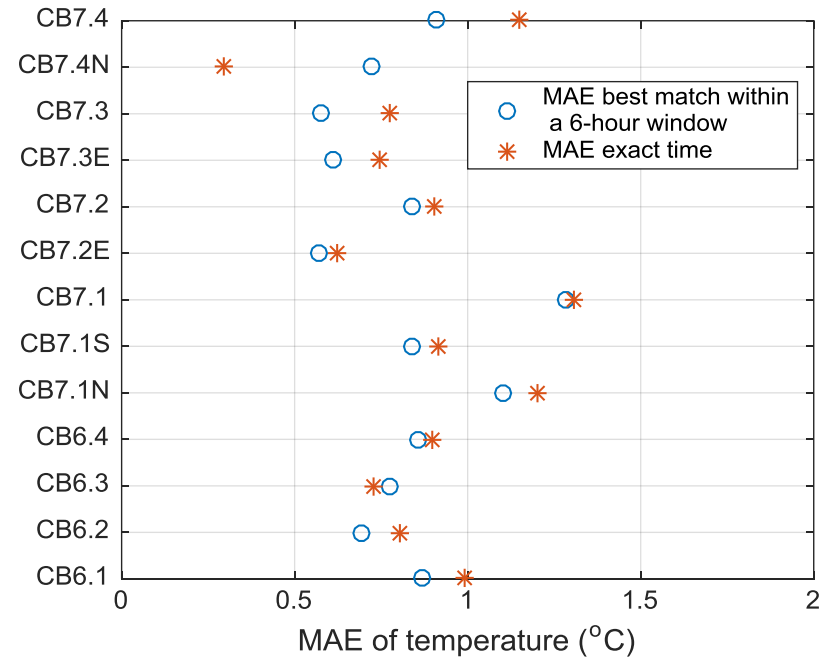Lower Bay temperature, at all sampling depths, 2011-2013

Figure B-18: Statistical comparison of modeled versus observed salinity and temperature from January, 2011 to December, 2013 in MAE (mean absolute error)